

Load-dependence and regulation of actin-myosin interactions in muscle

© Yu-Shu Cheng

Department of Kinesiology and Physical Education

Faculty of Education

McGill University, Montreal

May, 2019

A thesis submitted to McGill University in partial fulfillment of the requirements of the degree of

Doctor of Philosophy in Kinesiology

TABLE OF CONTENTS

Acknowledgments.....	4
Contribution of Authors	5
List of Figures.....	6
List of Tables.....	11
Abstract.....	12
Résumé.....	14
CHAPTER 1 – LITERATURE REVIEW.....	16
1. Introduction.....	17
2. The skeletal muscle sarcomere	22
3. Actin, myosin and the cross-bridge cycle	24
3.1 Actin.....	24
3.2 Troponin and tropomyosin.....	28
3.3 Myosin	29
3.4 The cross-bridge cycle	34
4. Load dependence of myosin force production.....	39
5. Structures of myosin responsible for the power stroke.....	42
6. Objective, hypotheses and research outline	45
7. Experimental methods for a load-dependent myosin-actin interactions.....	47
7.1 Loaded in-vitro motility assay (IVMA).....	47
7.2 Force measured system with microfabricated cantilevers	49
EXPERIMENTAL STUDY 1	51
CHAPTER 2 – LOAD DEPENDENCE OF ACTOMYOSIN INTERACTION.....	51
8. The load dependence and the force-velocity relation in intact myosin filaments from skeletal and smooth muscles	52
8.1 Abstract	53
8.2 Introduction.....	54
8.3 Methods.....	57
8.4 Results.....	64
8.5 Discussion.....	72
EXPERIMENTAL STUDY 2	78

CHAPTER 3 – ACTOMYOSIN INTERACTION REGULATION BY LOOPS 1 AND 2	78
9. Cleavage of loops 1 and 2 in skeletal muscle heavy meromyosin (HMM) leads.....	79
to a decreased function.....	79
9.1 Abstract	80
9.2 Introduction.....	81
9.3 Method	84
9.4 Results.....	90
9.5 Discussion.....	103
CHAPTER 4 – CONCLUSIONS AND FUTURE DIRECTIONS	109
10. Conclusions.....	110
11. Future directions	112
REFERENCE.....	114
CHAPTER 5 –APPENDICES AND SUPPLEMENTAL INFORMATION	131
12. Supplemental Information	132
12.1. Detailed protocols and methods for the experimental study 2.....	132
12.2. Supplemental material of Mass spectrometry for the experimental study 2.....	142

Acknowledgments

First and foremost, I would like to thank my supervisor, Dr. Dilson E. Rassier, for supervising my studies. He has been a great professor, mentor and friend. I have never met anyone like him, dynamic, resourceful, with willingness to share his wealth of knowledge with me. He works well in a multi-cultural and diverse work force, where his stable personality and high sense of responsibility is desirable. For all above, it is my great honor to work with him. Secondly, I would like to express my appreciation to the Natural Science and Engineering Research Council of Canada (NSERC) and Manulife Fellowship Fund (Bloomberg Manulife award) for the financial support of this thesis research. Thirdly, I would like to thank all my best friends who supported me and cheered me up in my PhD journey: Oleg S. Matusovsky, Lorne Taylor and Amy Wang who help me with the mass spectrometry experiments and data analysis, Lennart Hilbert who developed an automated video customized analysis software for an in-vitro motility assay. Also, I would like to thank Felipe de Souza Leite, Fabio Carderelli Minozzo, Nabil Shalabi, Daren Elkrief, Ricarda Haeger, Caitlin MacEachen, Md Rezuhanul Haque Saikat, Andrea Mendoza, Giulia Del Guercio Green, Albert Kalganov, and everyone who helped me on this amazing period of my life. Last, but most importantly, I would like to thank my family. They lovingly supported me from the other side of the earth.

Contribution of Authors

This study incorporates two manuscripts that are primarily the work of Yu-Shu Cheng, including data analysis and collection, writing and preparation for publication. The work for all the manuscripts was performed under the supervision of Dr. Dilson E. Rassier, who contributed in their conception, writing and data analysis. Dr. Oleg S. Matusovsky participated in the mass spectrometry experiments and data analysis. Dr. Lennart Hilbert conceived and wrote a mathematical model and software for experimental analysis and discussion. Dr. Felipe De Souza Leite helped me to set up the experimental systems and buffer preparations.

List of Figures

Figure 1. Structure of skeletal striated muscle (Adapted from Bhagavan, 2002). (A) A myofibril is a long cylinder containing sarcomeres. A sarcomere consists of the A-band (myosin thick filaments), and two adjacent I-bands (actin thin filaments). As the sarcomere contracts, the thin filament increases its overlap over thick filament. (B) A muscle fiber is composed by hundreds of myofibrils. (C) A bundle of muscle fibers composed by enormous myofibers. (D) Bundles of muscle cells are arranged into larger bundles connected with tendon..... 19

Figure 2. (A) Illustration of the contractile machinery in smooth muscles. The smooth muscle cell cytoplasm is packed with thick and thin filaments, and other structural components (dense bodies, dense bands, intermediate filaments). Myosin thick filaments and actin thin filaments are anchored to dense bodies (Adapted from Aguilar & Mitchell, 2010). (B) A schematic diagram showing the arrangement of smooth muscles in uncontracted/contracted states..... 21

Figure 3. Schematic representation of a myofibril, showing how myosin and actin filaments are organized within a sarcomere (adapted from Marieb & Hoehn, 2008). The Z-discs are located at the ends of the sarcomeres, which are centrally divided by the M-line. The I-band is the area between the A-band and the Z-disc, and consists of thin filaments only. The A-band is the area that consists mainly of thick filament that may overlap with thin filaments. 23

Figure 4. (A) Crystal structure of the monomeric actin form (adapted from Graceffa & Dominguez, 2003) with four domains. (B) Image of the helical structure of F-actin taken with cryo-electron microscopy (Dominguez & Holmes, 2011). The molecules are arranged as a single helix with 13 molecules repeating in six left-handed turns. (C) Model of a thin filament. Two regulatory proteins, troponin and tropomyosin, are attached to the thin filament at the myosin binding domain. Troponin contains three polypeptides and binds to both actin and tropomyosin. 27

Figure 5. Schematic view of troponin and tropomyosin interacting with the acto-myosin complex. (A) Tropomyosin blocks the myosin-binding site on actin in low Ca^{2+} concentration. (B) Ca^{2+} binds to troponin, causing a conformational change in tropomyosin. This change allows the myosin head to bind to actin. 29

Figure 6. Pictures taken with electron microscopy showing negatively stained myosin molecules in the absence of nucleotide. (A) Two globule heads connected by a long thin tail. Bar: 20 nm. (B) The myosin heads are shown containing different orientations. Bar: 20 nm. (Burgess, Walker, White, & Trinick, 1997)..... 31

Figure 7. Schematic representation of the major structural features of the myosin molecule. Heavy meromyosin (HMM) contains subfragment-1 (S1), a partially coiled-coil, and the regulatory (R) and essential (E) light chains. Light meromyosin (LMM) is a helical polypeptide coiled-coil structure. The thickness of LMM is about 2nm. (Adapted from Bhagavan, 2002).... 31

Figure 8. The details of actin-myosin interaction showing different stages of the cross-bridge cycle (Adapted from Sweeney & Houdusse, 2010). **A**: Actin, **M**: Myosin, **D**: ADP (adenosine diphosphate), **T**: ATP (adenosine triphosphate), **P**: Inorganic phosphate group..... 35

Figure 9. The ribbon diagram of the myosin II molecule in four structure states: rigor, post-rigor, pre-powerstroke and post-powerstroke. The lever arm position is controlled by the position of the converter, which swings relative to the rest of the motor domain. Model designed by Y.S. Cheng in Rassier’s laboratory, specifically for this thesis..... 39

Figure 10. (A) A ribbon representation of domains and fragments of myosin subfragment-1 (Rayment, 1996). The three regions of the motor domain include the upper and lower 50kDa domains (actin-binding) and the nucleotide pocket. The Essential (ELC) and the regulatory (RLC) light chain are actin binding regulatory domains. (B) A schematic illustration of myosin subfragment-1 indicating the different loops and segments structures (Adapted from Sweeney & Houdusse, 2010). 43

Figure 11. In-vitro motility assay, a method that tracks fluorescently-labeled actin filament over myosin heads under fluorescence microscopy in the presence of ATP (Adapted from Lauzon et al., 2012). 48

Figure 12. A schematic of the interaction between actin binding proteins and actin in the fractional loading in-vitro motility assay. Actin binding proteins (α -actinin) provide a fractional force against the driving force induced by myosin when added to the coverslip (adapted from Bing et al., 2000; Greenberg & Moore, 2010). 49

Figure 13(A). A schematic illustration of micro-fabricated cantilevers attached with the single myosin and actin filaments. (B) Forces were generated by myosin-actin interaction, the cantilever was bended by the forces. 50

Figure 14. (A) Schematic view of the micro-fabricated cantilevers. There are four pairs of flexible cantilevers (from left) and one set of inflexible cantilever (right) manufactured from thin silicon nitride. Each pair of cantilevers has identical stiffness. (B) Schematic view of the experimental chamber. The cantilevers were attached to metal holder where placed in the chamber. The actin filaments, thick filaments and all solution exchanges were inputted and outputted through side ports of the chamber. (C) A schematic diagram showing the experimental set-up. Thick filament and actin filaments were attached to the cantilevers, and were brought into contact. (D) When the filaments start to slide past each other, they produce force that causes the displacement of the flexible cantilever (Δd), which enabled us to measure the force. The signal from the cantilever displacement is also used to input the actuator in the rigid cantilever so it can change positions to induce changes in load as required for the experiments. 60

Figure 15. Force traces collected during filaments interactions during experiments. When there is no load applied to the system, the filaments slide and produce force until they are stabilized (blue). When the load was increased during the interactions (red trace), the force increased, and the load was decreased (green) the force was decreased. The gray trace shows the movement of the rigid cantilever to change the load – in this case only one trace is shown for clarity. Note that the signal to background noise ratio (black trace in the inset) is very high. 65

Figure 16. Force produced by the filaments at different ATP concentrations. (A) Mean force. (B) Force normalized per degree of filaments overlap. (C) Increase in force observed during the increase in load imposed to the filaments. Data are given as means \pm SEM. 68

Figure 17. The force-velocity relationship in skeletal (A) and smooth (B) myosin filaments with different ATP concentrations. The blue symbols represent the maximal velocity measure with in-vitro motility assays. 70

Figure 18. 10% SDS-PAGE showing the time course for proteolytic digestion of skeletal muscle HMM without (A) and with (B) addition of actin, to partially protect loop 2 from digestion. HMM (0.1 mg/ml) was digested at 1:50 enzyme-to-substrate ratio in 20 mM KCl, 20 mM

Tris-HCl (pH 7.5) and 5ug of protein were loaded for each column in the gel. The red squares show the bands that were chosen for subsequent mass spectrometry analysis. The digestion time corresponding to each lane is shown at bottom of the figure. 91

Figure 19. Myosin II sub-fragment 1 (PDB:2MYS) with the sequences of loop 1, ATP loop, loop 2 and the actin-binding domain 2 obtained by mass spectrometry, and highlighted by UCSF Chimera software..... 93

Figure 20. Label-free mass-spectrometry quantification of rabbit skeletal HMM and its tryptic fragments, when the digestion protocol was performed without protection of loop 2. Extracted ion chromatograms profiles were used to calculate the 50% peak areas of peptides covering loop 1 (A), part of loop 2 (B) ATP-loop (C), and actin-binding domain 2 (D) at different times during the protocol. Data were normalized to the 50% peak area of non-trypsinized HMM. Reproducibility of the data were tested in two independent experiments with at least three runs for quantification of peak area of selected peptides..... 95

Figure 21. Label-free mass-spectrometry quantification of rabbit skeletal HMM and its tryptic fragments when the digestion protocol was performed in the presence of actin to partially protect loop 2. Extracted ion chromatogram profiles were used to calculate the 50% peak areas of peptides covering loop 1 (A), part of loop 2 (B) ATP-loop (C), and actin-binding domain 2 (D) at different times. Data were normalized to the 50% peak area of non-trypsinized HMM. The reproducibility of the data was tested in two independent experiments with at least three runs for quantification of peak area of selected peptides. 96

Figure 22. Distribution of velocities of actin filaments sliding in the in-vitro motility assay. The data showed on the panels (A) and (C) represent the condition where both loops 1 and 2 were cleaved (1 minute and 8 minutes of digestion, respectively). Non-linear fits for the histograms rendered peaks produced velocities of $3.91\mu\text{m}/\text{sec}$ and $2.74\mu\text{m}/\text{sec}$, showing a shift in the mean velocity. The data showed on the panels (B) and (D) represent the condition when loop 1 was cleaved in the presence of actin to partially protect loop 2 (1 minute and 4 minutes of digestion, respectively). Non-linear fits for the histograms rendered peaks produced velocities of $4.42\mu\text{m}/\text{sec}$ and $1.93\mu\text{m}/\text{sec}$, respectively, showing a shift in the mean velocity. The velocity of actin motility (E) and the fraction of moving actin filaments (F) for the control HMM, and during cleavage of loops 1 and 2, with and without partial protection of loop 2, are shown as mean \pm SEM. Each

experiment was repeated three times. The values for the experiments including sample sizes are indicated in supplementary Tables 3 and 4. 98

Figure 23. The relation between the concentration of α -actinin and the velocity of actin motility over HMM in the different conditions investigated in this study (A) and when all data are grouped (B). There is an inverse, linear relationship such that an increase in the concentration of α -actinin decreases the velocity of actin motility. The lower panels show the relative velocity of actin motility obtained during cleavage of loops 1 and 2, without (C) and with (D) partial protection of loop 2. These experiments were conducted with the addition of different concentrations of α -actinin (0.5, 0.75, 1.0, 1.25 and 1.5 μ g/mL) in the motility assay. The graph shows data collected during 30 minutes of digestion. The number of actin filaments analyzed in each group. Data are presented as mean \pm S.E.M. 100

Figure 24. Effect of cleavage of loops 1 and 2 on actin-activated Mg^{2+} -ATPase. HMM: 0.01 mg/ml, F-actin: 0.05 mg/ml. Data are given as mean \pm S.E.M. (N=15 for each group). 102

Supplementary Figures

Supplementary Figure 1. A flowchart of experimental study 2 133

Supplementary Figure 2. Extracted ion chromatograms used to count peptide content in the loops and domains investigated in this study. Panels A-D: Representative peak area of selected peptides in different proteolytic fragments of HMM cleaved in both loops 1 and 2; Panels E-H: Representative peak area of selected peptides in different proteolytic fragments of HMM cleaved in loops 1 and 2 when loop 2 was partially protected with 2-fold excess of F-actin. 143

List of Tables

Table 1. The values for a/P_o representing the curvatures of the force-velocity curves in the experiments conducted with skeletal and smooth myosin filaments, with different ATP concentrations. 70

Supplementary Tables

Supplementary Table 1: Protein-Peptide Database of rabbit skeletal HMM (Uniprot database: accession number Q28641, highlighted by blue color) and its tryptic fragments with corresponding peptide counted areas obtained without protection of loop 2. The highlighted peak area of peptides covering ATP-loop, loop 1, actin binding domain 1-loop 2 and actin-binding domain 2 are shown. Reproducibility of obtained data was tested in two independent experiments with at least three runs for quantification of peak area of selected peptides. 144

Supplementary Table 2: Protein-Peptide Database of rabbit skeletal HMM (Uniprot database: accession number Q28641) and its tryptic fragments with corresponding peptide counted areas obtained with protection of loop 2. The highlighted peak area of peptides covering ATP-loop, loop 1, actin binding domain 1-loop 2 (part of loop 2) and actin-binding domain 2 are shown. Reproducibility of obtained data were tested in two independent experiments with at least three runs for quantification of peak area of selected peptides..... 149

Supplementary Table 3: Mean velocities ($\mu\text{m}/\text{sec}$) of actin filaments in the in-vitro motility assay form enzymatic HMM. 155

Supplementary Table 4: Mean of motile fraction (fraction of time that filaments are moving) of actin filaments in the in-vitro motility assay form enzymatic HMM. 156

Supplementary Table 5: Mean velocities of actin filaments cooperated with α -actinin in the in-vitro motility assay form enzymatic HMM. 157

Abstract

Muscle contraction is produced by the interaction between myosin and actin. In this thesis, we developed two studies looking into (i) the load dependence and the force-velocity relationship of myosin filaments interacting with actin, and (ii) the regulating effects of surface loops of the myosin molecule on the load-dependent actin motility. For the first study, we developed a method for evaluating the load dependence of force generation by isolated muscle myosin filaments. Single skeletal and smooth muscle myosin filament and single F-actin filament were attached to micro-fabricated cantilevers of known stiffness. We shortened or lengthened the myosin-actin filaments as they interacted with each other, and observed that increasing the load increased the force while decreasing the load decreased the force produced by myosin. We also performed additional experiments where we clamped the filaments at pre-determined levels of force. The filaments were forced to slide relative to each other and adjust the different loads which then allowed us to measure the velocity during the length changes and construct a force-velocity relation. The force-velocity curves for skeletal and smooth muscle myosin resembled the relations observed for muscle fibers. This measurement technique can be used to investigate many issues of interest and debate in the field of muscle biophysics.

In the second study, we used limited tryptic proteolysis of heavy meromyosin (HMM) to obtain different amounts of loops 1 and 2, the ATP-loop, and the actin-binding domain. The myosin-propelled actin motility, and the fraction of actin filaments motility were decreased in

association with the depletion of loop 1 in the HMM. Furthermore, the ATPase activity was decreased in close association with depletion of loops 1 and 2. We concluded that loop 1 in coordination with other surface loops is responsible for regulating the load-dependent velocity of actin motility. Therefore, myosin-actin interaction is closely regulated by the two flexible loops in the structure of myosin.

Résumé

La contraction musculaire est due à l'interaction entre actine et myosine. Dans cette thèse, nous avons développé deux études portant sur (i) la relation force-vitesse de filaments d'actine liés à myosine et son rapport en fonction de sa charge et (ii) les effets régulateurs des boucles de la surface de la molécule de myosine sur la motilité de l'actine qui est charge-dépendante. Dans la première partie de notre étude, nous avons développé une méthode pour évaluer la dépendance du voltage de la force générée par des filaments isolés de myosine musculaire. Un filament de myosine squelettique et de muscle lisse et un filament d'actine F étaient fixés sur des cantilevers micro-fabriqués de rigidité connue. Nous avons poussé ou tiré les filaments de myosine-actine lorsqu'ils étaient liés et nous avons observé que si nous augmentions la charge, la force augmentait, tandis que si nous diminuions la charge, la force générée par la myosine diminuait également. Nous avons également effectué des expériences supplémentaires au cours desquelles nous avons serré les filaments à des niveaux de force prédéterminés. Les filaments ont été forcés de glisser les uns par rapport aux autres et d'ajuster les différentes charges. Cela nous a permis de mesurer la vitesse lors des changements de longueur et de construire une relation force-vitesse. Les courbes force-vitesse de la myosine squelettique et lisse ressemblaient aux relations observées pour les fibres musculaires. Cette technique peut également servir à enquêter nombreuses questions d'intérêt et de débat dans le domaine de la biophysique musculaire.

Dans la deuxième partie de notre étude, nous avons épuisé les boucles dans la surface de la molécule de myosine, y compris la boucle 1, la boucle 2, la boucle ATP et les boucles de fixation de l'actine. Les boucles règlent la motilité voltage-dépendant des filaments d'actine propulsés par

les molécules de myosine. Les charge-dépendants vitesses et la fraction de la motilité des filaments d'actine ont été diminués en accord avec l'épuisement des boucles 1 dans le méromyosine lourde. Par la suite, l'activité ATPase a été diminué en accord avec l'épuisement des boucles 1 et 2. Nous concluons que la boucle 1, en coordination avec les autres boucles de surface, est responsable de la régulation de la vitesse en fonction de sa charge de la motilité d'actine. Par conséquent, l'interaction myosine-actine est fortement réglementé par les deux boucles flexibles de la structure de la myosine.

CHAPTER 1 – LITERATURE REVIEW

1. Introduction

Muscles are the motors of life and allow for a broad range of movements. Muscle contraction is the result of cyclic interactions of protein filaments driven by adenosine triphosphate (ATP) hydrolysis. The muscle myosin motor domain acts as an ATPase, breaking ATP into ADP and phosphate (P_i), releasing energy that results on mechanical work.

In vertebrates, muscles can be divided into three different types: skeletal, cardiac and smooth muscles. Skeletal and cardiac muscles have a form of striated muscle tissue, whereas smooth muscle is less organized as skeletal muscle. Striated muscle filaments are organized in contractile structures called sarcomeres, which repeat along the fiber axes. Skeletal and cardiac muscles have similar intracellular structure and physiological responses to high concentration of calcium (Ca^{2+}). On the other hand, smooth muscles are not organized in sarcomeres; they have a fusiform (spindle-shaped), non-striated organization that provides great elasticity, and a large operating working range.

There are three main types of muscle fibers identified in skeletal muscles: type I, type IIA, and type IIB (Brooke & Kaiser, 1970). These are further classified as fast (type II) or slow (type I) based on the speeds of fiber shortening (Barany, 1967). The muscle fiber types can be categorized via chemical staining for ATPase on myosin, myosin heavy chain (MHC) isoform identification, and metabolic enzymes identification (Scott, Stevens, & Binder-Macleod, 2001). The population of fiber types varies throughout a muscle. A motor unit consists of a group of individual muscle fibers that are activated by a single motor neuron. For each specific type of

fiber, motor units transmit signals to contract the fibers. Type I fibers correspond to slow-contracting motor units and type II fibers correspond to fast-contracting motor units (Burke, Levine, Tsairis, & Zajac, 1973; Edstrom & Kugelberg, 1968).

There are a number of morphological differences among fiber types. Type I fibers are somewhat red in color indicating high amounts of myoglobin and capillary content which enables high oxidative capacity compared with that of white muscles. Type IIA and IIB fibers contain different MHC isoforms sequenced by different genes (Dalla Libera, Sartore, Pierobon-Bormioli, & Schiaffino, 1980; Pierobon-Bormioli, Sartore, Libera, Vitadello, & Schiaffino, 1981). The pattern of energy metabolism is different in Type IIA and IIB where IIA fibers are generally more oxidative than IIB fibers (Izumo, Nadal-Ginard, & Mahdavi, 1986; Wieczorek, Periasamy, Butler-Browne, Whalen, & Nadal-Ginard, 1985). Type II fibers contain a larger content of glycolytic enzymes which leads to reduced mitochondria content and an efficient anaerobic glycolysis for high force production (Grichko, Gettelman, Widrick, & Fitts, 1999).

Figure 1 illustrates the different structural levels of a striated skeletal muscle. It is composed of many long poly-nucleated cells, also called muscle fibers. Every fiber in turn is composed of thousands of myofibrils, which contain tubules of contractile subunits. Each of these myofibrils is organized into thousands of serially-repeating blocks called sarcomeres. There are two main types of contractile filaments in a sarcomere: the thin (primarily actin-formed) filaments and the thick (primarily myosin-formed) filaments, which are organized into a crystalline hexagonal arrangement. Each thick filament is surrounded by 6 thin filaments

and each thin filament is surrounded by 3 thick filaments (H. E. Huxley, 1969).

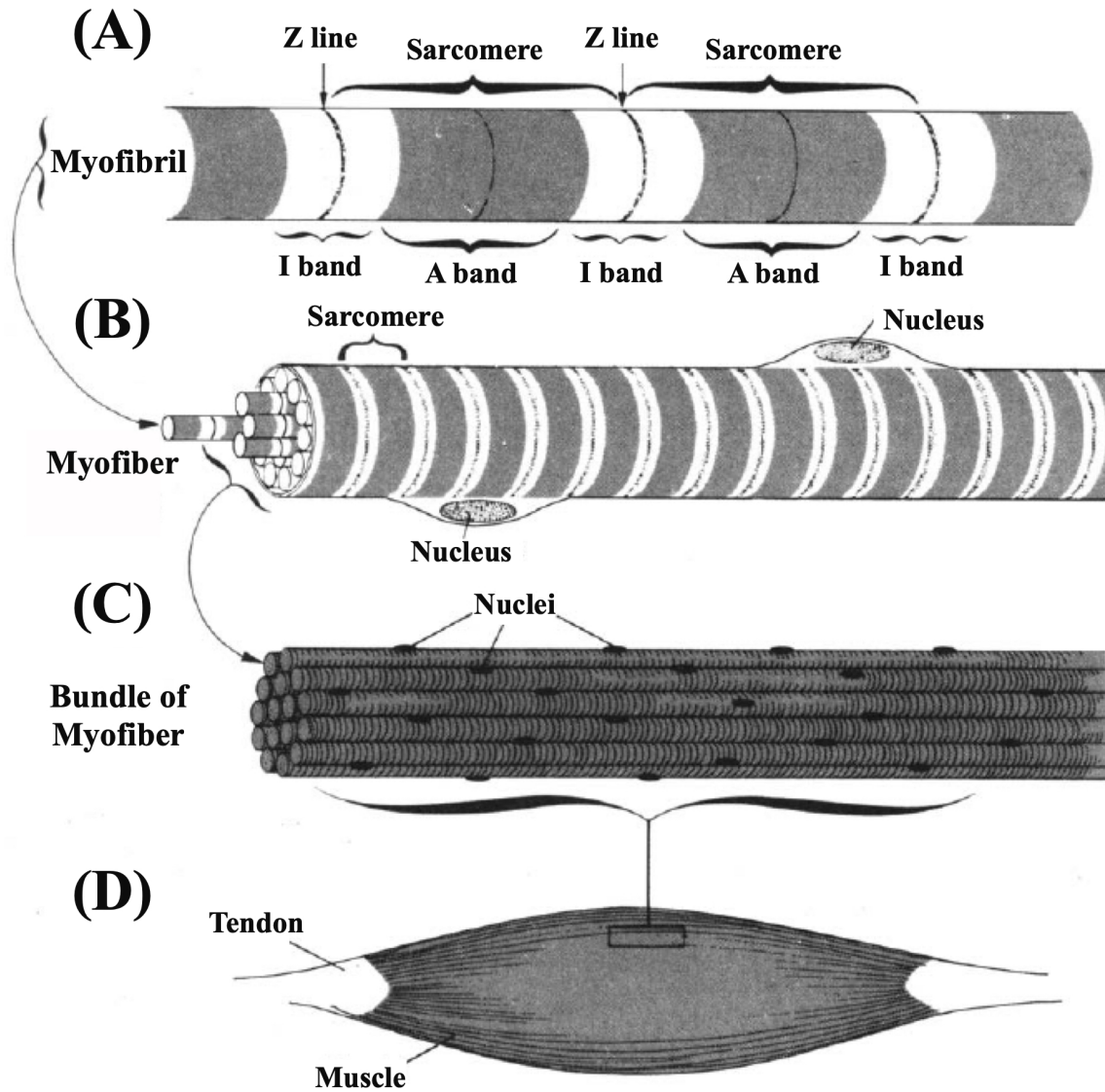
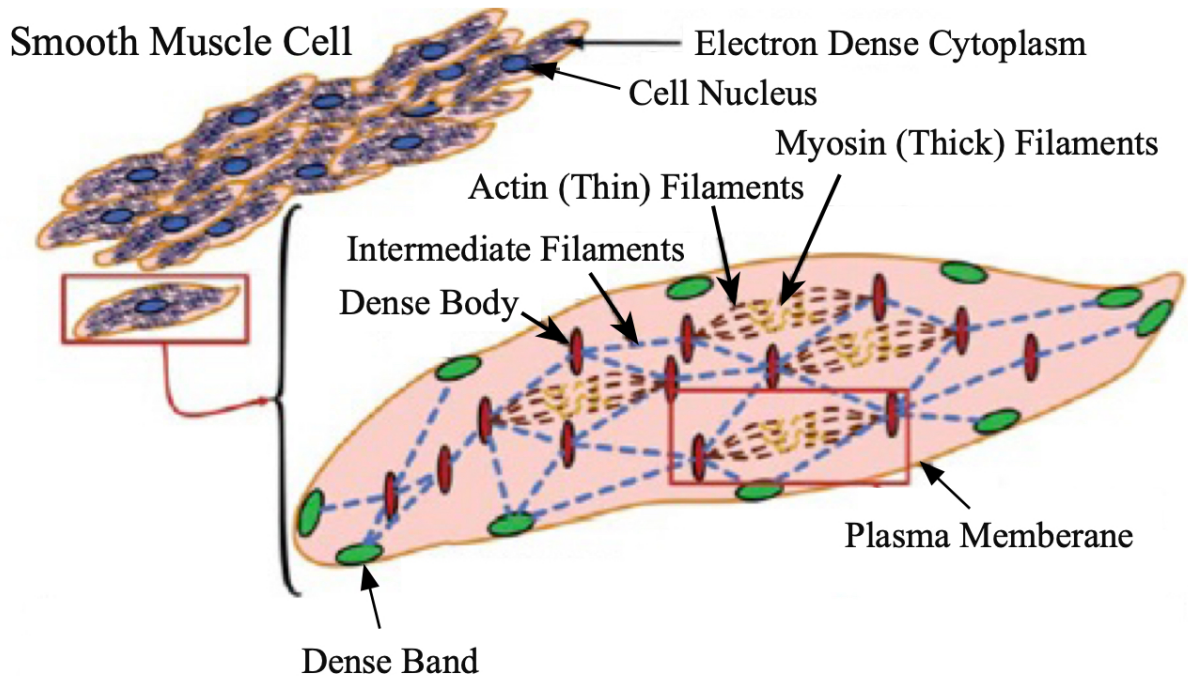


Figure 1. Structure of skeletal striated muscle (Adapted from Bhagavan, 2002). (A) A myofibril is a long cylinder containing sarcomeres. A sarcomere consists of the A-band (myosin thick filaments), and two adjacent I-bands (actin thin filaments). As the sarcomere contracts, the thin filament increases its overlap over thick filament. (B) A muscle fiber is composed by hundreds of myofibrils. (C) A bundle of muscle fibers composed by enormous myofibers. (D) Bundles of muscle cells are arranged into larger bundles connected with tendon.

Smooth muscles differ from skeletal muscles in a number of ways, including the morphology, molecular structure, and the arrangement of actin and myosin filaments (Figure 2A). Nonetheless, skeletal and smooth muscles share the same motor responsible for contraction: the myosin class II isoform. Smooth muscles are arranged in intermediate filament networks connected by nodes called 'dense bodies', which work together when a smooth muscle cell is activated. These dense bodies act as anchors to bridge thin filaments together along the contractile plane of the muscles determined by the direction in which myosin and actin filaments overlap.

Shortening of the smooth muscle cell occurs when myosin in the thick filament interacts with actin thin filaments between two dense bodies. Upon activation, the two actin filaments move towards each other (Figure 2B) (Aguilar & Mitchell, 2010).

(A)



(B)

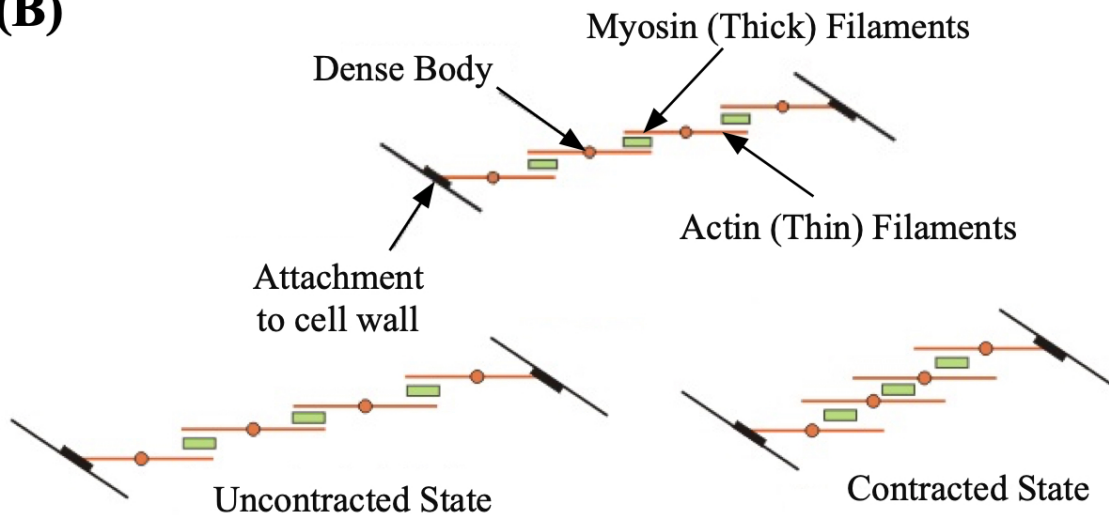


Figure 2. (A) Illustration of the contractile machinery in smooth muscles. The smooth muscle cell cytoplasm is packed with thick and thin filaments, and other structural components (dense bodies, dense bands, intermediate filaments). Myosin thick filaments and actin thin filaments are anchored to dense bodies (Adapted from Aguilar & Mitchell, 2010). (B) A schematic diagram showing the arrangement of smooth muscles in uncontracted/contracted states.

2. The skeletal muscle sarcomere

The organized arrangement of muscle proteins in the sarcomere plays an important role in active and passive force generation. The sarcomere contains unique sections of protein arrangements organized into regions called the Z-disk, I-band and A-band (Figure 3).

The boundaries of the sarcomere are determined by neighboring Z-discs. The average optimal length of one sarcomere is approximately 2.2 - 2.4 μm . The Z-disc is the connecting region for both the thin and thick filaments. Several actin binding proteins (ABPs), α -actinin, titin and nebulin, are needed for optimal arrangement of the thin filaments (Luther, 2009), and to help maintain sarcomere structure. The thickness of the Z-disc varies based on muscle fiber types and species. The difference between Z disks thickness in fiber types is related to α -actinin content (Luther, 2009).

The thick filament is anchored to the Z-disc by titin, another important component of muscle. Titin is a giant, 3 MDa protein approximately 1 μm long. Titin is composed of repeating coiled-coil structural (amphiphilic α -helices) motifs, which often acts as a highly stable polymerization domain (Bang et al., 2001; Cohen & Parry, 1990). Titin is one of the most abundant proteins of vertebrate striated muscle (Kurzban & Wang, 1988; Maruyama, Kimura, Yoshidomi, Sawada, & Kikuchi, 1984).

A giant protein in the sarcomere is nebulin (600-900kDa), which is coextensive with the actin filament. Nebulin is an integral component in the assembly and alignment of the Z-disks. It is directly responsible for regulating the length of thin filaments. Nebulin has functional

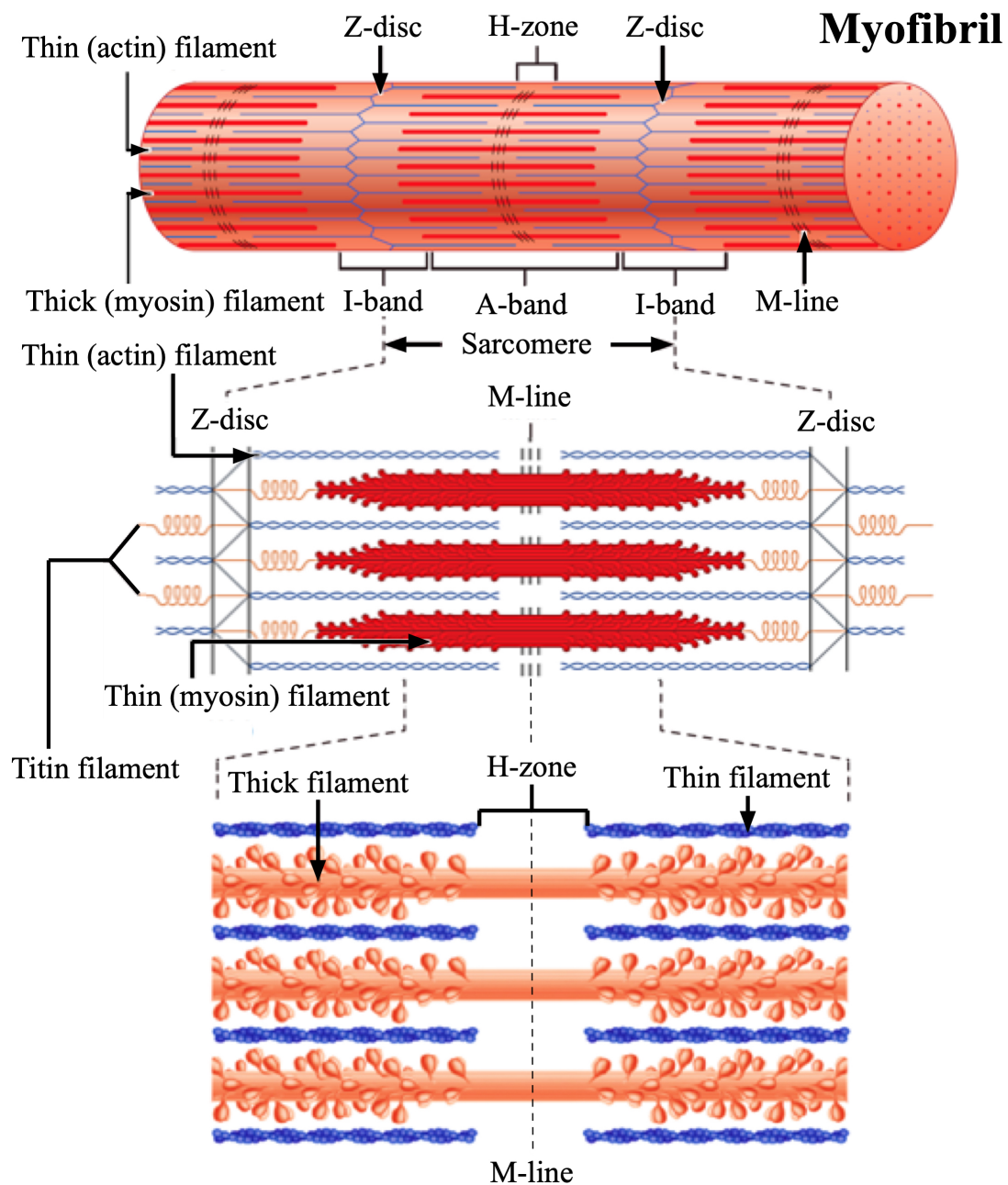


Figure 3. Schematic representation of a myofibril, showing how myosin and actin filaments are organized within a sarcomere (adapted from Marieb & Hoehn, 2008). The Z-discs are located at the ends of the sarcomeres, which are centrally divided by the M-line. The I-band is the area between the A-band and the Z-disc, and consists of thin filaments only. The A-band is the area that consists mainly of thick filament that may overlap with thin filaments.

characteristics as well; it affects myofibril calcium sensitivity and may change the kinetics of myosin-actin interactions (Labeit, Ottenheijm, & Granzier, 2011; Witt et al., 2006).

The A-band of the sarcomere is composed mostly by an assembly of thick filaments. The thick filaments are linked by a network of antiparallel myosin molecules organized in a filamentous structure, centrally divided by the M-line. The M-line is found within the H-zone of the sarcomere. The H-zone is a subdivision of the A-band in the center of the sarcomere, and is the only region where the thick filament cannot overlap the thin filament. The I-band is the region between two A-bands and is composed mostly by thin filaments.

3. Actin, myosin and the cross-bridge cycle

3.1 Actin

Actin is a highly conserved protein essential for filament interaction. It can transition between globular monomeric (G-actin) and filamentous (F-actin) states under the control of nucleotide hydrolysis. Actin plays an important role in cellular motility, maintenance of cell structure, cell polarity and in the regulation of transcription. Furthermore, the interaction of F-actin with myosin is the basis of force generation during muscle contraction (Szent-Gyorgyi, 2004). Free G-actin has a strong affinity for Mg^{2+} -ATP, but will be denatured readily in the absence of bound nucleotide (Carlier et al, 1988). At critical nucleotide concentrations (0.1mM), G-actin will assemble into F-actin spontaneously in physiological ionic strength buffers and

disassemble at low ionic strengths (N.V. Bhagavan, 2002).

There are three differential isoforms of actin expressed in mammals: α -actin, β -actin and γ -actin. The molecular weight of actin is approximately 42,000 Da (Elzinga, Collins, Kuehl, & Adelstein, 1973). The difference between actin isoforms is a few amino acids, with most of the variations occurring near the N terminus (Herman, 1993).

There are four globular subdomains I, II, III and IV which comprise the G-actin structure. It has a rectangular shape with the dimensions of approximately 5.5 x 5.5 x 3.5 nm, containing a nucleotide binding cleft located between subdomain II and IV (Dominguez & Holmes, 2011; Kabsch, Mannherz, Suck, Pai, & Holmes, 1990), as shown in Figure 4. These subdomains in G-actin bind non-covalently with an adjacent G-actin to initiate actin polymerization. These interaction sites in the domains are specific, so that all the G-actin assembling into a filament has the same polarity. This results in nucleotide binding cleft toward the same end of the filament by hydrogen bond. Moreover, most ABPs interact with target-binding clefts which are located between subdomains I and III of the actin molecule, a region also known as the hydrophobic cleft (Dominguez & Holmes, 2011).

A sequence located at the end of subdomain II (residues 39-51) is referred to as the DNase I-binding loop (or D-loop) because it mediates important interactions in the complex with DNase I (Kabsch et al., 1990).

Each G-actin interacts with four neighboring monomers. The monomers are named in relation to a reference monomer (subunit 0). Neighboring subunits are called +2 and +1 (+ denoting the barbed end) or -1 and -2 (- denoting the pointed end), as shown in figure 4B. In

order to stabilize the F-actin filament structure, the interaction between monomers made along the filament axis where subdomain IV of subunit 0 interacts with subdomain III in subunit -2, which in turn interact with the D-loop of subunit 0 and the target binding cleft of subunit -2. These interactions are critical for stabilizing the F-actin arrangement (Dominguez & Holmes, 2011).

The actual symmetry of F-actin, as explored by electron microscopy, resembles a single left-hand helix, with a repetition of 13 G-actins over 6 turns, with an axial distance of 35.9 nm. Each monomer in F-actin is rotated $-166.6 \pm 6^\circ$ from its compared to the neighbor, with a 2.76 nm axial increase, and a diameter of roughly 10 nm (Fujii, Iwane, Yanagida, & Namba, 2010) as shown in Figure 4C. However, given that the -166.6° monomer twist is close to 180° , the structure appears as a double stranded right-handed polymer chain. The two ends of F-actin are usually referred to as the fast-growing barbed (+) end and the slow-growing pointed (-) end. In-vitro, actin monomers connect to the barbed end of the filament when ATP is present and dissociates from the pointed end in the absence of ATP. This steady state mechanism of actin polymerization and depolymerization is called actin filament treadmilling (Wegner & Isenberg, 1983).

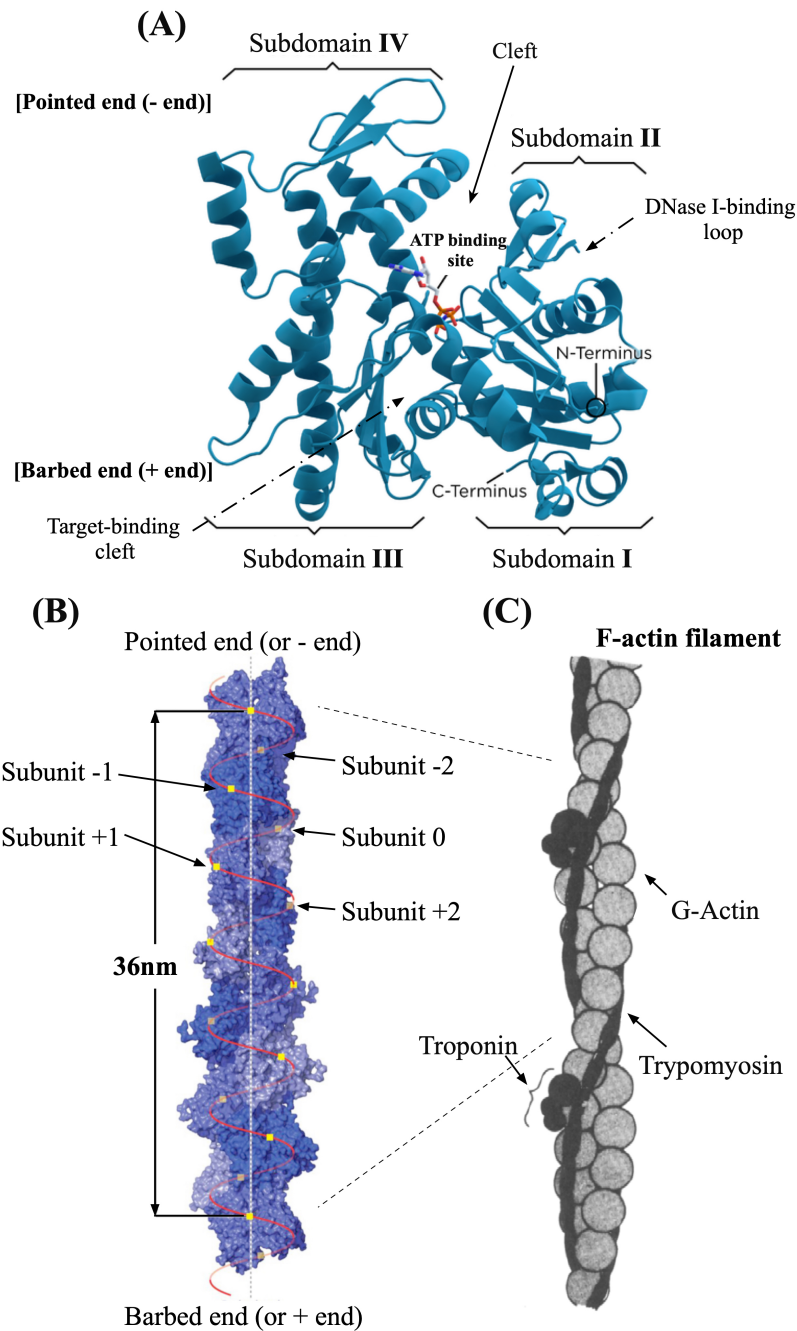


Figure 4. (A) Crystal structure of the monomeric actin form (adapted from Graceffa & Dominguez, 2003) with four domains. (B) Image of the helical structure of F-actin taken with cryo-electron microscopy (Dominguez & Holmes, 2011). The molecules are arranged as a single helix with 13 molecules repeating in six left-handed turns. (C) Model of a thin filament. Two regulatory proteins, troponin and tropomyosin, are attached to the thin filament at the myosin binding domain. Troponin contains three polypeptides and binds to both actin and tropomyosin.

3.2 Troponin and tropomyosin

Tropomyosin (~37KDa) was first discovered and investigated by Bailey in 1946 (Bailey, 1946), the protein has enormous coiled-coil α -helical content (Cohen, 1955). Its non-polar side chains result in its two-stranded coiled-coil shape (Hodges & Smillie, 1972). When tropomyosin is combined with troponin, each tropomyosin binds one troponin molecule (Ohtsuki, 1979). There are three different subunits in troponin, which include Troponin C (TnC), Troponin I (TnI) and Troponin T (TnT). TnC (18KDa) binds Ca^{2+} , which serves as a Ca^{2+} sensor. TnI (20-24KDa) serves as an inhibitor that binds between TnC and actin, inhibiting myosin from binding to actin. TnT (31-36KDa) serves as a regulator for conformational change in troponin when Ca^{2+} is bound, and links the other two subunits and tropomyosin to the actin filament (Figure 5A) (Greaser & Gergely, 1971).

Troponin and tropomyosin regulate the myosin binding sites on the actin filament in the absence of Ca^{2+} (Ebashi, Kodama, & Ebashi, 1968). When Ca^{2+} binds to troponin it causes a conformational change resulting in the tropomyosin moving toward troponin (Figure 5B). Once tropomyosin moves, the myosin-binding site on the actin filament opens, allowing the myosin head to rapidly attach to actin, which initiates the cross-bridge cycle (Lehman, Craig, & Vibert, 1994).

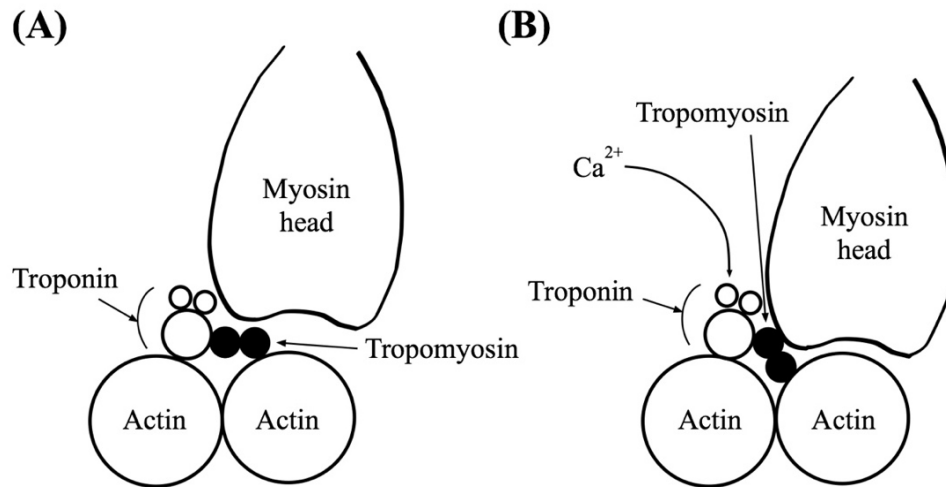


Figure 5. Schematic view of troponin and tropomyosin interacting with the acto-myosin complex. (A) Tropomyosin blocks the myosin-binding site on actin in low Ca^{2+} concentration. (B) Ca^{2+} binds to troponin, causing a conformational change in tropomyosin. This change allows the myosin head to bind to actin.

3.3 Myosin

In 1864 W. Kühne extracted a protein from muscle using high salt solution, which he named “myosin” (Kühne, 1864). In 1935, Weber created a new technique for the in-vitro study of muscle contraction using myosin preparation from a concentrated salt solution (Weber, 1935). In 1934, Lohmann suggested that ATP was the likely source of energy for muscle contraction (Lohmann, 1934). However, the concept that myosin was an ATPase enzyme was not widely accepted, because enzymes were considered to be small globular proteins, while myosin is not a globular protein (Polis & Meyerhof, 1947). The idea that myosin had ATPase activity was only proven in 1939 by W. A. Engelhardt and M. N. Lyubimova (Engelhardt & Lyubimova, 1939).

In 1942, Banga and Szent-Györgyi reported a protocol to extract myosin and actomyosin

from high ionic strength solution, which precipitated upon decreasing ionic strength (Banga & Szent-Györgyi, 1942). In 1943, Straub reported that actin existed in two forms; globular actin (G-actin) that was stable in the absence of salt and filamentous actin (F-actin) that was polymerized in the presence of ions and ATP (Straub, 1943).

Each gram of fresh skeletal muscle contains 70-100 mg of myosin (Needham & Williams, 1963), which means 40-50% of the total muscle proteins. Myosin molecules are able to polymerize into filament at low ionic strength (0.03M KCl), and the filaments are depolymerizing while at high ionic strength (0.6M KCl). Myosin is a highly asymmetric globulin molecule that represents a large superfamily of proteins which shares a common domain responsible for interaction with actin, ATP hydrolysis and force production (Mermall, Post, & Mooseker, 1998). However, the variety in the myosin superfamily generates diversity in functions and structures according to specific myosin isoform. So far, 35 classes of myosin have been identified in organisms – these classes are classified according to the phylogenetic tree of the motor domains (Odrionitz & Kollmar, 2007). Researchers have investigated 18 major classes of myosin, and at least 7 occur in mammalian species. Myosin class II, also called myosin II, is the most studied since it is responsible for contractions of skeletal, smooth and cardiac muscles (Harris, Work, Wright, Alpert, & Warshaw, 1994; F. Minozzo & D. E. Rassier, 2013).

Figure 6A and 6B, shows an example of negatively stained myosin structures. Myosin has a pair of heads and one long tail.

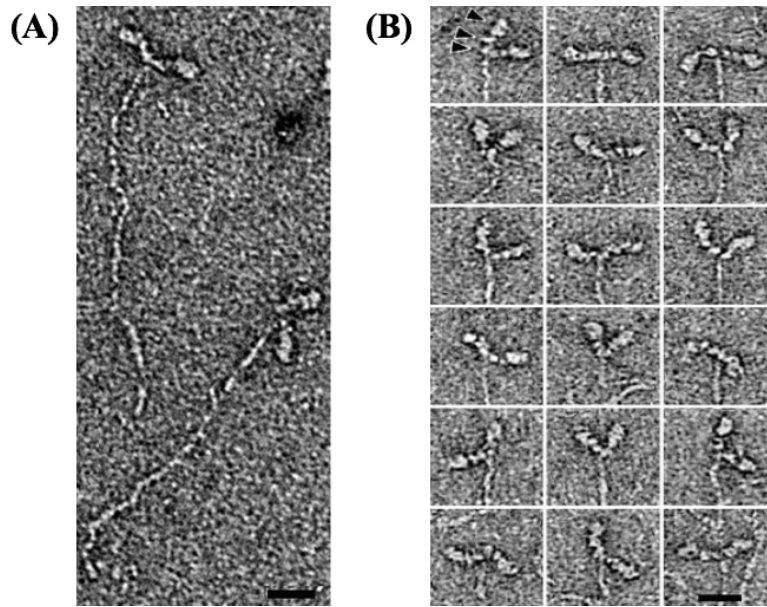


Figure 6. Pictures taken with electron microscopy showing negatively stained myosin molecules in the absence of nucleotide. (A) Two globule heads connected by a long thin tail. Bar: 20 nm. (B) The myosin heads are shown containing different orientations. Bar: 20 nm. (Burgess, Walker, White, & Trinick, 1997)

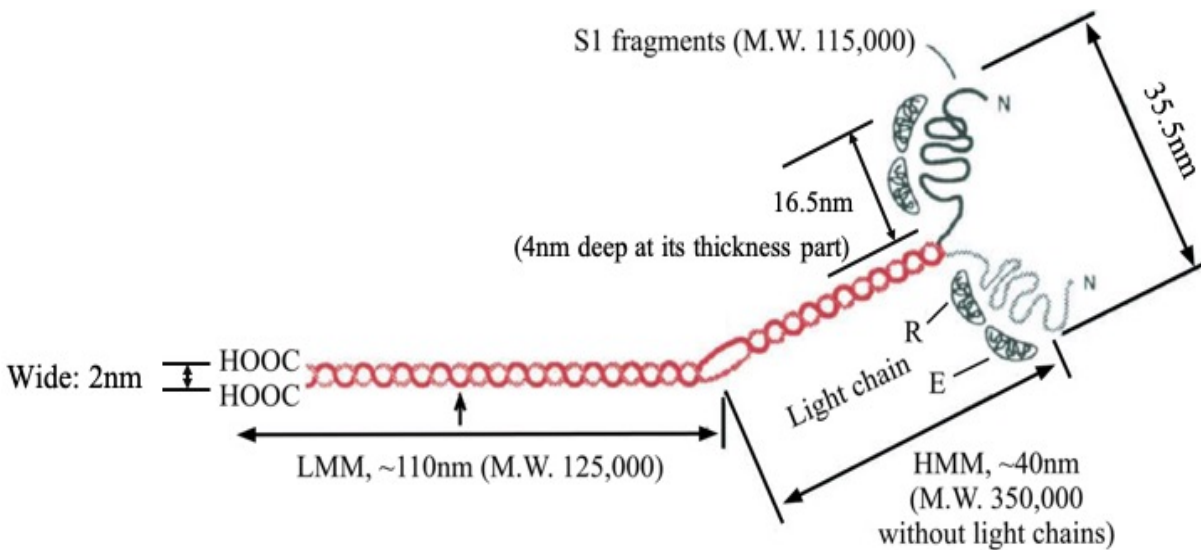


Figure 7. Schematic representation of the major structural features of the myosin molecule. Heavy meromyosin (HMM) contains subfragment-1 (S1), a partially coiled-coil, and the regulatory (R) and essential (E) light chains. Light meromyosin (LMM) is a helical polypeptide coiled-coil structure. The thickness of LMM is about 2nm. (Adapted from Bhagavan, 2002).

Myosin II consists of two identical heavy chains, a pair of essential light chains and a pair of regulatory light chains. The heavy chain contains a motor domain with an ATPase and an actin binding site (Figure 7). The structure of myosin II can be divided into two fragments by enzymatic cleavage: Heavy Meromyosin (HMM) and Light Meromyosin (LMM). LMM composes the lower part of the myosin tail (rod-like, α -helix coiled-coil part) that self-assembles to the main protein structure with other myosins to form a thick filament (Burgess et al., 2007; Young, Himmelfarb, & Harrington, 1964). HMM is responsible for ATPase activity and interactions with actin filaments (Barouch & Moos, 1971; Dancker, 1975). The region between the HMM and the LMM can be digested by specific enzyme treatments: trypsin can cleave the hinge region (64 residues) to separate LMM and HMM rapidly (Harrington, Von Hippel, & Mihalyi, 1959). The results obtained with proteolysis of myosin is very similar to that obtained by adding chymotrypsin to myosin preparations (Gergely, Gouvea, & Karibian, 1955).

HMM contains sub-fragments 1 and 2 (S1 and S2). S2 refers to upper part of the myosin tail and S1 is composed of two myosin heads. Each myosin head has three subunits: one globular motor domain and two myosin light chains (MLCs). The MLCs can be divided further into two groups: an essential light chain and a regulatory light chain. The MHC can also be divided into 3 fragments coupled with structural, flexible loops; these are secondary structures that reverse the peptide chain in protein folding. Each of these sub-structures in the globular motor domain have their own molecular weight: 25kDa (N-terminal), 50kDa (Central) and 20kDa (C-terminal) (Levi-Valensin et al., 1979).

The S1 fragment illustrated in Figure 7 can individually support force production and drive

actin motility, since it can drive ATP hydrolysis and bind to actin. Even when the S1 region of myosin is chemically isolated from the remaining sections of the molecule by different types of enzyme treatment, it maintains its affinity to bind with actin filaments. Based on the molecular weight of the different regions of the S1 fragment, and its high-resolution crystal structure (Rayment, Rypniewski, et al., 1993; Yang et al., 2007), we now know that the S1 has four major subdomains: the N-terminal domain, the upper 50K domain, the lower 50K domain and the converter domain (Houdusse et al., 1999).

The upper and the lower 50kDa domains (Figure 10), collectively called the 50kDa cleft, separate loop 1 and loop 2. The 50kDa cleft is connected through switch 2, loop 2 and the so-called strut loop (Fisher et al., 1995; Rayment, Rypniewski, et al., 1993; C. A. Smith & Rayment, 1996). There are two regions in this cleft, called inner cleft and outer cleft. The outer cleft interacts and binds with actin monomers. The inner cleft is near the switch II that binds the γ -phosphate released from ATP (Rayment, Rypniewski, et al., 1993). Near the inner cleft, the seven-stranded β -sheet-associated α -helices stretch from the N-terminal domain to the upper 50K domain. They act together as an internal tension transducer of the myosin head (Fujita-Becker, Reubold, & Holmes, 2006; Nikolaeva, Orlov, Bobkov, & Levitsky, 2002). The β -sheet is also linked to switch II and the relay helix, both of which are important structures in the lower 50K domain that communicate between the ATP-binding site and the converter domain. (Coureux et al., 2003; Sweeney & Houdusse, 2010).

The nucleotide-binding site located between the N-terminal domain and the upper 50K domain binds Mg^{2+} -ATP (Holmes & Geeves, 2000). It has been identified that nucleotide binding

and sensing of the hydrolysis state of the nucleotide involves many key structural motifs such as the p-loop, switch I and switch II (Sasaki, Shimada, & Sutoh, 1998). The switch II plays a critical role in the conversion of energy derived from ATP hydrolysis into actin sliding and force generation (Ruppel & Spudich, 1996; Uyeda, Ruppel, & Spudich, 1994). Switch I and switch II conformational states are referred to as closed (ATP binding) and open (ADP or no-nucleotide) states of the nucleotide-binding site. Finally, the p-loop, or the phosphate-binding loop, is a short polypeptide which cooperates with switch I and switch II to sense when ATP and ADP are bound to the nucleotide binding site (Koppole, Smith, & Fischer, 2007).

3.4 The cross-bridge cycle

The mechanisms of muscle contraction are directly associated with the sliding filament theory, proposed originally by Andrew Huxley, Hugh Huxley, and colleagues in separate studies published in 1954 (A. F. Huxley & Niedergerke, 1954; H. Huxley & Hanson, 1954). The theory has suffered many modifications since first developed, but it is still considered the best model of how muscles contract and produce force. It states that contraction happens as a result of actin and myosin filaments sliding past each upon muscle activation. The driving force for the sliding of the actin filament is the myosin motor, the basis for the “cross-bridge theory”. The cross-bridge theory, which is complementary to the sliding filament theory, was first proposed by Andrew F. Huxley in 1957 (A. F. Huxley, 1957) and later modified by the same author and collaborators (A. F. Huxley & Simmons, 1971). Since these initial studies, the cross-bridge model has become a paradigm in the muscle field, and virtually all studies have been interpreted within the theory’s framework. The cross-bridge model can be mostly described by structural changes in the myosin

molecules that happen while interacting with actin. Such changes take place cyclically, powered by energy derived from ATP hydrolysis. A simplified version of the cross-bridge cycle is depicted in Figure 8.

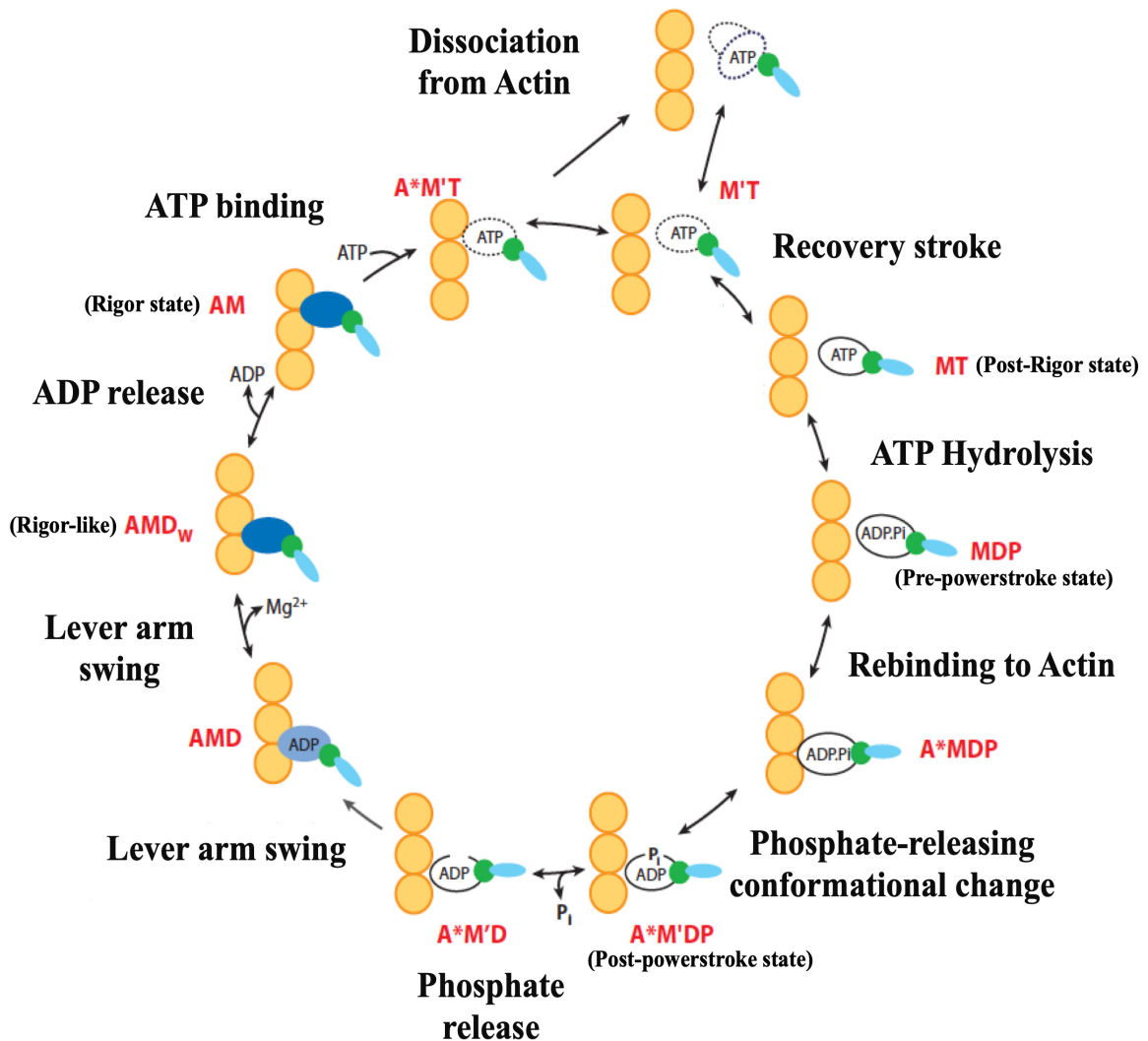


Figure 8. The details of actin-myosin interaction showing different stages of the cross-bridge cycle (Adapted from Sweeney & Houdusse, 2010). **A**: Actin, **M**: Myosin, **D**: ADP (adenosine diphosphate), **T**: ATP (adenosine triphosphate), **P**: Inorganic phosphate group.

In the first part of the cross-bridge cycle, the actomyosin complex is in the rigor (AM) state. Then, ATP binds into the nucleotide pocket due to its high affinity and myosin detaches from actin. Second, in the M state, the myosin transitions into the ADP·P_i form and myosin re-attaches to actin due to an increase in actin affinity caused by ATP hydrolysis. Third, P_i dissociates from the binding pocket, which is followed by the release of ADP, finally concluding the cross-bridge cycle. During these late phases, the myosin produced the so-called power stroke, transforming the chemical energy released from ATP hydrolysis into mechanical work.

During the first part of the cross-bridge cycle, in the AM state, the myosin affinity for ATP is high, while the myosin affinity for actin is low. The upper 50kDa domain of myosin moves to the AM state and causes switch 1 to follow its movement. As stated earlier in this thesis, the switch 1 is the myosin domain responsible for the communication between the nucleotide-binding pocket and the actin-binding domain (Boriack-Sjodin, Margarit, Bar-Sagi, & Kuriyan, 1998). As the switch 1 leaves its former position, the nucleotide pocket opens, allowing ATP to bind to switch 1 and initiate the upper 50K domain to move backwards. With ATP attached, the nucleotide pocket closes in the MT state. In the MT state, ATP binds to switch 1, the p-loop on the right, and switch 2 underneath it, which together comprise the “active” site for ATP hydrolysis. Switch 2 is responsible for conformational changes at the level of the relay helix, and positions the lever arm for the pre-power stroke state (Holmes & Geeves, 2000). Mutagenesis studies have provided support for these functions of switch 1 and switch 2 (Forgacs et al., 2009; Shimada, Sasaki, Ohkura, & Sutoh, 1997). In this way, the p-loop is an important motif for communicating the conformational changes from the active site to the protein effector-binding

site (Kull, Vale, & Fletterick, 1998).

ATP is hydrolyzed in the nucleotide pocket and contains α , β and γ -phosphate groups attached to an adenosine molecule. The γ -phosphate is only 5Å apart from switch 2 once it is bound to the nucleotide pocket (Geeves & Holmes, 2005). The movement of switch 2 in the active site toward the P_i of ATP brings amino acid residues to specific active positions in the molecule (Kintses et al., 2007). In the MT state, switch 2 moves towards the lower 50K domain due to hydrolysis of the P_i hydrogen bond. With ATP hydrolysis, actin affinity is increased allowing rebinding of the myosin to actin, transitioning the MDP to an A*MDP state. The movement of switch 2 causes the 50-kDa cleft to also move downward and close up, trapping γ -phosphate. The lower 50K domain forces the secondary structure to change its conformation. Finally, the converter movement causes a recovery-stroke in the lever arm which initiates myosin to enter the A*M'DP state- and the pre-power stroke state.

Two events take place during the A*M'DP – A*M'D state: the swing of the lever arm and the release of P_i , followed by the dissociation of ADP, resulting in the AMD state. The dissociation of P_i from the nucleotide pocket happens prior to release of ADP, leading to the AM state. The swing in the lever arm causes the myosin to bind actin more tightly causing the filament to slide and the nucleotide pocket to close and enter the AM·ADP state – the power stroke. Assuming that dissociation of P_i happens prior to the lever arm swing, both the ADP position and the lever arm position need to be maintained through these phases.

We do not have the crystal structure of myosin-actin for all steps that lead to force generation. We therefore used some of the structures that are available in the literature and the

information presented in the previous paragraphs to develop an independent, qualitative cross-bridge model.

Figure 9 shows the crystal structure of the myosin II states during the cross-bridge cycle and most importantly, the force-generating cycle. Consistent with the lever arm model, it has four distinct conformations: rigor state (PDB: 3I5G), post-rigor state (PDB:1SR6), pre-powerstroke state (PDB:1BR1) and post-powerstroke state (PDB:2MYS). These states illustrate that small conformational changes in the motor domain are coupled to large changes in the position of the lever arm.

The lever arm distance between the rigor state and the pre-powerstroke state is approximately 12 nm (Sweeney & Houdusse, 2010), which is illustrated in Figure 9. In the rigor state, the myosin is docked with actin filament without bound ATP. The myosin is detached from actin filament once nucleotide pocket binds ATP, which results in the post-rigor state. After hydrolysis of ATP, P_i is trapped at the active site. Myosin's affinity for actin increases from the pre-powerstroke state to the post-powerstroke state. The lever arm swings after ADP and P_i are released from nucleotide pocket, and force is produced after which myosin returns to the rigor state.

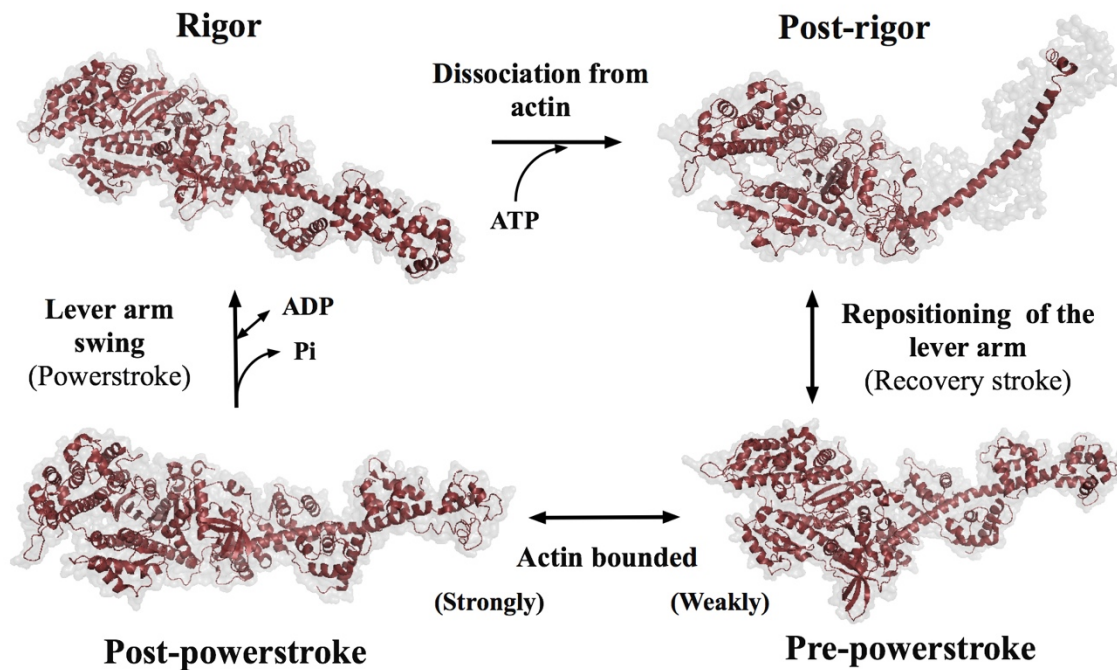


Figure 9. The ribbon diagram of the myosin II molecule in four structure states: rigor, post-rigor, pre-powerstroke and post-powerstroke. The lever arm position is controlled by the position of the converter, which swings relative to the rest of the motor domain. Model designed by Y.S. Cheng in Rassier’s laboratory, specifically for this thesis.

4. Load dependence of myosin force production

The model developed above, and all models that are developed using data from crystallography studies or based on biochemistry studies, propose a cross-bridge cycle with subsequent force generation when no load is applied to the actomyosin system. However, the force produced by the myosin cross-bridges during interactions with actin is highly dependent on the external load imposed on the cells and myofibrils during contractions. In fact, a pioneer study developed many years ago (Fenn, 1924) reported that under low loads, the muscle shortens

quickly, and under high loads the muscle contracts slowly, sustaining tension economically. Most intriguingly, the same study showed that when muscles shorten against any load and produce work, the magnitude of ATP hydrolysis is higher than during contractions developed without load (Fenn, 1923). Such an observation implies that the rate of ATP hydrolysis is directly linked to the cross-bridge cycle and varies in different muscle working conditions.

Since Feen's classic study, other scientists have investigated the load dependence of force production. It is now clear that the myosin power stroke is constrained by external loads, allowing muscles to shorten at high speeds under low loads and to sustain high forces while shortening slowly under high loads (Piazzesi, Lucii, & Lombardi, 2002; Reconditi et al., 2004). Ultimately, the load dependence of muscle contraction is the basis for the classic force-velocity relation of skeletal muscles (Hill, 1938).

The load dependence of myosin has been investigated across many levels of muscle organization, including intact fibers from the frog (Piazzesi et al., 2002; Reconditi et al., 2004) and single myosin molecules (Debold, Patlak, & Warshaw, 2005; Veigel, Molloy, Schmitz, & Kendrick-Jones, 2003). The results of these studies suggest that the load dependence of force production is closely associated with a load-dependent regulation of the overall rate between release and reattachment of myosin with ADP and P_i (Baker, Brosseau, Joel, & Warshaw, 2002; D. Smith & Sleep, 2006b).

Studies with the molecular motors myosin I and V (Debold et al., 2005; Veigel et al., 1999; Veigel, Wang, Bartoo, Sellers, & Molloy, 2002), show that the attachment time ($>100\text{ms}$) is shortened with increasing ATP concentration, suggesting that it is terminated when ATP binds to

myosin and ADP release (Guilford et al., 1997; Rief et al., 2000; Tyska et al., 1999a). The delay will cause longer attachment times between myosin and actin, resulting in more force produced at low velocity. Nevertheless, previous research (Takagi, Homsher, Goldman, & Shuman, 2006) reports that increasing loads accelerates ADP release in skeletal muscle myosin. The mechanisms behind the load dependence of force production are still a matter of debate.

Interpretation of studies with single molecules is also complex, as skeletal muscle myosin attaches to actin for a very brief period of time in near physiological ATP concentrations (<40ms) (Finer, Simmons, & Spudich, 1994; Kaya & Higuchi, 2010). As a result, studies with single myosin molecules in which the load can be controlled have not been performed in physiological ATP conditions. Skeletal muscle myosins work cooperatively in the thick filaments, and therefore their work is not independent from each other (Mansson, Rassier, & Tsiavaliaris, 2015). There is one study that investigated several myosin molecules sparsely distributed along on the surface of an optical fiber (Pertici et al., 2018), but without repeating the well-organized arrangement of thick filaments. They investigated the force-velocity relation in their system, but have not looked at the load-dependence of the force production.

The mechanism that regulates the load dependence of force is unclear. More specifically, the details behind the effects of load on the chemo-mechanical cycle of myosin heads when they work cooperatively are not well understood. Given the importance of the load-dependent power stroke for myosin molecules, and the fact that no studies have been conducted yet looking at the effects of load on the power stroke of myosin filaments, one of the goals of this thesis is to investigate the load dependence of the myosin power stroke in a configuration that the myosin

molecules act cooperatively in a filament.

5. Structures of myosin responsible for the power stroke.

The actomyosin complex is highly ionic strength-dependent, and the electrostatic interactions among the myosin motor functional loops and domains are important for the actin-binding site (Conibear, 1999; Geeves & Conibear, 1995; Geeves & Gutfreund, 1982; Geeves & Jeffries, 1988). The different subdomains and the flexible loops of myosin are shown in the schematic illustration in Figures 10A and 10B. These structures shown in the figures are all important in the actomyosin interaction, but we still do not know all the details surrounding their roles.

Loop 3, loop 4 and the HCM loop on the surface between the upper and the lower 50kDa domains of the myosin sub-fragment 1 cooperate with the actin-binding site and increase actin-binding affinity. Loop 3 is an actin-binding loop attach to the subdomain 1 of the adjacent actin monomer (Mentes et al., 2018). Loop 4 is a functional actin-binding region that regulates and stabilizes the interaction between actin and myosin in the weak actin binding states (Gyimesi, Tsaturyan, Kellermayer, & Malnasi-Csizmadia, 2008; Mentes et al., 2018). The HCM loop is related to the cardiomyopathy (CM) loop, which gives it its name, due to 29 missense mutations in the β -cardiac myosin (MYH7) gene (Rayment, Holden, Sellers, Fananapazir, & Epstein, 1995). It is located on the upper 50K domain of myosin. It is one of the loops that cooperates with

actin-myosin binding (Rayment, Holden, et al., 1993; Schroder et al., 1993) in the rigor state (Coureux et al., 2003; Holmes, Angert, Kull, Jahn, & Schroder, 2003).

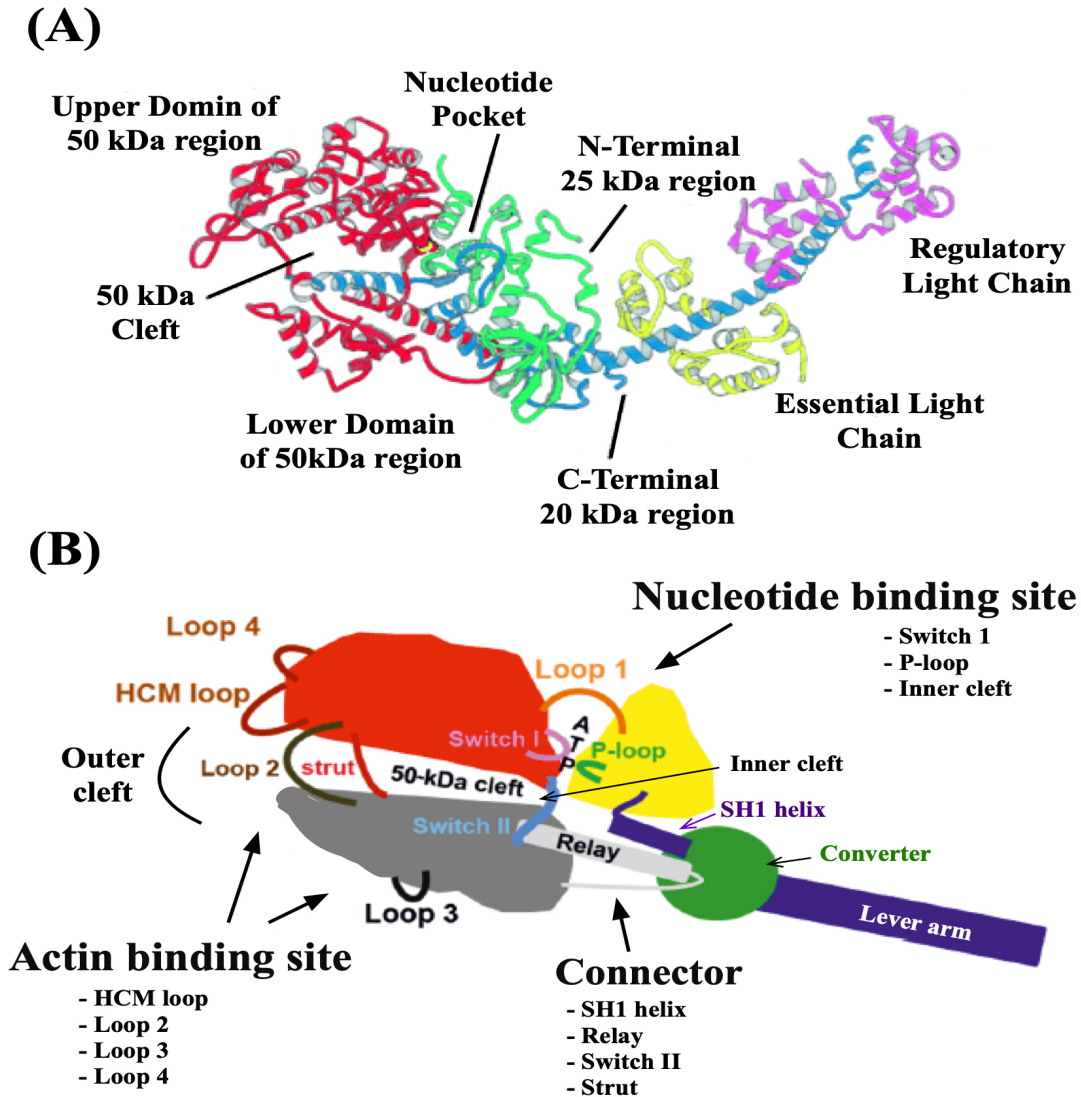


Figure 10. (A) A ribbon representation of domains and fragments of myosin subfragment-1 (Rayment, 1996). The three regions of the motor domain include the upper and lower 50kDa domains (actin-binding) and the nucleotide pocket. The Essential (ELC) and the regulatory (RLC) light chain are actin binding regulatory domains. (B) A schematic illustration of myosin subfragment-1 indicating the different loops and segments structures (Adapted from Sweeney & Houdusse, 2010).

Switch 1, switch 2 and the ATP-loop are essential during the cross-bridge cycle, force production and ATP hydrolysis. Switch 1 is the region responsible for the communication between the nucleotide-binding pocket and the binding region of the nucleotide exchange factor. Switch 2 communicates with P_i causing conformational changes of the relay helix during ATP hydrolysis. The ATP-loop is a protein motif that regulates conformational changes of the S1 region for ATP-binding pocket.

To sum up, myosin interacts with actin through loop 3, loop 4 and the HCM loop on the surface of the myosin molecule. Loop 2, loop 4 and the CM loop interact mainly with different regions of actin that are related with actin binding. These loops bind to actin at the same tropomyosin binding site, or “blocking” region (von der Ecken et al., 2015), which inhibits myosin activation. These loop regions could play an important role in myosin function and in the regulation of myosin kinetics.

The connector, converter and lever arm regions are essential – the main function of these regions is to amplify the conformational changes occurring at the active site of S1, which helps the movement of actin filaments by facilitating their interactions with myosin (Geeves & Holmes, 1999). The relay region is a conserved hydrophobic sequence that mediates conformational information between the converter domain, the nucleotide binding site and the actin-binding site (Tsiavaliaris et al., 2002).

The main of this thesis is the investigation of loop 1 and loop 2, as they have been implicated in direct regulation of ATP modulation and myosin-actin interactions. Loop 1 is one of the flexible loops of the myosin motor domain located at the 25-50kDa junction near the

nucleotide-binding pocket of the myosin head. It has been suggested that one of its functions is the modulation of ADP release (Eddinger & Meer, 2007). Loop 2 is located at the top of the motor domain, right on the 50 kDa cleft near the actin-binding surface, and has been suggested to participate in the actin activation by ATPase (Murphy & Spudich, 1998). It has also been suggested to have a role in reducing the duty ratio and thus increasing the shortening velocity of myosin (Clobes & Guilford, 2014). Loops 1 and 2 can also establish a high affinity, primarily hydrophobic, for actin. This affinity is a result of the cluster of positive charges in these loops and a cluster of negative charges on the actin N-terminal (Sutoh, 1983). However, up to date there is a lack of direct evidence to support this hypothesis. If this hypothesis were confirmed, these small, surface loops would have a decisive role in myosin-actin interactions and force transduction, and ultimately muscle contraction at the large scale.

Given the importance of the myosin structure and its domains in the myosin-actin interactions and the myosin power-stroke, and the intriguing hypothesis raised in the literature that loops 1 and 2 can regulate myosin's activity, actin binding and ATPase, a second goal of this thesis is to investigate the effects of loop 1 and loop 2 in myosin-actin interactions and activity.

6. Objective, hypotheses and research outline

Force production in muscle is driven by the interaction between thick and thin filaments in sarcomeres, coupled with ATP hydrolysis. The force is dependent on the external load imposed

on the muscle cells, myofibrils, and the myosin motor. However, the load dependence of force production has not yet been investigated in myosin molecules working in their natural configuration, i.e., in intact thick filaments. Such limitation in our knowledge also leaves a gap in our understanding of the force-velocity relationship in muscles.

The myosin structure is complex. Myosin transforms chemical energy into mechanical work through the interaction of different sub-structures in the molecule. Evidence suggests that flexible loops located at the surface of myosin are responsible for regulating the load dependent, myosin-driven actin motility. However, there is currently no detailed information on how the loops and domains of myosin S1 affects the cross-bridge cycle during myosin-actin interactions.

The main objectives of this thesis were to examine the load dependence of force generation and the sub-structures in myosin that are responsible for actin and ATPase activities during myosin-actin interactions. More specifically we aim to test the following hypotheses:

1. There is a load dependence of the myosin-actin interaction and force that is manifested at the molecular level;
2. The myosin-driven actin sliding and its load dependence are regulated by loops 1 and 2 in the myosin molecule.

In order to test these hypotheses we conducted two studies using advanced techniques to measure the force produced by myosin filaments while interacting with actin at different loads, and to evaluate the effects of depleting myosin from specific loops in the actin motility and force-velocity relation.

7. Experimental methods for a load-dependent myosin-actin interactions

There is an array of experimental methods that were used in this thesis. These assays were developed or modified in our laboratory specifically for the current studies, are not readily available in other laboratories and therefore need some explanation.

7.1 Loaded in-vitro motility assay (IVMA)

An in-vitro motility assay was developed in 1986 (Kron & Spudich, 1986) to investigate the motility of actin filaments over myosin molecules. In this assay, actin is induced to slide on a myosin-coated surface where performed on a nitrocellulose-coated coverslip (Sheetz & Spudich, 1983; Kron & Spudich, 1986). The experimental conditions (pH, temperature or ATP concentration) can be controlled and the actin motility can be visualized and easily detected. Figure 11 shows a diagram of the in-vitro motility assay. It can measure the velocity of actin motility, and fraction of actin filaments that slide over myosin.

In order to investigate the effects of load on actin motility, we used the frictional loading assay (Janson et al., 1992; Warshaw et al., 1990). In this assay, actin-binding proteins (ABPs) are added to the surface of the experimental chamber to produce frictional forces, which imparts load on the motility (Figure 12). There are many ABPs that can be used in this assay such as: α -actinin (Bing, Knott, & Marston, 2000; Cheng, Matusovskiy, & Rassier, 2019; Janson, Sellers, & Taylor, 1992), pPDM myosin (Warshaw, Desrosiers, Work, & Trybus, 1990) and filamin (Haeberle, Trybus, Hemric, & Warshaw, 1992). These ABPs interact with the actin filaments

during the myosin-induced sliding, creating counteracting forces against the driving force by the myosin motors, i.e., external loads. The magnitude of the external load changes in direct proportion to the amount of ABPs interacting with the actin filament. The frictional load exerted by ABP can be viscoelastic (velocity-dependent) and/or elastic (velocity-independent),

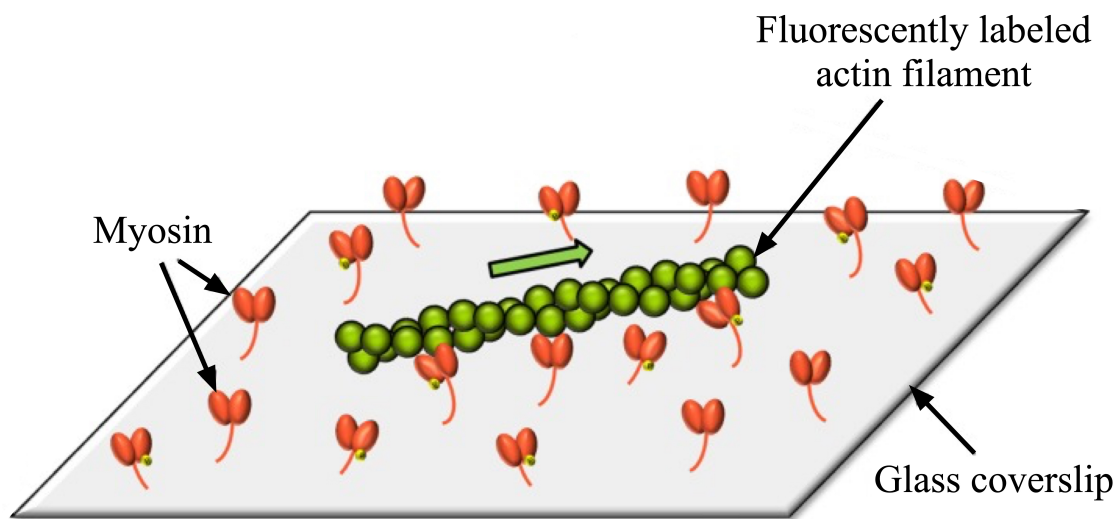


Figure 11. In-vitro motility assay, a method that tracks fluorescently-labeled actin filament over myosin heads under fluorescence microscopy in the presence of ATP (Adapted from Lauzon et al., 2012).

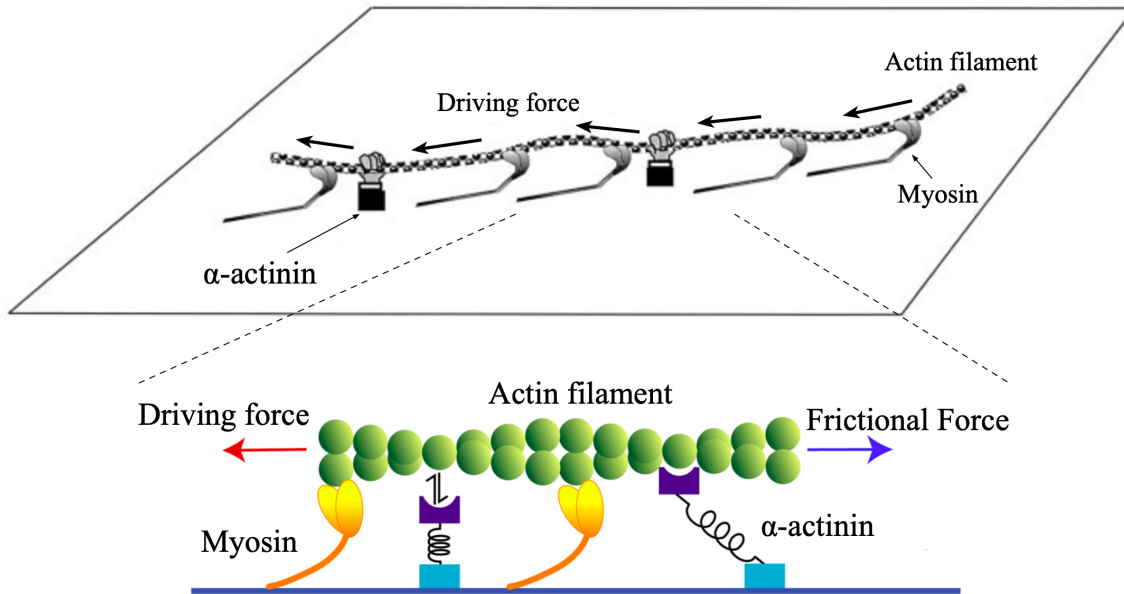


Figure 12. A schematic of the interaction between actin binding proteins and actin in the fractional loading in-vitro motility assay. Actin binding proteins (α -actinin) provide a fractional force against the driving force induced by myosin when added to the coverslip (adapted from Bing et al., 2000; Greenberg & Moore, 2010).

7.2 Force measured system with microfabricated cantilevers

We used a technique to measure the force generated during the interaction of actomyosin filaments while observing the degree of filaments overlap. We used micro-fabricated cantilevers of known stiffness (Kalganov, Novinger, & Rassier, 2010).

The cantilevers were micro-fabricated at the Cornell Nanoscale Facility (CNF). They were calibrated using a resonance frequency detection method (Fauver, Dunaway, Lilienfeld, Craighead, & Pollack, 1998).

The cantilevers were attached to metal holders, connected to micromanipulators that allow three-dimensional manipulation inside an experimental chamber, as shown in Figure 13A. Actin filaments labeled with Alexa-488-phalloidin fluorescence dye were bound to the surface of

flexible cantilever via α -actinin, and myosin filaments were bound on the surface of inflexible cantilever.

The apparatus works by bringing the cantilevers with the filaments close to each other. When the filaments attach, they produce force, and consequently displace the cantilevers. The two cantilevers in each flexible pair have identical stiffness; the forces are then calculated by assessing the displacement of the cantilevers and the angle of the filament overlap (Figure 13B).

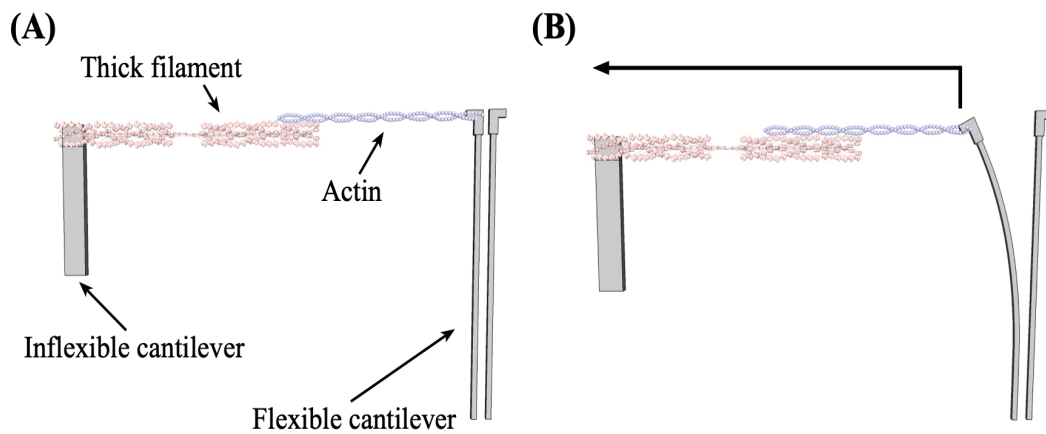


Figure 13(A). A schematic illustration of micro-fabricated cantilevers attached with the single myosin and actin filaments. (B) Forces were generated by myosin-actin interaction, the cantilever was bended by the forces.

EXPERIMENTAL STUDY 1

CHAPTER 2 – LOAD DEPENDENCE OF ACTOMYOSIN INTERACTION

8. The load dependence and the force-velocity relation in intact myosin filaments from skeletal and smooth muscles

Yu-Shu Cheng¹, Felipe de Souza Leite^{1#}, Dilson E. Rassier^{1*}

¹Department of Kinesiology and Physical Education, McGill University, 475 Pin Avenue West,
Room 308, Montreal, Canada

^{1#}Department of Genetics and Evolutionary Biology, Human Genome and Stem Cell Research
Center, Biosciences Institute, University of São Paulo, São Paulo, Brazil

Submitted to “American Journal of Physiology”

March, 2019.

8.1 Abstract

In this study, we developed a method for evaluating the load dependence of force produced by isolated muscle myosin filaments. Single filaments composed of skeletal muscle and smooth muscle myosin and single filaments of actin were attached between pairs of micro-fabricated cantilevers of known stiffness. The filaments were brought into contact to produce force, which caused sliding of the actin filaments over the myosin filaments. We applied load to the system by either pushing or pulling the filaments during interactions, and observed that increasing the load increased the force produced by myosin while decreasing the load decreased the force. We also performed additional experiments in which we clamped the filaments at pre-determined levels of force, which caused the filaments to slide to adjust the different loads, allowing us to measure the velocity of length changes to construct a force-velocity relation. Force values were in the range observed previously with myosin filaments and molecules. The force-velocity curves for skeletal and smooth muscle myosins resembled the relations observed for muscle fibers. The technique can be used to investigate many issues of interest and debate in the field of muscle biophysics.

8.2 Introduction

Muscle contraction is driven by cyclical interactions of the molecular motor myosin II with actin, a mechanical process coupled to the energy released from the breakdown of adenosine triphosphate (ATP) (Rayment, Holden, et al., 1993; Rayment, Rypniewski, et al., 1993). When myosin attaches to actin, it changes its configuration and produces the power stroke, sliding the actin filament towards the center of the muscle sarcomere. The myosin power stroke is constrained by external loads, allowing muscles to shorten quickly under low loads and to sustain high forces while shortening slowly under high loads (Piazzesi et al., 2002; Reconditi et al., 2004), determining the classic force-velocity relation of skeletal muscles (Hill, 1938). The load dependence of force production is linked to the *Fenn effect*, recognized for almost a century, but with molecular mechanisms that are still not completely known (Fenn, 1923, 1924).

The load dependence of myosin has been investigated by using intact fibres from the frog (Piazzesi et al., 2002; Reconditi et al., 2004) or with single molecules (Debold et al., 2005; Veigel et al., 2003). Studies with single fibres investigate the effects of external loads on force production, and indirectly the myosin power stroke, in situations in which the molecules work in the physiological array within sarcomeres. However, they do not allow for molecular measurements and the interpretation of these studies is complex. Studies with single molecules are challenging, as skeletal muscle myosin attaches to actin for a very brief period of time (<40ms) when tested in near physiological ATP concentrations (Finer et al., 1994; Kaya & Higuchi, 2010), and detecting binding events to apply loads during the power stroke is difficult. Furthermore, skeletal muscle myosins work cooperatively and in filamentous forms, and the

work of one myosin molecule affects the work produced by adjacent molecules and the kinetics of interactions with actin (Mansson et al., 2015).

The ensembles of myosin motors while attached to actin filaments were studied in several studies (Kalganov et al., 2013b; Kaya & Higuchi, 2013; Kaya, Tani, Washio, Hisada, & Higuchi, 2017). However, these studies have not investigated the development of steady-state forces with high, close to physiological ATP concentrations. One recent study presented a new “nano-machine” mimicking skeletal muscle myosin filaments, and was able to clamp forces at various levels and produce a steady force-velocity relationship (Pertici et al., 2018). The study advanced considerably our capacity to test with myosin ensembles, but also had an important limitation: myosin molecules were sparsely distributed along an optical fiber, without forming a filament, which would be directly comparable to the arrangement of myosins in a sarcomere. The thick myosin filaments are well organized within a sarcomere and their arrangements allow myosin molecules to produce force cooperatively in a highly synchronized fashion.

In this study, we investigated the load dependence of force production and the force-velocity relation in individual, intact filaments of myosin molecules while interacting with actin using a system newly designed in our laboratory. We tested filaments from both smooth and skeletal muscles and, for the first time, we were able to visualize the real time the effects of myosin power strokes and actin filament sliding while producing force. Furthermore, we used this system to clamp the force or the degree of filament overlap, so the force-velocity relation could be evaluated. Finally, we tested the effects of ATP on the load dependence of the myosin power stroke, in order to gain mechanistic insights into the Fenn effect. We observed that

increasing the load during myosin-actin interactions increased the force significantly, while decreasing the load decreased the force significantly. The force-velocity relation of intact myosin filaments from smooth and skeletal muscles followed an inverse hyperbolic relation similar to those in well-described in studies conducted with muscle fibers [e.g., (Edman, Reggiani, Schiaffino, & te, 1988; Edman, Reggiani, & te, 1985)], confirming that our system can repeat experiments conducted at higher levels of organization. Our system allowed mechanical experimentation and manipulation of myosin molecules working in their natural, filamentous formation, which represents an essential step into the investigations of the molecular mechanism of muscle contraction.

8.3 Methods

Proteins purification and preparation.

Native mussel thick filaments and native skeletal thick filaments were isolated according to standard procedures with minor modification (Cornachione et al., 2014; Kalganov et al., 2010; Kalganov et al., 2013b). Anterior byssus retractor muscles (ABRM) were isolated from fresh *Mytilus edulis* (mussel) and rabbit psoas muscles were taken from New Zealand White rabbits. The muscles were stored in Rigor solution with glycerol (50:50) for at least 24 hours at -20°C. The muscles were then defrosted for 12 hours at +4°C and placed on ice in buffer solution (140mM NaCl, 2mM MgCl₂, 10mM EGTA, 10mM PIPES, 2mM DTT, pH 7.4). 0.8 grams of muscles were diced in buffer (75mM KCl, 2mM MgCl₂, 10mM EGTA, 10mM PIPES, 10mM ATP, 2mM DTT, pH 7.0) and homogenized (16,000 RPM) (SNMX 1092, Omni Inc, USA) 3× for 7 sec on ice, with 1 min intervals. 25mM of KCl was added to the homogenate and placed on ice for 2 hours. The homogenate was precipitated in a centrifuge (5804R, Eppendorf) at 4500 ×g for 30 min, the supernatant was diluted with deionized water (4X) gradually, and kept on ice at 0°C overnight. The solution was centrifuged at 20,000×g for 120 min (5804R, Eppendorf), and the sediment was re-suspended in the buffer (140mM KCl, 2mM MgCl₂, 2mM EGTA, 10mM PIPES, 2mM DTT, pH 7.0).

Smooth and skeletal muscle myosin filament concentrations were measured at 595 nm using a commercial Bradford Protein Assay kit (Quick Start – BioRad, CA, USA) and a micro-plate reader (iMark Microplate Absorbance Reader, Bio Rad, USA). Thick filaments were used for experiments for a maximum of 3 days after preparation.

Actin filaments from skeletal muscles were prepared following standard procedures (Kron, Toyoshima, Uyeda, & Spudich, 1991) or were purchased from a company (AKL99, Cytoskeleton, Inc. USA), and were labeled with Alexa-488-phalloidin fluorescence dye (absorption/emission peaks at 488-520 nm) for fluorescence measurements (Kron, Toyoshima, et al., 1991). Fluorescence-labeled actin filaments were examined no more than 4 weeks after preparation. The protein α -actinin (A9776, Sigma) was dialyzed against AB buffer (25mM imidazole-HCl (pH 7.4), 25mM KCl, 4mM MgCl₂, 1mM EGTA, 1mM DTT) and was used during mechanical experiments to strengthen the attachment of actin to micro-fabricated cantilevers, which were used to measure forces generated during filament interactions.

Force measurements and micro fabricated cantilevers.

The mechanical experiments were conducted in an experimental chamber mounted on the stage of an inverted microscope (Nikon TE2000-U) equipped for dark field illumination, bright field illumination and fluorescence imaging. Dark field illumination was used to image myosin filaments (Kalganov et al., 2010; Kalganov et al., 2013b). Fluorescence microscopy was used to image actin filaments with a filter set for Alexa-488 (Exciter ET470/40x, Dichroic T495LP, Emitter ET525/50m, Chroma, USA). Images were captured with a Rolera-Mgi Plus video camera (Qimaging, Canada) and recorded using Streampix4 software (Norpix, Canada; pixel size: 120 nm; collection rate: 50 fps).

Micro-fabricated cantilevers were used for measurements of force during myosin-actin interactions (Cornachione et al., 2014; Kalganov et al., 2010; Kalganov et al., 2013b). The

cantilevers were made out of 400- μm thick silicon nitride wafer followed by photolithography process (Figure 14A-B), as previously used in our laboratory. The cantilever tips were coated with a 50nm platinum coating on the tip to improve reflectivity and optical contrast. The dimensions of flexible cantilevers were chosen to provide stiffness in the ranges of forces to be measured during the experiments (length: 550 μm , width: 1 μm , thickness: 0.6 μm). The stiffness of the cantilevers was obtained using a resonance frequency detection method as previously described (Fauver et al., 1998). Briefly, the cantilever tip was illuminated with a laser and the absorption peak was detected on a single photodiode detector (PIN-5D, UDT Sensors, Inc., Hawthorne, CA). Mechanical vibration was induced on the cantilever with a piezoelectric motor. When the vibration of the cantilever reached the maximum amplitude response the resonance frequency was measured. With the known resonance frequency, the elasticity modulus and the stiffness of the cantilevers were calculated. The stiffness obtained with this calibration method is not specific to a particular point on the cantilever tip, but the average stiffness for the cantilever tip. The stiffness of the cantilever is 0.179pN/nm in this study.

The cantilevers were glued on the bottom of the metal holders, which were connected to micromanipulators that allow three-dimensional manipulation inside of the experimental chamber (Figure 14C). Although native thick and actin filaments have a small degree of compliance (Liu & Pollack, 2002; Neumann, Fauver, & Pollack, 1998), filaments stretching or shortening was not observed in these experiments (Figure 14D), within the resolution of our system (120nm pixel size when measuring the overlap). Consequently, the degree of filament overlap should be proportional to the cantilever displacement.

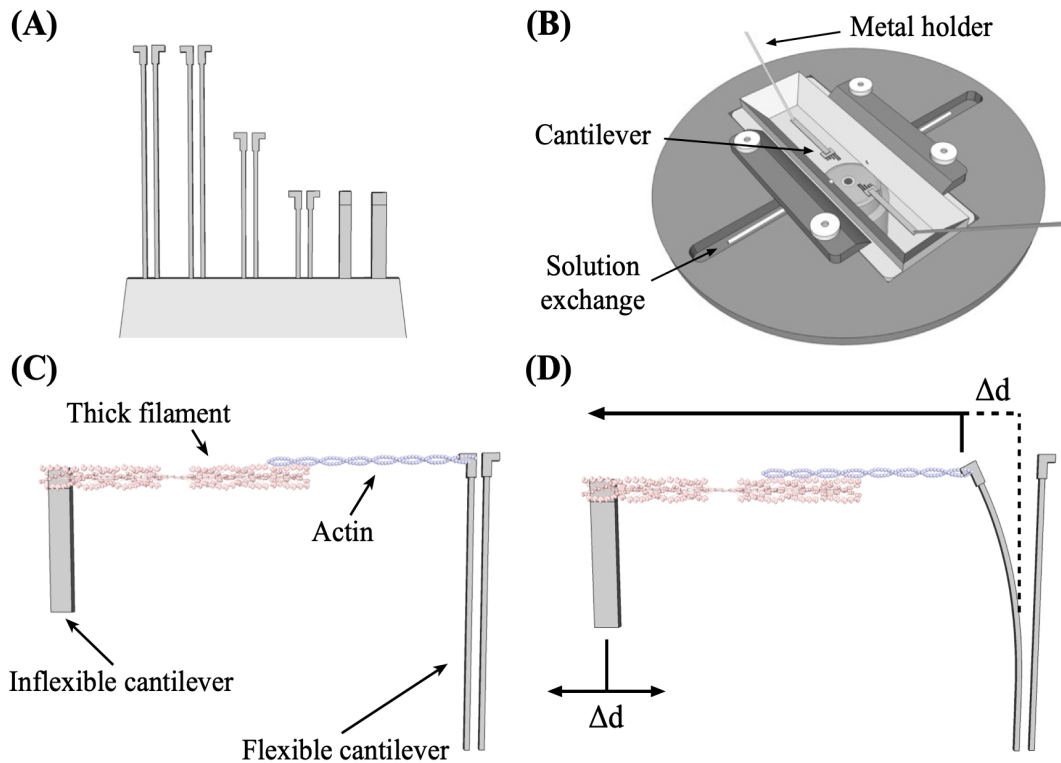


Figure 14. (A) Schematic view of the micro-fabricated cantilevers. There are four pairs of flexible cantilevers (from left) and one set of inflexible cantilever (right) manufactured from thin silicon nitride. Each pair of cantilevers has identical stiffness. (B) Schematic view of the experimental chamber. The cantilevers were attached to metal holder where placed in the chamber. The actin filaments, thick filaments and all solution exchanges were inputted and outputted through side ports of the chamber. (C) A schematic diagram showing the experimental set-up. Thick filament and actin filaments were attached to the cantilevers, and were brought into contact. (D) When the filaments start to slide past each other, they produce force that causes the displacement of the flexible cantilever (Δd), which enabled us to measure the force. The signal from the cantilever displacement is also used to input the actuator in the rigid cantilever so it can change positions to induce changes in load as required for the experiments.

The cantilevers were placed in the experimental chamber within a distance of $\sim 10\text{--}15\text{mm}$. $10\mu\text{l}$ of myosin filament solution was added near the rigid cantilever, and $10\mu\text{l}$ of α -actinin solution was added near the flexible cantilever, followed by a 10 min incubation period. A flow

of standard AB/BSA/GOC/ATP solution (AB: 0.5mg/ml BSA, 0.018 mg/ml catalase, 0.1mg/ml glucose oxidase, 3mg/ml glucose, 20mM DTT, ATP concentrations between 10 μ M and 1250 μ M) was injected into the chamber with a syringe pump (Pump 33, Harvard Apparatus, USA) at a speed of 0.5 ml/min. This flow washed the excess of α -actinin and myosin filaments. After 2 min, the flexible and the rigid cantilever were moved into close proximity in the field of view (100X magnification). Fluorescently labeled actin filaments (concentration: 2–4nM) were injected into the chamber and the flow facilitated their spontaneous attachment to one of the α -actinin-coated cantilever (Supplementary movie 1). The flow was maintained constant to align the actin filaments approximately 90° perpendicular to the cantilevers. Myosin filaments were then injected into the chamber and adhered spontaneously to the cantilevers. The cantilevers were not bent by the flow due to their stiffness.

One actin filament and one myosin filament attached at the cantilever's tips, or at a distance <50 μ m from the tip, was chosen for mechanical experimentation. Using the micromanipulators, the cantilevers were brought to close proximity until they interacted (Supplementary movie 2). Once the filaments interacted, they initiated force production and consequently displaced one of the cantilevers, which was tracked with Image software (NIH, USA). The force (F) during interactions was calculated from the displacements of the cantilevers as explained previously (Cornachione et al., 2014; Kalganov et al., 2010; Kalganov et al., 2013b): $F = k * \Delta d$, where k is stiffness and Δd is the amount of cantilever displacement. At times, the alignment of the filaments was not at 90° angle to the cantilever; in these cases, the force component on the vertical axis during cantilever displacement was enhanced by an angular

component represented by the vertical axis. The full force generated by the filaments during interaction was then adjusted such that $F = F_x + F_y$, where F_x is the vector component of force along the horizontal axis, and F_y is the vector component of force along the vertical axis. The images of the cantilever displacements were analyzed using an automatic algorithm (ABSsnake for ImageJ, NIH, USA). The system with cantilevers can be servo-controlled either in position or to be used for force feedback (Figure 14). The frequency response of the system in position feedback is limited by the noise in the system, but it was minimized to ~ 15 ms. We were able to induce changes of ~ 200 nm without significantly increasing the noise in the system.

Protocols.

Two protocols were utilized during this study. In protocol 1, the filaments were allowed to slide and produce force freely, and at intervals of 500ms a load was imposed to the myosin molecules; the load was increased or decreased by pulling or pushing the cantilever by 20nm, respectively. In protocol 2, after the force was stabilized it was clamped at a lower, pre-determined level. During the decrease in force the filaments overlap, and thus the length of the preparation, was changed. The slope of traces representing the changes in length were computed, and were taken as a measure of the velocity of shortening (Pertici et al., 2018).

Data analysis.

During protocol 1, the data were analyzed for the force produced during myosin-actin interactions at different ATP concentrations, and for the increase or decrease in force obtained

during the imposed changes in load. The force trace was analyzed as an average of data points over 50 ms after the force has stabilized following initial development. Comparisons between forces were done by analysis of variance (ANOVA). A significance level of $p < 0.05$ was used for all analysis. During protocol 2, the velocity of shortening during the reductions of force below the isometric value was measured by calculating the slope of the changes in length. The values of force and velocity were used to construct a force-velocity relation, which was fitted with a hyperbolic Hill equation: $(P_0 + a)(V + b) = (V_0 + b)a$, where P_0 is the maximal force, a and b are the distances of the asymptotes from the ordinate and abscissa, respectively, and V_0 (the ordinate intercept) estimates the maximum shortening velocity. a/P_0 is a parameter that expresses the degree of curvature of the FV relation, such that the greater the curvature the smaller the value of a/P_0 . All data are expressed as mean \pm SEM unless otherwise stated.

8.4 Results

Myosin filaments produce sliding of actin filaments and produce load-dependent forces.

When the filaments were brought to interact, force was generated which caused sliding of the actin filament over the myosin filament (Figure 15). The sliding of actin caused a displacement of one of the cantilevers. Supplementary Video 2 shows clearly the top cantilever moving during the interactions, as a result of power strokes produced by the myosin molecules. As far as we know, this is the first time that sliding of myosin-actin filaments can be visualized in real time. One of the cantilevers did not bend during interactions because of its high stiffness (>1000 times higher than the flexible cantilever). We used an algorithm to track the centroid of the tip of the cantilever in real time to determine the force produced by the filaments.

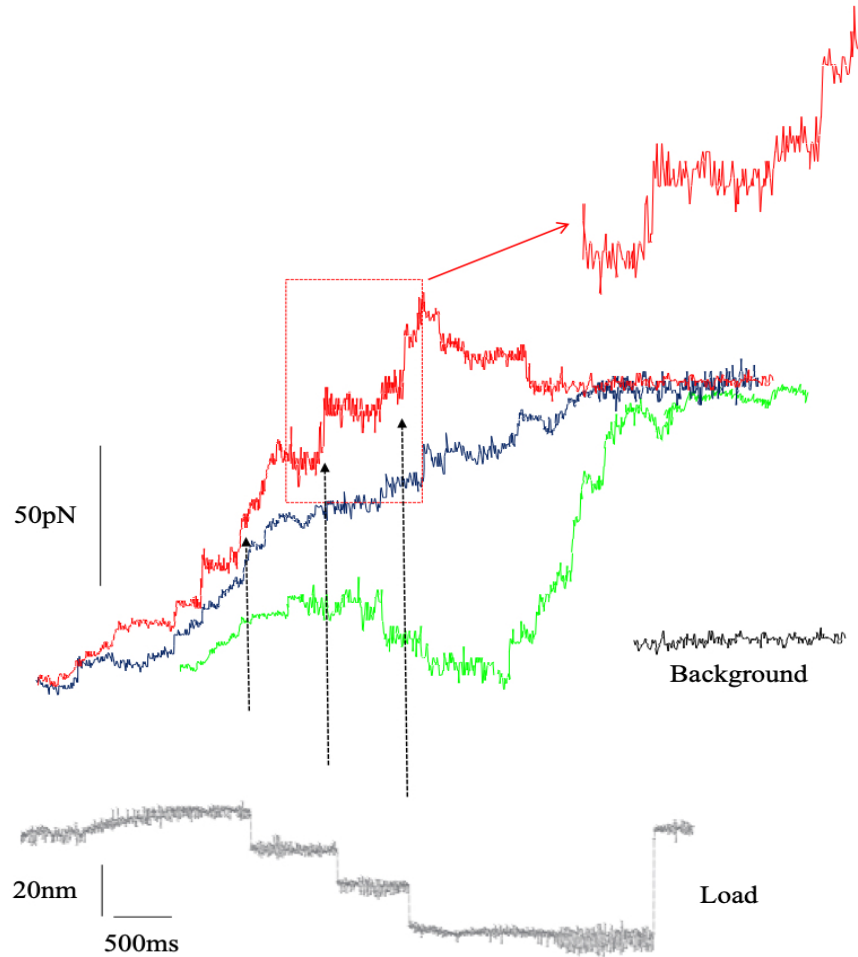


Figure 15. Force traces collected during filaments interactions during experiments. When there is no load applied to the system, the filaments slide and produce force until they are stabilized (blue). When the load was increased during the interactions (red trace), the force increased, and the load was decreased (green) the force was decreased. The gray trace shows the movement of the rigid cantilever to change the load – in this case only one trace is shown for clarity. Note that the signal to background noise ratio (black trace in the inset) is very high.

Figure 15 shows records of three filament interactions, one without load applied to the system (blue trace), one in which the load was increased three times during interactions (red trace) and one in which the load was decreased three times during the interaction (green trace). When there was no load, the force raised during the filaments interaction until it stabilized at a

certain level (Figure 15); in this example, the filaments produced 123.4pN of force before it stabilized in an isometric condition. The result was consistent across several preparations. Using this method, we tested the ATP-dependence of force measurements, in concentrations ranging between 10 μ M to 1250 μ M. We wanted to confirm that the forces that we were measuring with our system were in the range of those published in the literature. We observed force values varying between 120pN and 150pN for smooth muscle myosin, but when we normalized the forces per the degree of filament overlap we obtained values between 60 and 100 pN/ μ m (Figure 16). We could not develop the experiments with skeletal muscle myosin in all ATP concentrations, because the force produced at ATP concentrations below 500 μ M was too low for detection using our method. However, when we compare the contractions that were performed in similar ATP concentrations, the forces were lower in skeletal muscle myosin than those in smooth muscle myosin, but similar when the forces were normalized per filament overlap. The result is consistent with a previous report comparing myosins from different muscles (Guilford et al., 1997; Kalganov et al., 2013b).

The force produced by myosin filaments is a load-dependence.

Once force was generated, we applied a load to the myosin-actin filaments by pulling or pushing the rigid cantilever with a computer-controlled piezoelectric motor. We changed the position of the cantilever by 20nm, which is enough to induce load to the thick myosin filament without disconnecting the actin filaments. We were able to apply load several times (2-5) to the filaments before they disconnected or broke. Every time the load was increased, i.e., the filament

was pulled against sliding and thus against the power stroke (Video 2 in Supplementary Material), the force increased by approximately 20pN (Figure 15), relatively similar to studies looking to the load dependence of muscle myosin molecules measured with an optical laser trap (Pertici et al., 2018; Veigel, Schmitz, Wang, & Sellers, 2005). After the load was applied, the force restored to a pre-load level and the filaments continued to slide. When the load was applied to push the filaments (decreased the load, same direction of the power stroke), the force decreased by varying levels ranging between 10-35pN. After the consecutive decreases in force, force returned to baseline, and the filaments continued to slide. Provided the filaments did not break, the forces were all restored to similar levels after we stopped applying. The time for the force of return to baseline levels varied from experiment to experiment. The results for the load dependence of the power stroke were similar for the smooth and skeletal muscle filaments, albeit the absolute force values varied (Figure 16).

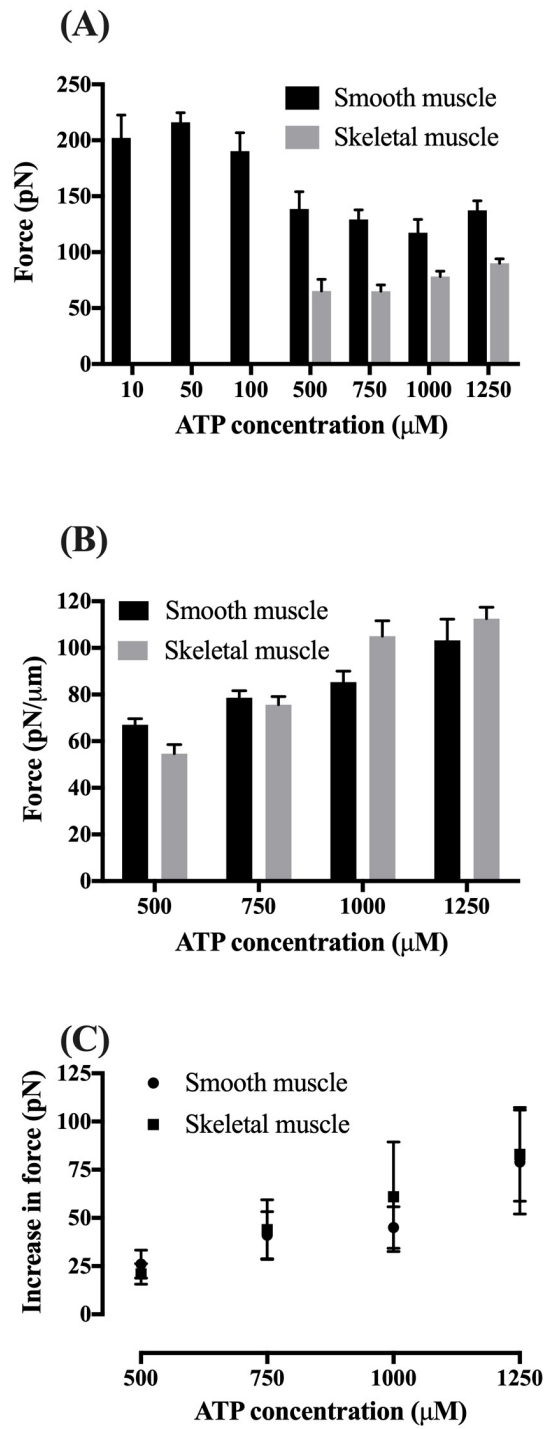


Figure 16. Force produced by the filaments at different ATP concentrations. (A) Mean force. (B) Force normalized per degree of filaments overlap. (C) Increase in force observed during the increase in load imposed to the filaments. Data are given as means \pm SEM.

The curvature force-velocity relation in myosin filaments resembles studies produced with muscle fibers.

We performed experiments in which we controlled the force produced by the system to build a force-velocity relation produced by the myosin filaments while interacting with actin to build a force-velocity relation. In these experiments, after the filaments interacted and produced maximal force, we clamped the force and the filaments interaction was kept constant for a pre-determined period of time. Such interaction would correspond to an “isometric” contraction. We then decreased the load by clamping one cantilever in a pre-determined force level. When the force was lowered, the filaments started to change the overlap in a velocity-dependent manner, which is a sign that the myosin molecules are able to continuously attach-detach during the changes in force. We measured the slopes of such changes in length to determine the velocity of sliding. We applied the protocol 5-6 times during each interaction, and we were able to construct a force-velocity relation (Figure 17). The force-velocity relation for these preparations presented the classic inverse hyperbolic shape as described initially by Hill (Hill, 1938) and repeated in studies with isolated muscle fibers. The curvatures of the fitted curves, estimated by the Hill coefficient (a/P_o), are comparable with other studies in the literature (Debold et al., 2005; Pertici et al., 2018) (Table 1). The curvatures were different for the three ATP concentrations measured in these experiments; it decreased in smaller ATP concentrations.

	1250 μM ATP	750 μM ATP	500 μM ATP
Skeletal muscle myosin	0.27 ± 0.03	0.35 ± 0.04	0.40 ± 0.05
Smooth muscle myosin	0.25 ± 0.05	0.32 ± 0.04	0.39 ± 0.03

Table 1. The values for a/P_0 representing the curvatures of the force-velocity curves in the experiments conducted with skeletal and smooth myosin filaments, with different ATP concentrations.

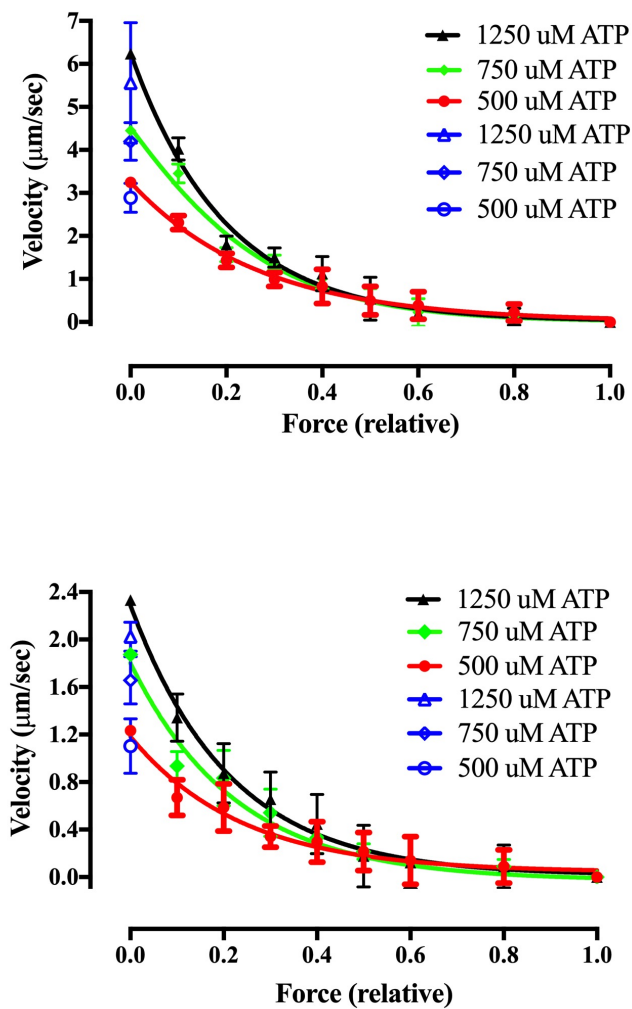


Figure 17. The force-velocity relationship in skeletal (A) and smooth (B) myosin filaments with different ATP concentrations. The blue symbols represent the maximal velocity measure with in-vitro motility assays.

The maximum sliding velocity of actin filaments propelled by myosin filaments fitted well the force-velocity relationship.

In order to produce a full force-velocity relation for our filaments, we determined the maximum sliding velocity of the actin filaments. We performed in-vitro motility assays with purified myosin heavy-meromyosins (HMM). We observed velocities that were well within the range published in the literature (Figure 17). The maximal sliding velocities of actin propelled by filaments or by isolated HMM (blue symbols on the Figure 17) were similar. The values measured using the in-vitro motility assays were slightly smaller than those predicted by the fitted curve, as result that was also observed in previous studies (Pertici et al., 2018).

8.5 Discussion

The system described in this study is the first to allow load-dependent measures of myosin II in intact filaments, while visualizing the sliding of acting filament during force production. It opens new possibilities for studying the molecular mechanisms of muscle contraction, with far-reaching implications; the system can be used to investigate the cooperativity of myosin molecules in filaments that can be extracted from different tissues, from healthy or diseased muscles.

There are other systems that have been developed to allow the study of individual myosin molecules or ensembles of myosin molecules, and that have been instrumental in our understanding behind the action of myosin II. Studies with single molecules are commonly performed with the three-bead assay, where two beads are trapped by optical tweezers which are in turn attached to the end of an actin filament [e.g., (Debold et al., 2005; Finer et al., 1994; Veigel et al., 2003)]. The actin is then brought in contact with a myosin (or HMM) molecule sitting in the third bead, and upon attachment produces the power stroke.

The system is unique as it allows the mechanics of single molecules. However, depending of the goal of the study, it also has its limitations. The stiffness of the optical traps must be lower than that of the myosin molecules so they can undergo the power stroke unhindered, which leads to significant Brownian motions. Consequently, the signal/noise ratio in the system is reduced. Furthermore, interpretation of these studies must assume that the power stroke is similar to that of naturally oriented myosin molecules attached to the thick filaments. While one study has confirmed such assumptions (Ruff, Furch, Brenner, Manstein, & Meyhofer, 2001), others

observed an error associated with the orientation of myosin can amount to a factor of two (Ishijima et al., 1996; Tanaka, Ishijima, Honda, Saito, & Yanagida, 1998). Finally, there is an assumption that the power stroke after initial attachment occurs with equal probability at all positions along the actin filament, but forces generated by the laser traps may induce distortion of the attached myosin molecules, resulting in non-equal probability to execute the power stroke.

Although it is not simple to compare our results with single molecule studies, we can estimate the force produced by the myosin molecules in our experiments. The force produced by skeletal muscle myosins was between 54.6 pN/ μm and 112.5 pN/ μm of overlap, respectively, corresponding to 0.0546 pN/nm and 0.1125 pN/nm. If we assume that there is one myosin cross-bridge per 14.3 nm of length of thick filament actively interacting with an actin filament (Gordon, Homsher, & Regnier, 2000), the skeletal muscle filaments produced between 0.78 pN and 1.61 pN per myosin molecule. If we estimate that ~30% of cross-bridges interact with an actin filament in any given time during force production (Linari, Caremani, Piperio, Brandt, & Lombardi, 2007), the force produced by single myosin molecules would be at least 3 times higher, reaching values close to 5 pN. The values that are in the range of the data obtained with optical trap experiments, which commonly observe forces between 5–7 pN (Finer et al., 1994; Molloy, Burns, Kendrick-Jones, Tregear, & White, 1995).

There are previous studies that investigated ensembles of myosin motors while attached to actin filaments, but they have not experimented with steady-state forces with high ATP concentrations and the force produced by myosin molecules never stabilized completely (Kalganov et al., 2013b; Kaya & Higuchi, 2013; Kaya et al., 2017). These studies also did not

clamp the force in pre-determined values, not allowing the investigation of the load-dependent, force velocity-relation. The exception is a recent study that developed a new “nano-machine” mimicking skeletal muscle myosin filaments, which was able to produce a steady force-velocity relationship (Pertici et al., 2018). The study advanced considerably advanced our capacity of measuring the mechanics of myosin ensembles and shall be used in the future in a range of biophysical applications, but it also had a limitation: myosin molecules were sparsely distributed along an optical fiber. Therefore, they were not tested in a physiological arrangement, as they have not formed filaments, which would be directly comparable to the arrangement of myosin molecules in a sarcomere.

Finally, there are studies that tested intact filaments before, but without controlling for the load and thus not enabling to measure stable forces with different velocities of shortening. Liu and Pollack (Liu & Pollack, 2004) used intact filaments from mussels in a system that is relatively similar to the one used in this study, and observed maximal forces before the filaments disconnected in the range of 200–270pN, similar to ours. Yamada et al. (A. Yamada, Ishii, Shimmen, & Takahashi, 1989) used myosin filaments bound on a glass surface and actin filaments attached to a glass needle, away from the surface. They did not measure the active force produced by the filaments, but their binding strength, with values ranging between 130–550 pN/ μm of overlap. Based on electron microscopy pictures, the authors estimated an active force of 200 pN/ μm , also close to the values obtained in our experiments.

The main results of this study confirm a load dependence of force production that is observed at the molecular level, and a force-velocity relation that presented the same inverted

hyperbolic shape that has been observed in previous studies using other systems. When we increased the load imposed to the myosin filaments, the force increased by 30-80%, depending on the ATP concentration used during the experiments. The increase in force was larger with increasing concentrations of ATP, which elicited a strong and longer binding between myosin and actin. The larger increase in force can be attributed to an increased resistance to stretch, as it has been shown that strong binding between myosin and actin leads to larger forces during stretch (Karatzaferi, Chinn, & Cooke, 2004; Minozzo, Altman, & Rassier, 2015). Although the mechanisms of force increase during stretch and increased load has been the focus of much investigation (Colombini, Nocella, Benelli, Cecchi, & Bagni, 2007; Getz, Cooke, & Lehman, 1998; Karatzaferi et al., 2004; F. C. Minozzo & D. E. Rassier, 2013), this is the first time that this phenomenon is observed at the filament level, confirming it is a molecular property that can explain how the form that myosin adapt to the mechanical strain during contractions.

Muscle myosins are highly efficient motors that adjust their power output according to external loads, exerting higher force at slow velocities and lower forces when the tasks demand fast movements. The force and velocity of myosin-induced actin motility are highly regulated by ATPase kinetics and ADP release in the MHC. It has been proposed that the overall rate between release and re-attachment of myosin with ADP and P_i may be affected by load (Baker et al., 2002; D. Smith & Sleep, 2006a; D. A. Smith & Geeves, 1995). Studies with the molecular motors myosin I, V, and kinesin (De La Cruz, Wells, Rosenfeld, Ostap, & Sweeney, 1999; Veigel et al., 1999; Veigel et al., 2003; Veigel et al., 2002) suggest that increasing loads delay ADP release. Such delay in ADP release would allow for a longer attachment between myosin and

actin, and consequently more force produced at lower velocity. Furthermore, studies performed with the processive myosins I, V and kinesin show that their attachment time (usually >100ms) is shortened with increasing ATP concentrations, suggesting that it is terminated when ATP binds to myosin and ADP is released (Guilford et al., 1997; Rief et al., 2000; Tyska et al., 1999b; Veigel et al., 2005; Visscher, Schnitzer, & Block, 1999). Such results indicate that ADP release may modulate the duration and magnitude of the power stroke. However, processive motors have high ADP affinity and undergo substantial conformational changes associated with ADP release, while skeletal muscle myosin has weak ADP affinity (Dantzig, Barsotti, Manz, Sweeney, & Goldman, 1999; Gollub, Cremo, & Cooke, 1996) and small conformational changes associated with ADP release (Gollub et al., 1996).

The classic experiments showed that muscle metabolism responds to the prevailing mechanical conditions (Fenn, 1923, 1924). The observation ultimately led to the cross-bridge model describing the effect of load on the kinetics of tension recovery in muscle fibers proposed by Huxley and Simmons (A. F. Huxley & Simmons, 1971). The model proposed that cross bridges under high load proceed through attachment states slowly, whereas those under low load proceed more rapidly. Our results give additional support for the model.

Finally, we obtained a force-velocity relation in our experiments that is similar to that observed in studies with single fibers [e.g., (Edman et al., 1988; Edman et al., 1985; Hill, 1938)], myosin ensembles (Pertici et al., 2018) and myosin molecules (Debold et al., 2005). The curvature of the fitted force-velocity curves in the two filaments tested in this study and while using different ATP concentrations – the Hill coefficient expressed as a/P_o – were well within the

values reported in the literature. This finding strengthens our results and implies that our system is able to measure the power of the myosin filaments while interacting with actin and producing power strokes.

EXPERIMENTAL STUDY 2

CHAPTER 3 – ACTOMYOSIN INTERACTION REGULATION BY LOOPS 1 AND 2

**9. Cleavage of loops 1 and 2 in skeletal muscle heavy meromyosin (HMM) leads
to a decreased function**

Yu-Shu Cheng¹, Oleg S. Matusovsky¹, Dilson E. Rassier^{1*}

¹Department of Kinesiology and Physical Education, McGill University, 475 Pin Avenue West,
Room 308, Montreal, Canada

Published to “Archives of Biochemistry and Biophysics”

October, 2018.

9.1 Abstract

Background. The mechanical work and the actin-activated ATP kinetics in skeletal muscles are closely associated with two surface loops that are present in the myosin molecule: loop 1 and loop 2. They are located close to the ATP-loop (loop 1), and the actin binding domain (loop 2). In this study we investigated the roles of loops 1 and 2 in the regulation of the load-dependent velocity of actin sliding and ATPase activity.

Methods. Heavy meromyosin (HMM) from rabbit skeletal muscle was subjected to limited tryptic proteolysis to obtain fragments containing different amounts of loops 1 and 2. The amino-acid sequences of these fragments were confirmed with quantitative mass-spectrometry. The velocity of actin motility propelled by the HMM fragments was measured using in-vitro motility assays, with varying loads induced by the addition of different concentrations of α -actinin.

Results. The load-dependent velocity of the myosin-propelled actin motility and the fraction of motile actin filaments were decreased in close association with the depletion of loop 1 in the HMM. The ATPase activity was decreased in close association with depletion of loops 1 and 2.

Conclusions. Loop 1 is responsible for regulating the load-dependent velocity of actin motility.

General significance. Myosin-actin interaction is closely regulated by two flexible loops in the structure of myosin. The results of this study are important for the understanding of the molecular mechanisms of contraction, and therefore the most basic functions of life, such as locomotion, heart beating, and breathing.

9.2 Introduction

Muscle contraction is a result of cyclic interactions of the molecular motor myosin II with actin filaments. This process is driven by the chemical energy released from ATP hydrolysis, which is translated into mechanical work and force generation (Chock, Chock, & Eisenberg, 1976; Lynn & Taylor, 1971; Stein, Schwarz, Chock, & Eisenberg, 1979). Force generation is closely linked to conformation changes in the myosin molecule, initiated by binding with actin and release of phosphate (P_i) (Goldman & Brenner, 1987; H. E. Huxley, 1969). These conformation changes of specific regions of myosin are transferred through the molecule, producing the “power-stroke” responsible for the sliding of actin filaments.

The details behind the myosin-actin interactions, and the role of different domains of myosin during force generation have yet to be identified. There is evidence suggesting that the actin binding site comprises sections of the upper and lower 50K domains of myosin (Rayment, Holden, et al., 1993; Rayment, Rypniewski, et al., 1993; Sweeney & Houdusse, 2010; von der Ecken, Heissler, Pathan-Chhatbar, Manstein, & Raunser, 2016), separated by a cleft that closes on strong binding with actin. A major difficulty in fully characterizing the myosin-actin cycle is the presence of flexible loops in the structure of myosin that may be essential for contraction (Spudich, 1994). Proteolysis of skeletal myosin at these loops cleaves the head into segments of 25K, 50K and 20K (Mornet, Pantel, Audemard, & Kassab, 1979). The loops connecting these segments (the 25–50K and 50–20K loops), called loop 1 and loop 2, are not resolved in the crystal structures of the chicken skeletal myosin II sub-fragment 1 (S1) (Rayment, Rypniewski, et al., 1993) or *Dictyostelium* S1 (Fisher et al., 1995), suggesting that they adopt various

conformations. While the rest of the myosin II head is well conserved [60–80% identical (Sellers & Goodson, 1995)], the loops vary considerably (Goodson, Warrick, & Spudich, 1999). Loop 1 (residues 204-216) is located close to the ATP-loop and in the vicinity of the active site of the myosin sub-fragment 1 (S1), while loop 2 (residues 627-646) is situated in the vicinity of the actin-binding domain (Mornet et al., 1979).

It has been suggested that loop 1 is responsible for regulating the velocity at which myosin propels actin (Clark, Ansari, Dash, Geeves, & Coluccio, 2005; Knetsch, Uyeda, & Manstein, 1999; Lauzon, Trybus, & Warshaw, 1998; Lauzon, Tyska, et al., 1998; Murphy & Spudich, 1998; Rovner, Freyzon, & Trybus, 1997; Uyeda, Patterson, Mendoza, & Hiratsuka, 2002), and loop 2 is involved with the binding with actin and ATPase activity (Joel, Sweeney, & Trybus, 2003; Joel, Trybus, & Sweeney, 2001; Knetsch et al., 1999; Murphy & Spudich, 1999; Uyeda et al., 2002). Studies using selective, tryptic digestion of loops in myosin have strengthened these hypotheses (Bobkov, Bobkova, Lin, & Reisler, 1996; Holmes, Schroder, Sweeney, & Houdusse, 2004; Murphy & Spudich, 1999). However, a limitation in these studies was that the depletion of specific regions of myosin was not directly quantified, and may have led to digestion of other structures that are important during myosin-actin interactions. For example, it may affect the ATP loop and the actin-binding domain loop which are essential for myosin regulation. The studies also did not investigate how these loops regulate the load-dependent actin motility, a situation that is closely related to a constrained environment within the sarcomeres, where the resistance imposed by external and internal loads may change the effects of the loops in the myosin activity.

In this study, we aimed to better understand the effects of loops 1 and 2 in the

myosin-propelled velocity of actin sliding. We examined the effects of cleaving heavy meromyosin (HMM) into fragments that eliminate loop 1 and loop 2, and also the ATP loop and the actin-binding domain that work in close connection with loops 1 and 2. As in previous studies, we used trypsin, that can cleave the loops while the activity of the remaining regions of the molecule are functional (Holmes et al., 2004; Murphy & Spudich, 1999), but we used new-generation quantitative mass-spectrometry for a precise evaluation of the peptides in different fragments resulting from tryptic cleavage of HMM. We measured the actin motility in-vitro in unloaded conditions, and in conditions in which a load was added to the experimental assay during different times of HMM cleavage.

9.3 Method

Protein purification.

Myosin was purified from rabbit psoas muscle taken from New Zealand White rabbits using a protocol that has been previously described (Kalganov et al., 2013b), with minor modifications. Briefly, 5 grams of muscle tissue were homogenized with 15mL of Hasselbalch-Schneider buffer (0.1 M $\text{KH}_2\text{PO}_4/\text{K}_2\text{HPO}_4$ at pH 6.4; 0.6 M KCl, 10 mM $\text{Na}_4\text{P}_2\text{O}_7 \cdot 10\text{H}_2\text{O}$, 1 mM MgCl_2 , and 20 mM ethylene glycol tetra-acetic acid) using an Omni mixer homogenizer (Omni International, Inc., Georgia, USA) for myosin extraction. The solution was stirred continuously for 15 min at 4°C, and the myosin extraction was stopped by the addition of 20 mL of distilled water at 4°C. The mixture was centrifuged at 3,000×g for 10 min, while the supernatant (myosin solution) was filtrated through a 55mm hardened circle filter paper (No. 54, GE healthcare companies, UK). The filtrate was next diluted with two-fold distilled water at 4°C and centrifuged at 10,000×g for 15 min. The resulting pellet was washed with buffer B (20mM K_2HPO_4 at pH 7.2; 0.12M KCl; 1mM EDTA and 1mM DL-Dithiothreitol (DTT)), re-suspended in 5 mL of buffer C (50mM Sodium pyrophosphate and 1mM DTT at pH 7.8), and centrifuged at 10,000×g for an additional 10 min. The supernatant was filtered (No. 54 filter paper, WHATMAN™, GE, USA), and the myosin solution was kept on ice and stored at 4°C until the time of the experiment. Proteins were always prepared one day before the motility assays were performed (Homsher, Wang, & Sellers, 1992).

HMM was prepared from whole myosin, following procedures adapted from a previous study (Kron, Uyeda, Warrick, & Spudich, 1991). Myosin stock was diluted in nine volumes of

solution 1 (0.1 mM NaHCO₃, 0.1 mM EGTA, and 1 mM DTT), left on ice for 15 min, and centrifuged at 25,000×g for 10 min. The pellet was dissolved in an equal volume of solution 2 (20 mM imidazole-HCl, 1 M KCl, 4 mM MgCl₂, and 10 mM DTT, pH 7.4). After a 10 minutes period of incubation at 25°C in a water bath (2239-Isotemp®, Fisher Science, USA), α-chymotrypsin (C-3142; Sigma-Aldrich, Canada) was added to the solution to reach a final concentration of 12.5 µg/ml. After 10 min of incubation, the solution was diluted in nine volumes of solution 1, mixed with 3 mM MgCl₂ and 0.1 mM PMSF, and kept in ice for 1 hour. The suspension was centrifuged at 25,000×g for 90 min. The supernatant containing HMM was collected and stored in ice for no more than 3 days before being used for experiments.

Actin filaments (AKL99, Cytoskeleton, Inc. USA) were labeled with Alexa-488-phalloidin fluorescence dye (absorption/emission peaks at 488–520 nm) for visualization under fluorescence microscopy during in-vitro motility assays.

Tryptic proteolysis of HMM.

Tryptic treatment of HMM to cleavage specific segments of the molecule was developed according to a previous study (Bobkov et al., 1996) with minor modification. The reaction mixture included 20 mM KCl, 20 mM Tris-HCl (pH 7.5). Final trypsin concentrations of 0.01 mg/ml and 0.5mg/ml of HMM (1:50 enzyme-to-substrate ratio) were used. The time course of enzymatic digestion was controlled from 1 min to 60 min, to produce HMM fragments with different percentages of cleaved loop 1 and loop 2. Partial protection of loop 2 and the actin-binding domain during the tryptic proteolysis of HMM was done with the presence of a 2-fold molar excess of F-actin (Mornet, Bertrand, Pantel, Audemard, & Kassab, 1981).

Sodium dodecyl sulfate gel electrophoresis and Bradford quantification.

Sodium dodecyl sulfate (SDS) polyacrylamide gel electrophoresis (PAGE) was prepared using slab gels 0.75mm thick (Mini Protein® electrophoresis-BioRad, USA). 10% acrylamide and a 4% bis/acrylamide were used for the stacking gels that were stained with SimpltBlue™ Safe Stain (Invitrogen, Carlsbad, CA). The molecular mass of the protein fragments was determined by comparing their electrophoretic motilities to molecular weight standards (SeeBlue™ Plus2 Pre-stained Protein Standard, Thermo Fisher Scientific, Canada). Myosin and HMM concentrations were also measured at 595 nm using a commercial Bradford Protein Assay kit (Quick Start - BioRad, CA, USA) using a micro-plate reader (iMark Microplate Absorbance Reader, Bio Rad, USA).

In-vitro motility assays.

In-vitro motility assays were performed as previously described (Kalganov et al., 2013b) with minor modifications. Briefly, a flow-through chamber was constructed from a microscope glass coverslip (22x50-1.5, Fisherbrand®, USA) coated with 1.0% nitrocellulose (LADD Inc. VT, U.S.A). The experiments were performed in a homemade chamber with a water thermal exchange column (SC-20, Harvard apparatus, Canada) that fixed the temperature at 30°C. 100uL of 100µg/ml non-cleaved or cleaved HMM were passed through the chamber to allow it to randomly attach to a nitrocellulose-coated coverslip. Next, 250 uL of assay buffer (0.1% fluorescence-labeled actin filament and 25 mM Imidazol, 25 mM KCl, 4 mM MgCl₂, 14 mM

Glucose, 0.5 mM BSA, 0.018 mg/ml catalase, 0.1 mg/ml glucose oxidase, 17.8 mM dithiothreitol-containing 1mM ATP and an oxygen-scavenging system) was perfused into the chamber.

The velocity of actin propelled by non-cleaved and cleaved HMM was measured after different digestion times (Bobkov et al., 1996). The actin filaments were imaged using fluorescence with a filter set using Exciter HQ480/40X, Dichroic Q505LP, Emitter HQ535/50m, Chroma, USA (dye: Alexa-488). The fluorescent light signals emitted by the actin were collected with a 100X oil-immersion objective (Nikon, Plan Fluor, NA: 0.5–1.3). A video was recorded by a high-speed digital EMCCD Camera (Qimage, ROL-MGi-PLUS-F-M-14-C, 512 x 512 pixels BC, Canada). The velocity of actin sliding was analyzed by a customized software (Matlab 8.3.0, MathWorks® Massachusetts, U.S.A.) (Hilbert, Balassy, Zitouni, Mackey, & Lauzon, 2015; Hilbert et al., 2013). All actin filaments were tracked during the experiments, but the results of filaments with velocities lower than 0.05µm/sec were discarded from analysis.

Mass spectrometry.

The peptides in the different fragments that were selected for analysis were identified by liquid chromatography-tandem mass spectrometry (LC-MS/MS) using an Ultimate 3000 nanoLC coupled to an Orbitrap Fusion Tribrid mass spectrometer (Thermo Fisher Scientific). The samples were run on an SDS-PAGE, and the gel bands were cut and processed using standard methods (Shevchenko, Tomas, Havlis, Olsen, & Mann, 2006). The resulting peptides were loaded onto a Thermo Acclaim Pepmap precolumn (Thermo, 75µM ID X 2 cm C18 3µM beads)

and then onto an Acclaim Pepmap Easyspray analytical column separation (Thermo, 75 μ M X 15cm with 2 μ M C18 beads) using a Dionex Ultimate 3000 uHPLC at 220 nl/min with a gradient of 2-35% organic solution (0.1% formic acid in acetonitrile) over 1 hour. Peptides were analyzed using a Thermo Orbitrap Fusion Tribrid mass spectrometer, sequencing all peptides with a charge of 2+ or greater.

The raw data were converted into *.mgf files (Mascot generic format) for search using the Mascot 2.3 search engine (Matrix Science) against a rabbit database (Uniprot). The database search results were loaded onto Scaffold Q+ Scaffold 4.4.8 (Proteome Software, USA) for statistical analysis and data visualization. Ion currents (XIC's) for each peptide were analyzed and quantified by combining the *.raw files from the Thermo Orbitrap Fusion and the *.dat files from the output of Mascot 2.3 into Pinnacle software (v1.0.52.0, OptysTech, Thermo Scientific, USA) using the Targeted Quantitation; label free DDA or pSMART workflow. The mass tolerances for the precursor and fragment ions were set to 10ppm and 0.6Da, respectively. The control-enzyme was specified as trypsin and two miss cleavages were allowed. Cysteine carbamidomethylation was specified as a fixed modification and methionine oxidation was chosen as a variable modification.

Scaffold (version 4.6.1, Proteome Software Inc., Portland, OR) was used to validate MS/MS based peptide and protein identifications. Peptide identifications were accepted if they could be established at >95.0% probability by the Peptide Prophet algorithm with Scaffold delta-mass correction. The list of all observed peptides and their sequences are listed in the Supplementary Tables 1 and 2. For a quantitative data analysis of the myosin's functional loops, extracted ion

chromatograms for the ^{12}C , ^{13}C and double ^{13}C isotopes were used to calculate 50% peak areas of eluted peptides in the Pinnacle software as previously described (Matusovsky et al., 2017). 50% peak areas of specific peptides corresponding to the loop 1, loop 2, ATP-loop and actin-binding domain obtained during proteolysis of HMM were normalized to 50% peak areas of non-trypsinized HMM peptides.

ATPase activity.

The Mg^{2+} -ATPase activity of actomyosin was reconstituted from rabbit F-actin and HMM in a medium containing (in mM) 30 KCl, 0.1 CaCl_2 , 0.5 MgCl_2 , 2 DTT, and 20 Imidazole-HCl (pH 7.2). The ATPase reaction was started after 10 min of incubation at 25°C by adding 1 mM of Mg^{2+} -ATP and was ended after 10 min by adding 2.5% trichloroacetic acid. The final concentrations of ATP and Mg^{2+} in the assay were 1 mM and 1.5 mM, respectively. The amount of P_i liberated during the reactions was evaluated colorimetrically at 595nm. Mg^{2+} -ATPase activity of HMM was calculated as μM of P_i per mg of HMM per minute of ATPase reaction. All results are given as mean \pm S.E.M.

9.4 Results

SDS-PAGE patterns of selectively cleaved HMM.

HMM was subjected to limited proteolysis during 60 min in the presence or absence of actin, which partially protects loop 2. Figures 18A and 18B show the time course of the tryptic cleavage of HMM in 10% SDS-PAGE after different digestion times. Figure 18A shows an experiment without partial protection of loop 2 during the experiment. The major product in the first minute of proteolytic digestion is the 88-kDa fragment which is observed through the digestion until 30 min (from 1 to 30 minutes). During further cleavage of the MHC, the 88-kDa fragment degraded into 68-kDa and 57-kDa bands (from 8 to 60 minutes). When comparing the pattern of digestion of HMM, the 88-kDa, 68-kDa and 57kDa fragments observed in this study correspond to the 75-kDa, 67-kDa and 63-kDa fragments observed in a previous study using a similar proteolysis protocol [25]. The 57-kDa fragment was split during further digestion into a 30-kDa, produced by the cleavage of loop 1. The loop 2 was almost completely split by trypsin after 10 min of digestion, while loop 1 was not completely split until ~30 min (from 8 to 30 minutes). Thus, in agreement with a previous study (Bobkov et al., 1996), trypsin cleaved loop 2 faster than loop 1. The proteolysis of myosin light chain 1 and myosin light chain 2 (LC1 and LC2 bands) resulted in several small sub-products, which were not evaluated in the current study.

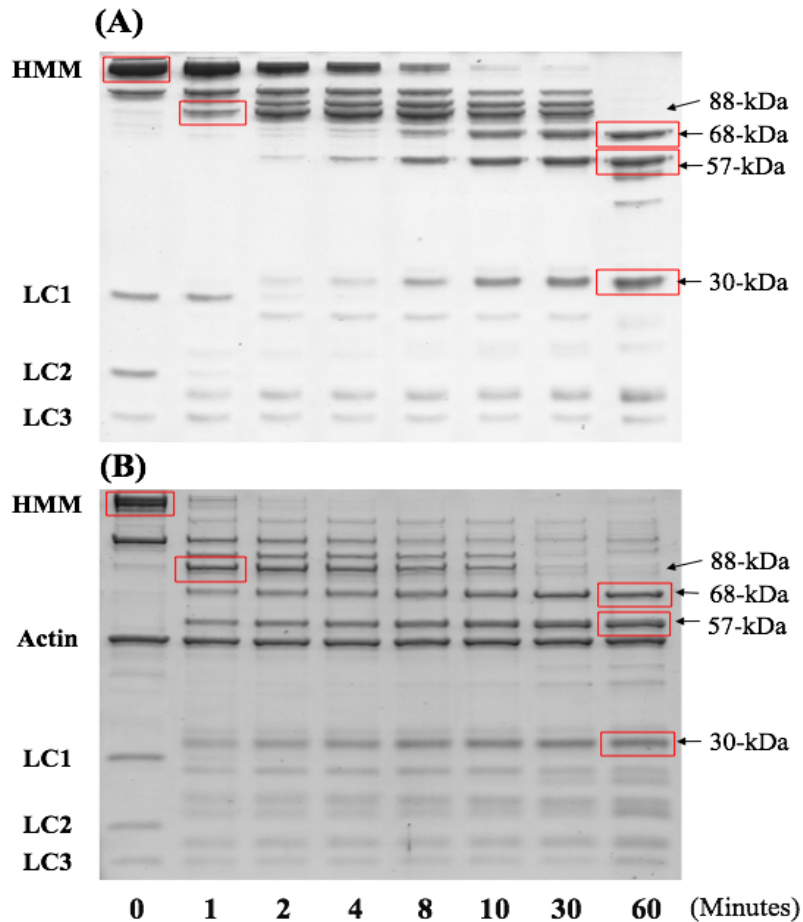


Figure 18. 10% SDS-PAGE showing the time course for proteolytic digestion of skeletal muscle HMM without (A) and with (B) addition of actin, to partially protect loop 2 from digestion. HMM (0.1 mg/ml) was digested at 1:50 enzyme-to-substrate ratio in 20 mM KCl, 20 mM Tris-HCl (pH 7.5) and 5ug of protein were loaded for each column in the gel. The red squares show the bands that were chosen for subsequent mass spectrometry analysis. The digestion time corresponding to each lane is shown at bottom of the figure.

When a 2-fold molar excess of F-actin was added over HMM to partially protect loop 2 and the actin-binding loop, the F-actin band representing actin (43kDa) was consistently visualized in the gel (Figure 18B). As observed in the previous analysis, a major 88kDa fragment was generated in the first minute of proteolysis. Two bands with 68kDa and 30kDa were then split

from the major 88-kDa fragment. Notably, bands with a high molecular weight were visible through the protocol until the end of proteolysis. Digestion of loop 1 was initiated after 1 min of treatment, showing that it was a major target of trypsin under this actin-protected condition. Cleavage of loop 1 was completed faster when loop 2 was partially protected by F-actin than in the condition without protection. The general pattern of proteolytic digestion in both protocols can be summarized as follows:



Mass spectrometry quantification of proteolytic fragments of HMM.

We used the bands extracted from the gels to investigate the content of peptides during the proteolysis of HMM using label-free quantitative mass spectrometry. We chose specific bands that showed a prominent molecular weight during different HMM digestion times (Figure 18). Based on the information collected in Uniprot database (accession number Q28641) and the mass-spectrometry peptides of HMM that we obtained, we investigated the presence of the flexible loops under investigation (Figure 19).

The peptide sequences of rabbit skeletal myosin loops 1 and 2, ATP-loop and actin-binding domain were obtained from mass fingerprint search in Uniprot database. We were able to identify peptides in rabbit skeletal myosin sequence that cover the whole sequences of loop 1 (VIQYFATIAITGDKK and KEEATSGK: residues 192-207 and 208-214, respectively), the ATP-loop (ENQSILITGESGAGK: residues 171-185), a sequence of loop 2 (GSSFQTVSALFR:

residues 644-655) and the actin-binding domain 2 (AGLLGLLEEMR: residues 770-780) (Supplementary Table 1). The specific location of these functional loops and identified peptides in myosin II is shown in Figure 19. Note that the loop 1 is situated close to the ATP-loop, and the loop 2 is situated close to the actin-binding domain.

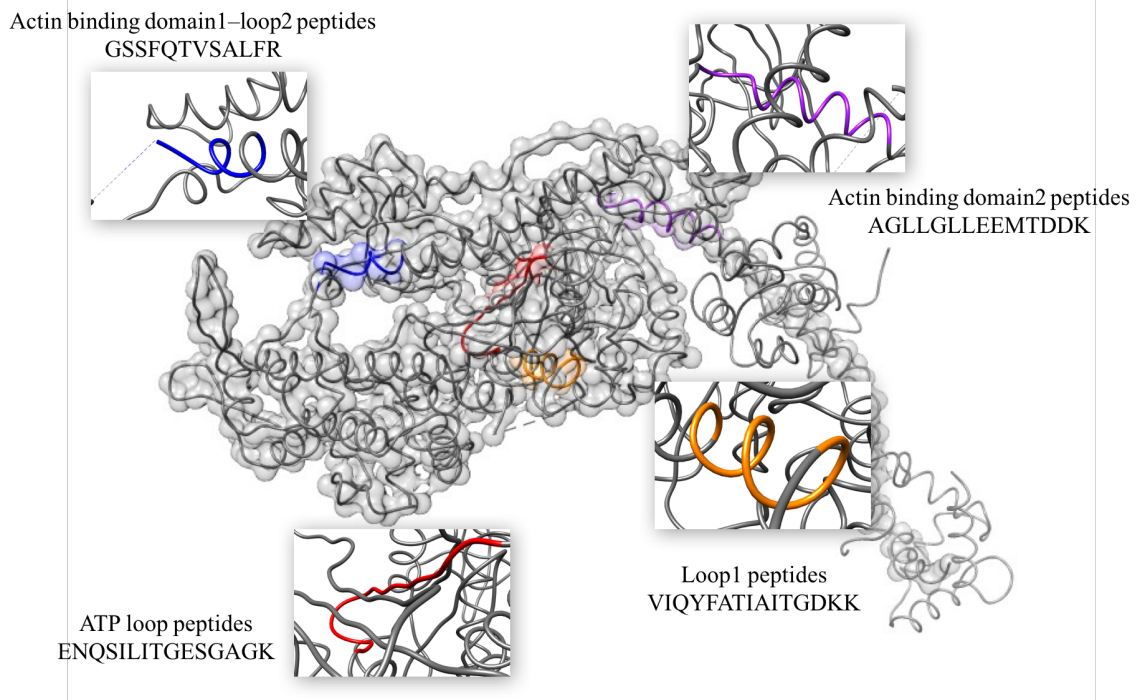


Figure 19. Myosin II sub-fragment 1 (PDB:2MYS) with the sequences of loop 1, ATP loop, loop 2 and the actin-binding domain 2 obtained by mass spectrometry, and highlighted by UCSF Chimera software.

Analysis of mass spectrometry data obtained from HMM fragments with and without actin protection revealed the absence of the peptides covering the entire loop 2 area of myosin. The possible reason is that loop 2 is rich in lysine, which is the most accessible amino acid for trypsin used to obtain peptides for mass-spectrometry. However, we were able to find peptides that

overlap the areas of the loop 2 (644-656 residues in skeletal myosin, Uniprot Access number Q28641) and the actin-binding domain 2. The majority of these overlapping peptides were observed in the 68-kDa fragment obtained during proteolysis. The peptides were also found in the 30-kDa fragment, but the content was low. Only small traces were observed in the 88-kDa and 57-kDa fragments (Figure 20).

Figure 20A shows that proteolytic digestion of HMM led to the splitting of loop 1 peptide very quickly. The 68kDa fragment did not contain loop 1, which was observed only in the 30kDa fragment, 60 minutes after the beginning of proteolysis. A very similar pattern was observed for the peptides in the ATP-loop, showing that the effects of trypsin are localized; in this case, in the vicinity of loop 1 and ATP loop.

When we treated HMM with trypsin in the presence of actin to partially protect loop 2, the trend of proteolysis was quite similar to that shown in Figure 21, except that the loop 1 was depleted more prominently - there was only a small number of peptides in the 88kDa fragment, just 1 min during digestion (Figure 21). There was a large number of peptides from loop 1 and the ATP loop in the 30kDa fragment, showing that they were digested almost entirely during 60 min of treatment. Although the ATP-loop peptides were present in the 88-kDa fragment, they were completely absent in the 68-kDa and 57-kDa fragments.

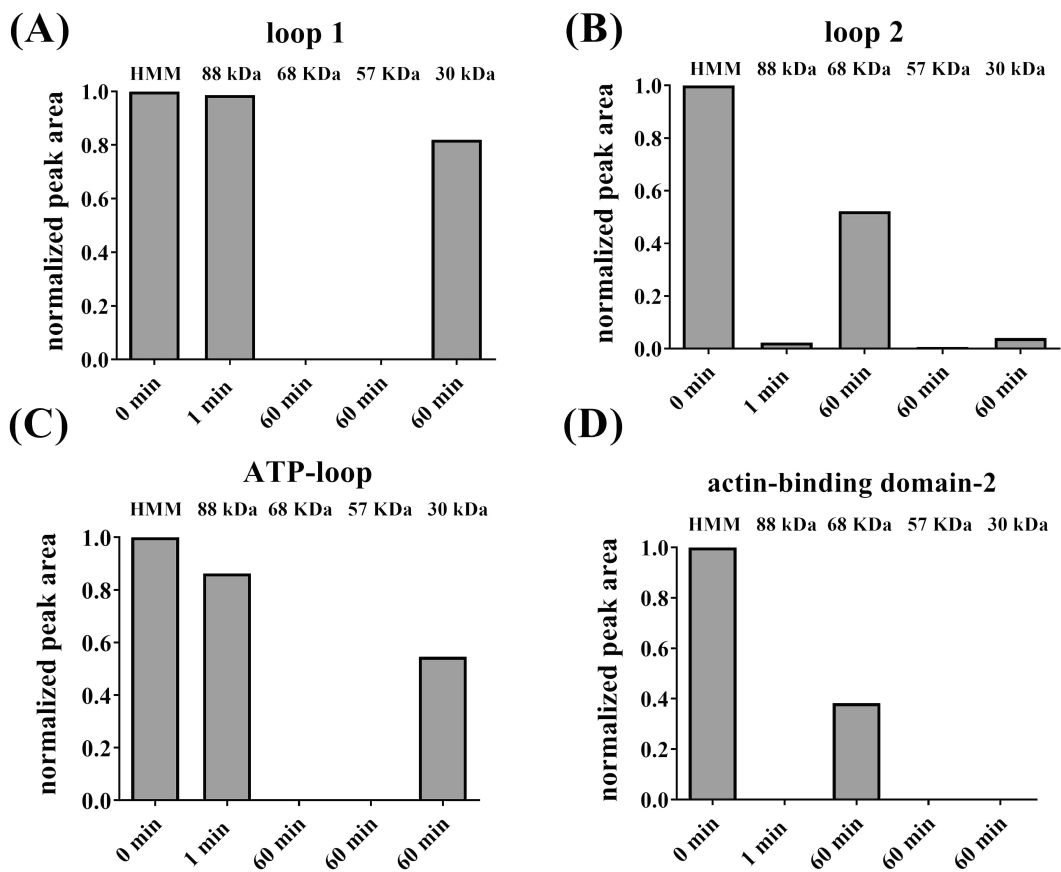


Figure 20. Label-free mass-spectrometry quantification of rabbit skeletal HMM and its tryptic fragments, when the digestion protocol was performed without protection of loop 2. Extracted ion chromatograms profiles were used to calculate the 50% peak areas of peptides covering loop 1 (A), part of loop 2 (B) ATP-loop (C), and actin-binding domain 2 (D) at different times during the protocol. Data were normalized to the 50% peak area of non-trypsinized HMM. Reproducibility of the data were tested in two independent experiments with at least three runs for quantification of peak area of selected peptides.

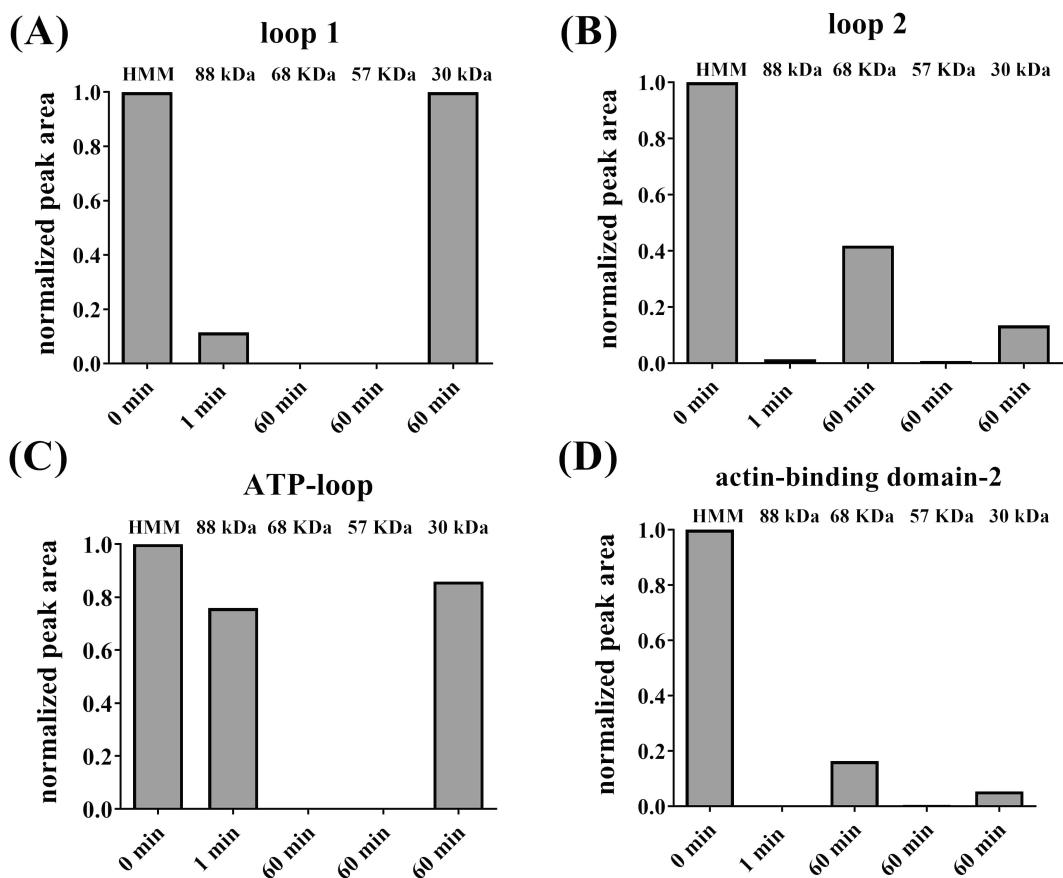


Figure 21. Label-free mass-spectrometry quantification of rabbit skeletal HMM and its tryptic fragments when the digestion protocol was performed in the presence of actin to partially protect loop 2. Extracted ion chromatogram profiles were used to calculate the 50% peak areas of peptides covering loop 1 (A), part of loop 2 (B) ATP-loop (C), and actin-binding domain 2 (D) at different times. Data were normalized to the 50% peak area of non-trypsinized HMM. The reproducibility of the data was tested in two independent experiments with at least three runs for quantification of peak area of selected peptides.

The effects of trypsinized HMM on actin motility velocity.

Figure 22 shows the distribution of the sliding velocities of actin filaments propelled by selected species of HMM cleaved during tryptic digestion. Notably, the velocity was decreased with increasing tryptic digestion of myosin, with and without partial protection of loop 2, as evidenced by a leftward shift in the histogram fitted with the data. The average velocities of the actin filaments measured are also shown in Figure 22. Before digestion of HMM, the velocity of actin motility was $3.29 \pm 0.08 \mu\text{m}/\text{sec}$, and did not change significantly when tested during 30 min without digestion (control); at the end of the protocol it was $3.57 \pm 0.02 \mu\text{m}/\text{sec}$. When actin motility was measured in HMM-trypsin treated fragments, the velocity was decreased from $4.05 \pm 0.13 \mu\text{m}/\text{sec}$ to $2.24 \pm 0.15 \mu\text{m}/\text{sec}$ with 4 minutes of digestion. The motility was stopped after 10 minutes of digestion. When actin was added to the preparation to partially protect loop 2, the velocity of motility was decreased from $3.82 \pm 0.10 \mu\text{m}/\text{sec}$ to $1.21 \pm 0.16 \mu\text{m}/\text{sec}$ after 2 minutes of digestion, and the motility was stopped after 8 minutes of digestion (Figure 22E).

The fraction of actin filaments propelled by HMM over 30 minutes of control testing or during proteolysis were also measured (Figure 22F). Virtually all filaments were moving through the protocol in control conditions, showing that the vast majority of HMM was functional. The fraction of moving actin filaments decreased during HMM digestion, in a pattern that was similar to that observed for the sliding velocity. The fraction of motility decreased faster when loop 2 was protected, likely due to the faster depletion of loop 1.

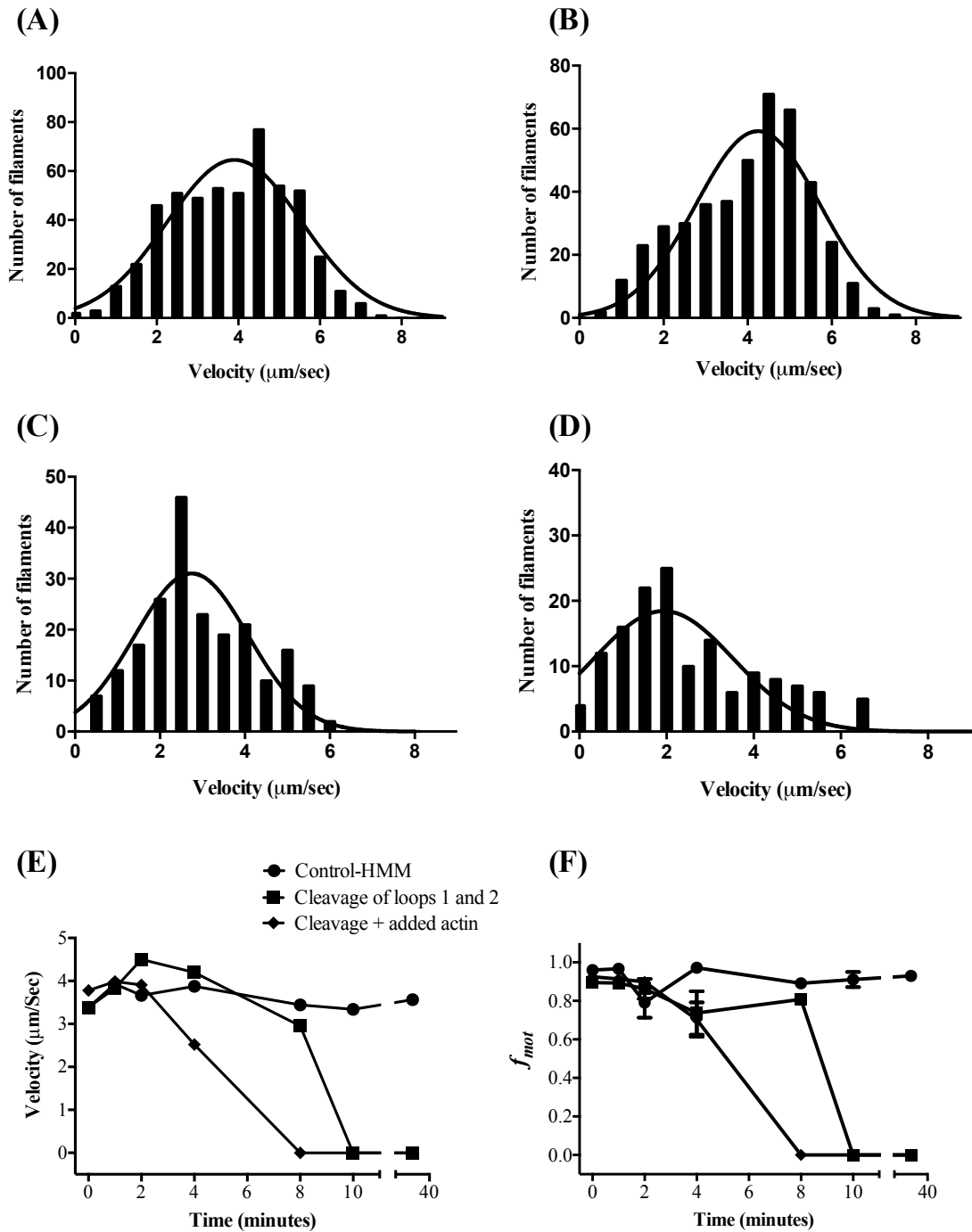


Figure 22. Distribution of velocities of actin filaments sliding in the in-vitro motility assay. The data showed on the panels (A) and (C) represent the condition where both loops 1 and 2 were cleaved (1 minute and 8 minutes of digestion, respectively). Non-linear fits for the histograms rendered peaks produced velocities of $3.91\mu\text{m}/\text{sec}$ and $2.74\mu\text{m}/\text{sec}$, showing a shift in the mean velocity. The data showed on the panels (B) and (D) represent the condition when loop 1 was

cleaved in the presence of actin to partially protect loop 2 (1 minute and 4 minutes of digestion, respectively). Non-linear fits for the histograms rendered peaks produced velocities of $4.42\mu\text{m}/\text{sec}$ and $1.93\mu\text{m}/\text{sec}$, respectively, showing a shift in the mean velocity. The velocity of actin motility (E) and the fraction of moving actin filaments (F) for the control HMM, and during cleavage of loops 1 and 2, with and without partial protection of loop 2, are shown as mean \pm SEM. Each experiment was repeated three times. The values for the experiments including sample sizes are indicated in supplementary Tables 3 and 4.

Effects of load on actin motility.

In a separate set of experiments, we added α -actinin to the motility assays (concentrations of $0.5\mu\text{g}/\text{mL}$, $0.75\mu\text{g}/\text{mL}$, $1.0\mu\text{g}/\text{mL}$, $1.25\mu\text{g}/\text{mL}$ and $1.5\mu\text{g}/\text{mL}$) and repeated the tests with the HMM fragments obtained during proteolysis (Figure 23). After incubating for approximately 1 min, the α -actinin is bound to the coverslip surface as well as loosely to actin filaments. In the absence of an added load, the HMM driving force propels actin at maximal velocity (V_{max}). α -actinin provides an exogenous, friction load to the actin filament that opposes the myosin driving force. The actin sliding velocity (V) is then determined by the balance of the forces acting on the actin filament. It has been shown that increasing concentrations of α -actinin changes the velocity of actin motility in a dose-dependent fashion (Bing et al., 2000). In fact, the **overall velocity** of actin motility in our study decreased significantly with all preparations that we used, showing a strong linear relation (Figure 23A). Assuming that increasing the load will increase the force that myosin exerts to propel actin filaments, our results resemble the original force-velocity relation that is characteristic of muscle myosin. When we group all analyses performed during these experiments (Figure 23B) we have a slope of -2.088 ± 0.19 ($Y = 2.088 * X$

+ 3.518, $r^2: 0.97$, $p = 0.0004$).

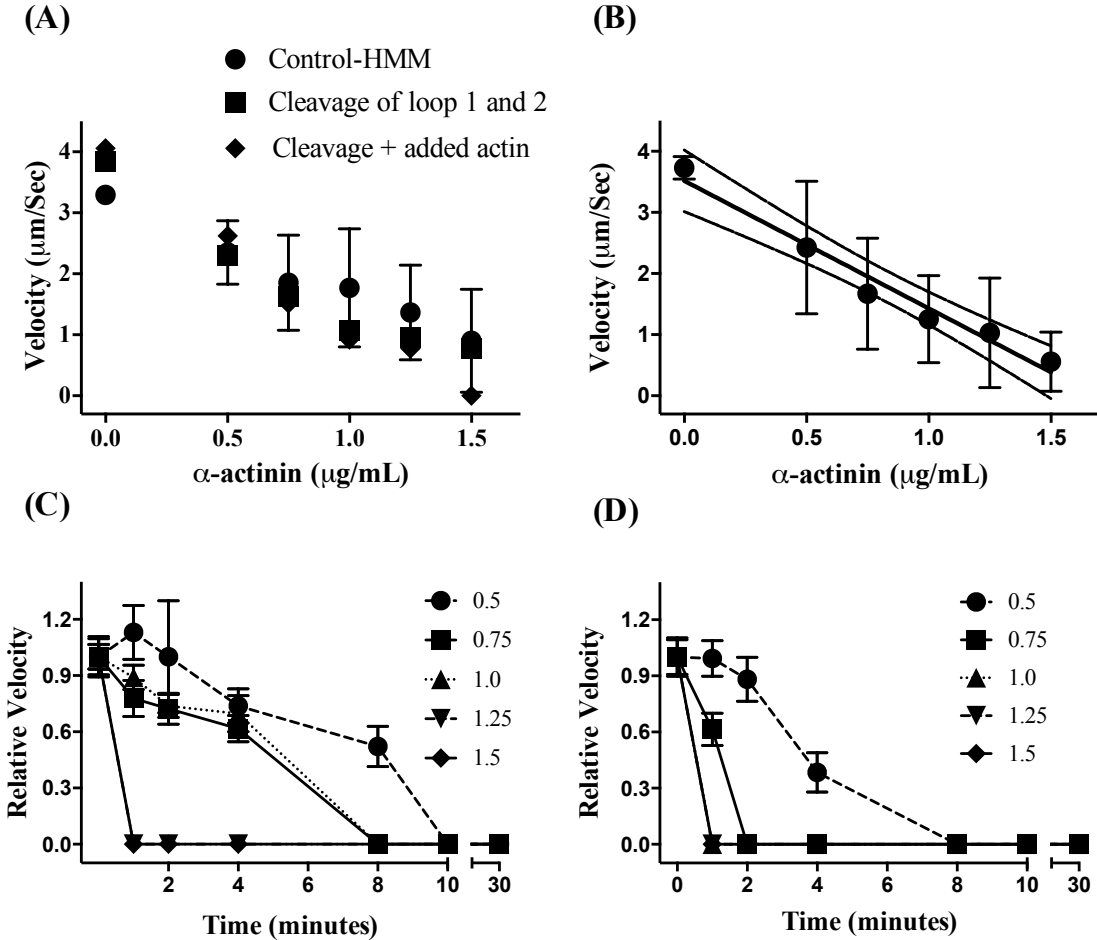


Figure 23. The relation between the concentration of α -actinin and the velocity of actin motility over HMM in the different conditions investigated in this study (A) and when all data are grouped (B). There is an inverse, linear relationship such that an increase in the concentration of α -actinin decreases the velocity of actin motility. The lower panels show the relative velocity of actin motility obtained during cleavage of loops 1 and 2, without (C) and with (D) partial protection of loop 2. These experiments were conducted with the addition of different concentrations of α -actinin (0.5, 0.75, 1.0, 1.25 and 1.5 $\mu\text{g}/\text{mL}$) in the motility assay. The graph shows data collected during 30 minutes of digestion. The number of actin filaments analyzed in each group. Data are presented as mean \pm S.E.M.

When we normalized the velocities of motility based on data obtained before proteolytic digestion, we observed some important features (Figures 23C and 23D). First, increasing concentrations of α -actinin decreased the velocity of actin motility in almost all times during digestion, i.e. there was a downward shift in the α -actinin-velocity relation, for those experimental points where motility was observed. Second, although motility was observed with all α -actinin concentrations before digestion, soon after HMM proteolysis started, motility ceased with high concentrations of α -actinin. Finally, with the partial protection of loop 2 and consequently a faster digestion of loop 1, the effect of α -actinin was more pronounced, and a concentration of $\geq 1.0\mu\text{g/mL}$ was sufficient to stop actin motility. One potential explanation for the larger effect of α -actinin when loop 1 was depleted more rapidly is that there was also a decrease in the fraction of actin filaments motility, indicating less force produced by HMM fragments to propel the actin filaments against the loads.

ATPase activity.

Tryptic digestion of HMM decreased the ATPase activity significantly over 60 minutes (Figure 24). Note that the decrease in ATPase was similar in the two groups of fragments – with or without the addition of extra actin to the preparation. Conceptually, this result was not expected, as protection of loop 2 would have maintained the levels of ATPase activity during the digestion protocol. However, the result is consistent with the major effect of adding actin to the preparation; accelerating the digestion of loop 1 while not significantly changing the content of loop 2. Therefore loop 1 is not suspected to be closely associated with ATPase activity.

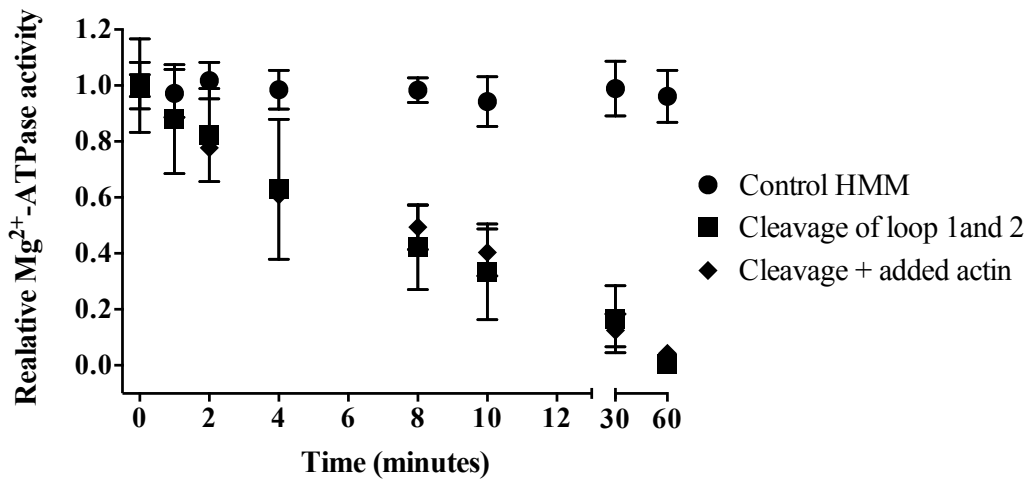


Figure 24. Effect of cleavage of loops 1 and 2 on actin-activated Mg^{2+} -ATPase. HMM: 0.01 mg/ml, F-actin: 0.05 mg/ml. Data are given as mean \pm S.E.M. (N=15 for each group).

9.5 Discussion

In this study, we observed that digestion of HMM that resulted in proteolysis of loop 1, loop 2, ATP-loop and the actin-binding domain decreased significantly the velocity of myosin-propelled actin motility in the in-vitro motility assay. These results were strengthened by analysis of high-resolution mass spectrometry, revealing that loop 1 and the ATP-loop, as well as loop 2 and the actin-binding domain, are closely located and undergo a similar process of proteolysis during HMM digestion. When we added different loads to the motility assay, there was a decrease in the actin sliding velocity, leading to an inverse, linear load-velocity relation. This load-dependent decrease in actin velocity was related to the proteolysis of loop 1 and ATP-loop. Altogether, these findings suggest that the myosin loops are necessary for the regulation of myosin-actin interactions and that the load-dependent velocity of actin motility is regulated mostly by loop 1 and the ATP-loop.

It has been proposed that loops 1 and 2, not resolved in the crystal structure of myosin (Rayment, Rypniewski, et al., 1993), are critical for modulating the ATPase cycle and the maximum velocity of actin motility (Spudich, 1994). Proteolysis at these loops divides skeletal myosin S1 into three fragments of 25kDa, 50kDa, and 20kDa (Mornet et al., 1979). A previous study (Bobkov et al., 1996) showed that proteolysis of the 50-20K loop affects the actin-activated ATPase activity while proteolysis of the 25-50K loop affects actin motility. The 25-50K loop, or loop 1, lies nearer the ATP-binding pocket, and due to this proximity it can affect P_i release (Clark et al., 2005; Knetsch et al., 1999; Lauzon, Trybus, et al., 1998; Lauzon, Tyska, et al., 1998; Murphy & Spudich, 1998; Rovner et al., 1997; Uyeda et al., 2002).

Meanwhile the 50-20K loop, or loop 2, proximal to the actin-binding face, which modulates actin-activated ATPase activity (Joel et al., 2003; Joel et al., 2001; Knetsch et al., 1999; Murphy & Spudich, 1999; Uyeda et al., 2002). Interestingly, our results with mass spectrometry showed that the process of proteolysis in this study led to very similar results between the loop 1 and the ATP-loop, and also between loop 2 and the actin-binding domain, which are situated in close proximity. Loop 2 and the acting binding-domain in fact have overlapping peptides (Supplementary Table 1).

Loop 1 varies naturally with alternative splicing in different myosin isoforms, in close association with their function (Kelley, Takahashi, Yu, & Adelstein, 1993). These variations are observed in different vertebrate smooth and non-muscle myosin II isoforms and alter the rate of actin filament movement in-vitro (Kelley et al., 1993; Rovner et al., 1997). Consequently, loop 1 has been proposed as the primary factor determining the rate of ADP release from myosin, which dictates actin sliding velocity in-vitro (Spudich, 1994). There is also evidence that loop 1 controls ADP release during the acto-myosin cycle in catch muscles and striated muscles from the scallop (Kurzawa-Goertz, Perreault-Micale, Trybus, Szent-Gyorgyi, & Geeves, 1998).

In smooth muscle myosin, the naturally occurring difference in amino acids incorporated into loop 1 is tissue specific, and correlates with their functions (Kelley et al., 1993; Leguillette et al., 2005); they contain two isoforms with a natural mRNA splicing at the amino-terminus, differing by the presence (+) or absence (-) of the 7 amino acid insert (QGPSFAY). Rapidly contracting phasic muscle is predominantly composed of the (+)insert isoform, whereas slowly contracting, tone-maintaining tonic muscle is mostly composed of the (-)insert isoform

(Leguillette et al., 2005; Tuck et al., 2004; White, Zhou, Low, & Periasamy, 1998). Additionally, there is a direct relationship in the relative content of the insert and the activity of smooth muscle tissues (e.g. aorta, uterus, bladder, trachea, stomach, and intestine (Leguillette et al., 2005; Low, Leguillette, & Lauzon, 2006)), suggesting that loop 1 variations contribute to different mechanical properties of phasic and tonic muscles. Notably, alterations in the time course of bronchoconstriction in (+)insert knockout mice confirm this mechanism (Tuck et al., 2004). In a previous study we measured the velocity of motility of myosin filaments polymerized from turkey gizzard phasic smooth muscle myosin, and filaments polymerized from a mixture (50–50%) of phasic and tonic smooth muscle myosin purified from turkey gizzard and pig stomach fundus (Kalganov et al., 2013b). We also compared these preparations with skeletal and mussel (invertebrate) filaments, and observed that the activity of these myosins were well correlated with their loop 1 structure (Kalganov et al., 2013b).

In the current study, we observed that when we partially protected loop 2 from digestion, loop 1 was digested more rapidly. Importantly, a faster digestion of loop 1 was accompanied by an earlier decrease in the actin velocity during the digestion protocol, strengthening the hypothesis that loop 1 is responsible for ADP release. Previous studies agree with our results. Studies using chimera *Dictyostelium* myosins (Murphy & Spudich, 1998) or alternatively spliced smooth muscle myosin and scallop myosin (Perreault-Micale, Kalabokis, Nyitray, & Szent-Gyorgyi, 1996) show that changes in loop 1 affect in-vitro motility (Rovner et al., 1997) and therefore ADP release, while having little effect upon ATPase activity. A lack of direct correlation between actin-activated MgATPase activity and in-vitro motility was also observed

(Mornet et al., 1979; Siemankowski, Wiseman, & White, 1985; Umemoto & Sellers, 1990). Finally, a proteolytic study of rabbit skeletal HMM (Bobkov et al., 1996) showed that independent cleavage of loop 1 and loop 2 affects motility and ATPase activity separately, supporting the idea that the loops can independently affect these rate-limiting steps of the myosin-actin interaction cycle.

There has been limited information on the mechanisms of how load affects the power stroke of myosin molecules. This limitation is partially due to technical challenges; skeletal muscle myosin attaches to actin for a very brief period (<40ms), and detecting binding events while applying loads during the power stroke is difficult. Using our loaded motility assay, we provided new information on the mechanisms behind the load dependence of the myosin-actin interaction. We observed that increasing the load, as expected, decreased the velocity of the actin filaments sliding over HMM. Depletion of loops 1 and 2 caused a downward shift in the load-velocity relation, and a lower amount of α -actinin was needed to stop the actin motility. When loop 1 depletion was accelerated during the proteolysis process (Figs. 23C and 23D), the effects of load were less prominent. Since loop 1 is responsible for ADP release, the result suggests that the load dependence of the myosin power stroke is associated with ADP release. This result is in agreement with studies performed with the processive myosins I, V and kinesin that show that their attachment time with actin (usually >100ms) is shortened with increasing ATP concentrations, suggesting that it is terminated when ATP binds to myosin and ADP is released (Guilford et al., 1997; Rief et al., 2000; Tyska et al., 1999b; Veigel et al., 2005; Visscher et al., 1999). Therefore, our results together with previous studies suggest that loop 1 is responsible for

velocity of contraction, ADP release, and the load dependence of the power stroke in different myosins, including skeletal muscles.

Residues in loop 2 have a high probability of interaction with actin in the strongly bound state (Volkman et al., 2000), and thus this loop is likely critical for the actomyosin interface cycle throughout the ATPase cycle. The initial, weakly binding state between myosin and actin happens through electrostatic interactions between lysine residues in loop 2 (50–20kDa) which are positively charged with residues in the subdomain 1 of actin monomers that are negatively charged (Chaussepied, 1989; Cheung & Reisler, 1992). Removal of negative charges from subdomain 1 of actin decreases the affinity of actin for myosin in the presence of MgATP (Miller, Cheung, White, & Reisler, 1995), and deletion of lysines K652 and K653 at the C-terminal portion of loop 2 abolishes actin-activated ATPase activity and myosin-propelled in-vitro motility of actin (Joel et al., 2001).

Strong evidence for the connection between the loop 2 and actomyosin interactions also comes from studies using engineered myosins. Studies have shown that chimeric Dictyostelium myosin II molecules containing loop 2 structures derived from other myosins change their steady-state ATPase and V_{\max} (Uyeda et al., 1994) according to the characteristics of the parent myosins. Similar studies showed that chimeras of smooth muscle HMM containing loop 2 from skeletal and cardiac muscle myosins presented an increased affinity for actin, without significantly altering V_{\max} (Joel et al., 2003), typical from these myosins. These results agree with our findings that loop 2 overlap with the actin-binding site, with a previous study looking at the location of loop 2 (Mornet et al., 1979), and with data showing that proteolysis of loop 2

causes decreases in the actin-activated ATPase activity (Bertrand, Derancourt, & Kassab, 1989; Mornet et al., 1979). These results suggest that the sequence variability of the loops might help to fine-tune the activity of each myosin isoform (Spudich, 1994).

An intriguing hypothesis is that loops 1 and 2 have evolved to optimize myosin's activity and by varying the sequence at key sites outside the core of the enzyme, the activity of a particular myosin can be fine-tuned for its cellular role. These two loops may co-vary to maintain the fraction of the ATPase cycle in which the myosin is strongly bound to actin. The proximity of loop 1 and loop 2 to the nucleotide and actin binding sites, coupled with the variability of their sequences make them ideal sites for affecting the rate-limiting steps of the actin–myosin ATPase cycle and force-generating steps.

CHAPTER 4 – CONCLUSIONS AND FUTURE DIRECTIONS

10. Conclusions

In this thesis, we presented two studies showing that skeletal and smooth muscle myosins are efficient motors that adjust their power output according to external loads. The force production and actin motility, which are controlled by ATPase kinetics and ADP release, are regulated at least partially by the surface loops 1 and 2 in the MHC.

In Chapter 2 of this thesis a new experimental method was used which allowed for the evaluation of the load dependence on force production in intact filaments of myosin II, while visualizing the sliding of actin filaments over myosin. As far as the authors are aware, it was the first time that the sliding of actin filaments on top of myosin filaments could be visualized in real time while producing force. We observed that increasing the load increases the force produced by the myosin molecules, while decreasing the load decreased the force. The force-velocity relation presented an inverse hyperbolic relation that was similar to early studies performed with single fibers. Therefore, the load dependence of the myosin power stroke and the force-velocity relation were observed at the molecular levels.

In Chapter 3 of this thesis, we observed that digestion of HMM that resulted in proteolysis of loop 1, loop 2, ATP-loop and the actin-binding domain decreased the velocity of myosin-propelled actin motility in the in-vitro motility assay. Loop 1, the ATP-loop, loop 2 and the actin-binding domain, are closely located and undergo a similar process of proteolysis during HMM digestion. We further observed that when we added different loads to the motility assay, there was a decrease in the actin sliding velocity, leading to an inverse, linear load-velocity relation. This load-dependent decrease in actin velocity was particularly related to the proteolysis

of loop 1 and ATP-loop. Altogether, these findings suggest that the myosin loops are necessary for the regulation of myosin-actin interactions, and that the load-dependent velocity of actin motility is regulated mostly by loop 1 and by the ATP-loop.

It is interesting to note that increasing the load during either filament interaction (Chapter 2) or during in-vitro motility assay (Chapter 3) has the same effect, leading to an almost identical force-velocity relationship.

Overall, the results of this thesis are the first to show the phenomenon of the load dependence of force production and the force velocity relation at the myosin-actin and molecular levels, providing valuable knowledge of the molecular mechanisms of muscle contraction to the scientific community.

11. Future directions

In the future, it would be important to follow these studies to investigate some questions that were raised during our experiments and data analysis. First, it would be important to evaluate the effects of the loops investigated in Chapter 3 in the force produced by filaments using the system developed in Chapter 2 or with other method that can reliably measure the myosin power stroke. We have made attempts to perform these experiments but after digesting the MHC from specific loops the filaments became too fragile to be attached to micro-fabricated cantilevers. It may be possible to cleave the myosin loops using other methods, but this need to be investigated. If such experiments become possible, the filaments with specific digestion of loops can be tested for the force, force-velocity relation and power output, with results that can reveal further the mechanisms behind myosin-actin interactions.

It would also be interesting to use the same methods developed in this study to investigate myosin and actin filaments in conditions affected by different diseases that may affect the muscular system. For example, there are several forms of cardiomyopathy that are closely linked to mutations on the MHC (Lowey et al., 2008) and changes in the myosin ATPase (Lowey et al., 2018), and thus may reveal changes in the myosin-induced power developed by the muscular system.

Finally, our laboratory has begun looking into the effects of oxidation and nitration of muscle filaments on contractile characteristics of muscle cells and myofibrils. It is known that oxidation and nitration can lead to significant decreases in force and have been linked to muscle weakness in a variety of forms (Pearson, McArdle, & Jackson, 2015; T. Yamada et al., 2006). A

next step will be to evaluate the load dependence of force in myosin filaments that have been treated for these conditions.

REFERENCE

- Aguilar, H. N., & Mitchell, B. F. (2010). Physiological pathways and molecular mechanisms regulating uterine contractility. *Hum Reprod Update*, 16(6), 725-744. doi:10.1093/humupd/dmq016
- Bailey, K. (1946). Tropomyosin: a new asymmetric protein component of muscle. *Nature*, 157, 368.
- Baker, J. E., Brosseau, C., Joel, P. B., & Warshaw, D. M. (2002). The biochemical kinetics underlying actin movement generated by one and many skeletal muscle myosin molecules. *Biophys.J.*, 82(4), 2134-2147.
- Bang, M. L., Centner, T., Fornoff, F., Geach, A. J., Gotthardt, M., McNabb, M., . . . Labeit, S. (2001). The complete gene sequence of titin, expression of an unusual approximately 700-kDa titin isoform, and its interaction with obscurin identify a novel Z-line to I-band linking system. *Circ Res*, 89(11), 1065-1072.
- Banga, I., & Szent-Györgyi, A. (1942). *Preparation and properties of myosin A and B* (Vol. 1). Institute of Medical Chemistry—University of Szeged.
- Barany, M. (1967). ATPase activity of myosin correlated with speed of muscle shortening. *J.Gen.Physiol*, 50(6), Suppl-218.
- Barouch, W. W., & Moos, C. (1971). Effect of temperature on actin activation of heavy meromyosin ATPase. *Biochim Biophys Acta*, 234(2), 183-189.
- Bertrand, R., Derancourt, J., & Kassab, R. (1989). Selective cleavage at lysine of the 50 kDa-20 kDa connector loop segment of skeletal myosin S-1 by endoproteinase Arg-C. *FEBS Lett*, 246(1-2), 171-176.
- Bhagavan, N. V. (2002). *CHAPTER 21 - Muscle and Nonmuscle Contractile Systems* (N. V. BHAGAVAN Ed.).
- Bing, W., Knott, A., & Marston, S. B. (2000). A simple method for measuring the relative force exerted by myosin on actin filaments in the in vitro motility assay: evidence that tropomyosin and troponin increase force in single thin filaments. *Biochem J*, 350 Pt 3, 693-699.
- Bobkov, A. A., Bobkova, E. A., Lin, S. H., & Reisler, E. (1996). The role of surface loops (residues 204-216 and 627-646) in the motor function of the myosin head. *Proc.Natl.Acad.Sci.U.S.A*, 93(6), 2285-2289.

- Boriack-Sjodin, P. A., Margarit, S. M., Bar-Sagi, D., & Kuriyan, J. (1998). The structural basis of the activation of Ras by Sos. *Nature*, *394*(6691), 337-343. doi:10.1038/28548
- Bradford, M. M. (1976). A rapid and sensitive method for the quantitation of microgram quantities of protein utilizing the principle of protein-dye binding. *Anal Biochem*, *72*, 248-254.
- Brooke, M. H., & Kaiser, K. K. (1970). Muscle fiber types: how many and what kind? *Arch Neurol*, *23*(4), 369-379.
- Burgess, S. A., Walker, M. L., White, H. D., & Trinick, J. (1997). Flexibility within myosin heads revealed by negative stain and single-particle analysis. *J Cell Biol*, *139*(3), 675-681.
- Burgess, S. A., Yu, S., Walker, M. L., Hawkins, R. J., Chalovich, J. M., & Knight, P. J. (2007). Structures of smooth muscle myosin and heavy meromyosin in the folded, shutdown state. *J Mol Biol*, *372*(5), 1165-1178. doi:10.1016/j.jmb.2007.07.014
- Burke, R. E., Levine, D. N., Tsairis, P., & Zajac, F. E., 3rd. (1973). Physiological types and histochemical profiles in motor units of the cat gastrocnemius. *J Physiol*, *234*(3), 723-748.
- Chaussepied, P. (1989). Interaction between stretch of residues 633-642 (actin binding site) and nucleotide binding site on skeletal myosin subfragment 1 heavy chain. *Biochemistry*, *28*(23), 9123-9128.
- Cheng, Y. S., Matusovskiy, O. S., & Rassier, D. E. (2019). Cleavage of loops 1 and 2 in skeletal muscle heavy meromyosin (HMM) leads to a decreased function. *Arch Biochem Biophys*, *661*, 168-177. doi:10.1016/j.abb.2018.11.002
- Cheung, P., & Reisler, E. (1992). Synthetic peptide of the sequence 632-642 on myosin subfragment 1 inhibits actomyosin ATPase activity. *Biochem Biophys Res Commun*, *189*(2), 1143-1149.
- Chock, S. P., Chock, P. B., & Eisenberg, E. (1976). Pre-steady-state kinetic evidence for a cyclic interaction of myosin subfragment one with actin during the hydrolysis of adenosine 5'-triphosphate. *Biochemistry*, *15*(15), 3244-3253.
- Clark, R., Ansari, M. A., Dash, S., Geeves, M. A., & Coluccio, L. M. (2005). Loop 1 of transducer region in mammalian class I myosin, Myo1b, modulates actin affinity, ATPase activity, and nucleotide access. *J Biol Chem*, *280*(35), 30935-30942.
- Clobes, A. M., & Guilford, W. H. (2014). Loop 2 of myosin is a force-dependent inhibitor of the

- rigor bond. *J Muscle Res Cell Motil*, 35(2), 143-152. doi:10.1007/s10974-014-9375-z
- Cohen, C. (1955). Optical rotation and helical polypeptide chain configuration in collagen and gelatin. *J Biophys Biochem Cytol*, 1(3), 203-214.
- Cohen, C., & Parry, D. A. (1990). Alpha-helical coiled coils and bundles: how to design an alpha-helical protein. *Proteins*, 7(1), 1-15. doi:10.1002/prot.340070102
- Colombini, B., Nocella, M., Benelli, G., Cecchi, G., & Bagni, M. A. (2007). Crossbridge properties during force enhancement by slow stretching in single intact frog muscle fibres. *J.Physiol*, 585(Pt 2), 607-615.
- Conibear, P. B. (1999). Kinetic studies on the effects of ADP and ionic strength on the interaction between myosin subfragment-1 and actin: implications for load-sensitivity and regulation of the crossbridge cycle. *J Muscle Res Cell Motil*, 20(8), 727-742.
- Cornachione, A. S., Leite, F. S., Wang, J., Leu, N. A., Kalganov, A., Volgin, D., . . . Kashina, A. (2014). Arginylation of myosin heavy chain regulates skeletal muscle strength. *Cell Rep*, 8(2), 470-476. doi:10.1016/j.celrep.2014.06.019
- Coureux, P. D., Wells, A. L., Menetrey, J., Yengo, C. M., Morris, C. A., Sweeney, H. L., & Houdusse, A. (2003). A structural state of the myosin V motor without bound nucleotide. *Nature*, 425(6956), 419-423.
- Dalla Libera, L., Sartore, S., Pierobon-Bormioli, S., & Schiaffino, S. (1980). Fast-white and fast-red isomyosins in guinea pig muscles. *Biochem Biophys Res Commun*, 96(4), 1662-1670.
- Dancker, P. (1975). ATPase activity and light scattering of acto-heavy meromyosin: dependence on ATP concentration and on ionic strength. *Z Naturforsch C*, 30(3), 379-384.
- Dantzig, J. A., Barsotti, R. J., Manz, S., Sweeney, H. L., & Goldman, Y. E. (1999). The ADP release step of the smooth muscle cross-bridge cycle is not directly associated with force generation. *Biophys.J.*, 77(1), 386-397.
- De La Cruz, E. M., Wells, A. L., Rosenfeld, S. S., Ostap, E. M., & Sweeney, H. L. (1999). The kinetic mechanism of myosin V. *Proc.Natl.Acad.Sci.U.S.A*, 96(24), 13726-13731.
- Debold, E. P. (2012). Recent insights into muscle fatigue at the cross-bridge level. *Front Physiol*, 3, 151. doi:10.3389/fphys.2012.00151
- Debold, E. P., Patlak, J. B., & Warshaw, D. M. (2005). Slip sliding away: load-dependence of velocity generated by skeletal muscle myosin molecules in the laser trap. *Biophys.J.*, 89(5), L34-L36.

- Dominguez, R., & Holmes, K. C. (2011). Actin structure and function. *Annu Rev Biophys*, 40, 169-186. doi:10.1146/annurev-biophys-042910-155359
- Ebashi, S., Kodama, A., & Ebashi, F. (1968). Troponin. I. Preparation and physiological function. *J Biochem*, 64(4), 465-477.
- Eddinger, T. J., & Meer, D. P. (2007). Myosin II isoforms in smooth muscle: heterogeneity and function. *Am J Physiol Cell Physiol*, 293(2), C493-508. doi:10.1152/ajpcell.00131.2007
- Edman, K. A., Reggiani, C., Schiaffino, S., & te, K. G. (1988). Maximum velocity of shortening related to myosin isoform composition in frog skeletal muscle fibres. *J.Physiol*, 395, 679-694.
- Edman, K. A., Reggiani, C., & te, K. G. (1985). Differences in maximum velocity of shortening along single muscle fibres of the frog. *J.Physiol*, 365, 147-163.
- Edstrom, L., & Kugelberg, E. (1968). Histochemical composition, distribution of fibres and fatiguability of single motor units. Anterior tibial muscle of the rat. *J Neurol Neurosurg Psychiatry*, 31(5), 424-433.
- Elzinga, M., Collins, J. H., Kuehl, W. M., & Adelstein, R. S. (1973). Complete amino-acid sequence of actin of rabbit skeletal muscle. *Proc Natl Acad Sci U S A*, 70(9), 2687-2691.
- Engelhardt, W. A., & Lyubimova, M. N. (1939). Myosin and adenosine triphosphatase. *Nature*, 144. doi:10.1038/144668b0
- Fauver, M. E., Dunaway, D. L., Lilienfeld, D. H., Craighead, H. G., & Pollack, G. H. (1998). Microfabricated cantilevers for measurement of subcellular and molecular forces. *IEEE Trans.Biomed.Eng*, 45(7), 891-898.
- Fenn, W. O. (1923). A quantitative comparison between the energy liberated and the work performed by the isolated sartorius muscle of the frog. *J.Physiol*, 58(2-3), 175-203.
- Fenn, W. O. (1924). The relation between the work performed and the energy liberated in muscular contraction. *J.Physiol*, 58(6), 373-395.
- Finer, J. T., Simmons, R. M., & Spudich, J. A. (1994). Single myosin molecule mechanics: piconewton forces and nanometre steps. *Nature*, 368(6467), 113-119.
- Fisher, A. J., Smith, C. A., Thoden, J. B., Smith, R., Sutoh, K., Holden, H. M., & Rayment, I. (1995). X-ray structures of the myosin motor domain of Dictyostelium discoideum complexed with MgADP.BeFx and MgADP.AlF₄. *Biochemistry*, 34(28), 8960-8972.
- Forgacs, E., Sakamoto, T., Cartwright, S., Belknap, B., Kovacs, M., Toth, J., . . . White, H. D. (2009). Switch 1 Mutation S217A Converts Myosin V into a Low Duty Ratio Motor.

- J.Biol.Chem.*, 284(4), 2138-2149.
- Fujii, T., Iwane, A. H., Yanagida, T., & Namba, K. (2010). Direct visualization of secondary structures of F-actin by electron cryomicroscopy. *Nature*, 467(7316), 724-728. doi:10.1038/nature09372
- Fujita-Becker, S., Reubold, T. F., & Holmes, K. C. (2006). The actin-binding cleft: functional characterisation of myosin II with a strut mutation. *J Muscle Res Cell Motil*, 27(2), 115-123. doi:10.1007/s10974-005-9047-0
- Geeves, M. A., & Conibear, P. B. (1995). The role of three-state docking of myosin S1 with actin in force generation. *Biophys J*, 68(4 Suppl), 194S-199S; discussion 199S-201S.
- Geeves, M. A., & Gutfreund, H. (1982). The use of pressure perturbations to investigate the interaction of rabbit muscle myosin subfragment 1 with actin in the presence of MgADP. *FEBS Lett*, 140(1), 11-15.
- Geeves, M. A., & Holmes, K. C. (1999). Structural mechanism of muscle contraction. *Annu.Rev.Biochem.*, 68, 687-728.
- Geeves, M. A., & Holmes, K. C. (2005). The molecular mechanism of muscle contraction. *Adv.Protein Chem.*, 71, 161-193.
- Geeves, M. A., & Jeffries, T. E. (1988). The effect of nucleotide upon a specific isomerization of actomyosin subfragment 1. *Biochem J*, 256(1), 41-46.
- Gergely, J., Gouvea, M. A., & Karibian, D. (1955). Fragmentation of myosin by chymotrypsin. *J Biol Chem*, 212(1), 165-177.
- Getz, E. B., Cooke, R., & Lehman, S. L. (1998). Phase transition in force during ramp stretches of skeletal muscle. *Biophys.J.*, 75(6), 2971-2983.
- Goldman, Y. E., & Brenner, B. (1987). Special topic: molecular mechanism of muscle contraction. General introduction. *Annu.Rev.Physiol*, 49, 629-636.
- Gollub, J., Cremo, C. R., & Cooke, R. (1996). ADP release produces a rotation of the neck region of smooth myosin but not skeletal myosin. *Nat.Struct.Biol.*, 3(9), 796-802.
- Goodson, H. V., Warrick, H. M., & Spudich, J. A. (1999). Specialized conservation of surface loops of myosin: evidence that loops are involved in determining functional characteristics. *J.Mol.Biol.*, 287(1), 173-185.
- Gordon, A. M., Homsher, E., & Regnier, M. (2000). Regulation of contraction in striated muscle. *Physiol Rev.*, 80(2), 853-924.
- Greaser, M. L., & Gergely, J. (1971). Reconstitution of troponin activity from three protein

- components. *J Biol Chem*, 246(13), 4226-4233.
- Greenberg, M. J., & Moore, J. R. (2010). The molecular basis of frictional loads in the in vitro motility assay with applications to the study of the loaded mechanochemistry of molecular motors. *Cytoskeleton (Hoboken)*, 67(5), 273-285. doi:10.1002/cm.20441
- Grichko, V. P., Gettelman, G. J., Widrick, J. J., & Fitts, R. H. (1999). Substrate and enzyme profile of fast and slow skeletal muscle fibers in rhesus monkeys. *J.Appl.Physiol*, 86(1), 335-340.
- Guilford, W. H., Dupuis, D. E., Kennedy, G., Wu, J., Patlak, J. B., & Warshaw, D. M. (1997). Smooth muscle and skeletal muscle myosins produce similar unitary forces and displacements in the laser trap. *Biophys.J.*, 72(3), 1006-1021.
- Gyimesi, M., Tsaturyan, A. K., Kellermayer, M. S., & Malnasi-Csizmadia, A. (2008). Kinetic characterization of the function of myosin loop 4 in the actin-myosin interaction. *Biochemistry*, 47(1), 283-291. doi:10.1021/bi701554a
- Haerberle, J. R., Trybus, K. M., Hemric, M. E., & Warshaw, D. M. (1992). The effects of smooth muscle caldesmon on actin filament motility. *J Biol Chem*, 267(32), 23001-23006.
- Harrington, W. F., Von Hippel, P. H., & Mihalyi, E. (1959). Proteolytic enzymes as probes of the secondary structure of fibrous proteins. *Biochim Biophys Acta*, 32(1), 303-304.
- Harris, D. E., Work, S. S., Wright, R. K., Alpert, N. R., & Warshaw, D. M. (1994). Smooth, cardiac and skeletal muscle myosin force and motion generation assessed by cross-bridge mechanical interactions in vitro. *J Muscle Res Cell Motil*, 15(1), 11-19.
- Herman, I. M. (1993). Actin isoforms. *Curr Opin Cell Biol*, 5(1), 48-55.
- Hilbert, L., Balassy, Z., Zitouni, N. B., Mackey, M. C., & Lauzon, A. M. (2015). Phosphate and ADP differently inhibit coordinated smooth muscle myosin groups. *Biophys J*, 108(3), 622-631. doi:10.1016/j.bpj.2014.12.008
- Hilbert, L., Bates, G., Roman, H. N., Blumenthal, J. L., Zitouni, N. B., Sobieszek, A., . . . Lauzon, A. M. (2013). Molecular mechanical differences between isoforms of contractile actin in the presence of isoforms of smooth muscle tropomyosin. *PLoS Comput Biol*, 9(10), e1003273. doi:10.1371/journal.pcbi.1003273
- Hill, A. V. (1938). The heat of shortening and the dynamic constants of muscle. *Proceedings of the Royal Society B-Biological Sciences*, 126(843), 136-195.
- Hodges, R. S., & Smillie, L. B. (1972). Cysteine sequences of rabbit skeletal tropomyosin. *Can J Biochem*, 50(3), 330-343.

- Holmes, K. C., Angert, I., Kull, F. J., Jahn, W., & Schroder, R. R. (2003). Electron cryo-microscopy shows how strong binding of myosin to actin releases nucleotide. *Nature*, 425(6956), 423-427. doi:10.1038/nature02005
- Holmes, K. C., & Geeves, M. A. (2000). The structural basis of muscle contraction. *Philos Trans R Soc Lond B Biol Sci*, 355(1396), 419-431. doi:10.1098/rstb.2000.0583
- Holmes, K. C., Schroder, R. R., Sweeney, H. L., & Houdusse, A. (2004). The structure of the rigor complex and its implications for the power stroke. *Philos.Trans.R.Soc.Lond B Biol.Sci.*, 359(1452), 1819-1828.
- Homsher, E., Wang, F., & Sellers, J. R. (1992). Factors affecting movement of F-actin filaments propelled by skeletal muscle heavy meromyosin. *Am.J.Physiol*, 262(3 Pt 1), C714-C723.
- Huxley, A. F. (1957). Muscle structure and theories of contraction. *Prog.Biophys.Biophys.Chem.*, 7, 255-318.
- Huxley, A. F., & Niedergerke, R. (1954). Measurement of muscle striations in stretch and contraction. *J.Physiol*, 124(2), 46-47P.
- Huxley, A. F., & Simmons, R. M. (1971). Proposed mechanism of force generation in striated muscle. *Nature*, 233(5321), 533-538.
- Huxley, H., & Hanson, J. (1954). Changes in the cross-striations of muscle during contraction and stretch and their structural interpretation. *Nature*, 173(4412), 973-976.
- Huxley, H. E. (1969). The mechanism of muscular contraction. *Science*, 164(886), 1356-1365.
- Ishijima, A., Kojima, H., Higuchi, H., Harada, Y., Funatsu, T., & Yanagida, T. (1996). Multiple- and single-molecule analysis of the actomyosin motor by nanometer-piconewton manipulation with a microneedle: unitary steps and forces. *Biophys.J.*, 70(1), 383-400.
- Izumo, S., Nadal-Ginard, B., & Mahdavi, V. (1986). All members of the MHC multigene family respond to thyroid hormone in a highly tissue-specific manner. *Science*, 231(4738), 597-600.
- Janson, L. W., Sellers, J. R., & Taylor, D. L. (1992). Actin-binding proteins regulate the work performed by myosin II motors on single actin filaments. *Cell Motil.Cytoskeleton*, 22(4), 274-280.
- Joel, P. B., Sweeney, H. L., & Trybus, K. M. (2003). Addition of lysines to the 50/20 kDa junction of myosin strengthens weak binding to actin without affecting the maximum ATPase activity. *Biochemistry*, 42(30), 9160-9166.
- Joel, P. B., Trybus, K. M., & Sweeney, H. L. (2001). Two conserved lysines at the 50/20-kDa

- junction of myosin are necessary for triggering actin activation. *J.Biol.Chem.*, 276(5), 2998-3003.
- Kabsch, W., Mannherz, H. G., Suck, D., Pai, E. F., & Holmes, K. C. (1990). Atomic structure of the actin:DNase I complex. *Nature*, 347(6288), 37-44. doi:10.1038/347037a0
- Kalaganov, A., Novinger, R., & Rassier, D. E. (2010). A technique for simultaneous measurement of force and overlap between single muscle filaments of myosin and actin. *Biochem Biophys Res Commun*, 403(3-4), 351-356. doi:10.1016/j.bbrc.2010.11.034
- Kalaganov, A., Shalabi, N., Zitouni, N., Kachmar, L. H., Lauzon, A. M., & Rassier, D. E. (2013a). Forces measured with micro-fabricated cantilevers during actomyosin interactions produced by filaments containing different myosin isoforms and loop 1 structures. *Biochim Biophys Acta*, 1830(3), 2710-2719. doi:10.1016/j.bbagen.2012.11.022
- Kalaganov, A., Shalabi, N., Zitouni, N., Kachmar, L. H., Lauzon, A. M., & Rassier, D. E. (2013b). Forces measured with micro-fabricated cantilevers during actomyosin interactions produced by filaments containing different myosin isoforms and loop 1 structures. *Biochim Biophys Acta*, 1830(3), 2710-2719.
- Karatzafiri, C., Chinn, M. K., & Cooke, R. (2004). The force exerted by a muscle cross-bridge depends directly on the strength of the actomyosin bond. *Biophys.J.*, 87(4), 2532-2544.
- Kaya, M., & Higuchi, H. (2010). Nonlinear elasticity and an 8-nm working stroke of single myosin molecules in myofilaments. *Science*, 329(5992), 686-689. doi:10.1126/science.1191484
- Kaya, M., & Higuchi, H. (2013). Stiffness, working stroke, and force of single-myosin molecules in skeletal muscle: elucidation of these mechanical properties via nonlinear elasticity evaluation. *Cell Mol Life Sci*, 70(22), 4275-4292. doi:10.1007/s00018-013-1353-x
- Kaya, M., Tani, Y., Washio, T., Hisada, T., & Higuchi, H. (2017). Coordinated force generation of skeletal myosins in myofilaments through motor coupling. *Nat Commun*, 8, 16036. doi:10.1038/ncomms16036
- Kelley, C. A., Takahashi, M., Yu, J. H., & Adelstein, R. S. (1993). An insert of seven amino acids confers functional differences between smooth muscle myosins from the intestines and vasculature. *J.Biol.Chem.*, 268(17), 12848-12854.
- Kintses, B., Gyimesi, M., Pearson, D. S., Geeves, M. A., Zeng, W., Bagshaw, C. R., & Malnasi-Csizmadia, A. (2007). Reversible movement of switch 1 loop of myosin determines actin interaction. *EMBO J*, 26(1), 265-274. doi:10.1038/sj.emboj.7601482

- Knetsch, M. L., Uyeda, T. Q., & Manstein, D. J. (1999). Disturbed communication between actin- and nucleotide-binding sites in a myosin II with truncated 50/20-kDa junction. *J.Biol.Chem.*, 274(29), 20133-20138.
- Konishi, M., & Watanabe, M. (1998). Steady state relation between cytoplasmic free Ca²⁺ concentration and force in intact frog skeletal muscle fibers. *J Gen Physiol*, 111(4), 505-519. doi:10.1085/jgp.111.4.505
- Koppole, S., Smith, J. C., & Fischer, S. (2007). The structural coupling between ATPase activation and recovery stroke in the myosin II motor. *Structure*, 15(7), 825-837. doi:10.1016/j.str.2007.06.008
- Kron, S. J., & Spudich, J. A. (1986). Fluorescent actin filaments move on myosin fixed to a glass surface. *Proc.Natl.Acad.Sci.U.S.A*, 83(17), 6272-6276.
- Kron, S. J., Toyoshima, Y. Y., Uyeda, T. Q., & Spudich, J. A. (1991). Assays for actin sliding movement over myosin-coated surfaces. *Methods Enzymol.*, 196, 399-416.
- Kron, S. J., Uyeda, T. Q., Warrick, H. M., & Spudich, J. A. (1991). An approach to reconstituting motility of single myosin molecules. *J.Cell.Sci.Suppl*, 14, 129-133.
- Kühne, W. (1864). *Untersuchungen über das Protoplasma und die Contractilität* (Vol. Vii): W. Engelmann.
- Kull, F. J., Vale, R. D., & Fletterick, R. J. (1998). The case for a common ancestor: kinesin and myosin motor proteins and G proteins. *J Muscle Res Cell Motil*, 19(8), 877-886.
- Kurzawa-Goertz, S. E., Perreault-Micale, C. L., Trybus, K. M., Szent-Gyorgyi, A. G., & Geeves, M. A. (1998). Loop I can modulate ADP affinity, ATPase activity, and motility of different scallop myosins. Transient kinetic analysis of S1 isoforms. *Biochemistry*, 37(20), 7517-7525. doi:10.1021/bi972844+
- Kurzban, G. P., & Wang, K. (1988). Giant polypeptides of skeletal muscle titin: sedimentation equilibrium in guanidine hydrochloride. *Biochem Biophys Res Commun*, 150(3), 1155-1161.
- Labeit, S., Ottenheijm, C. A., & Granzier, H. (2011). Nebulin, a major player in muscle health and disease. *FASEB J*, 25(3), 822-829. doi:10.1096/fj.10-157412
- Laemmli, U. K. (1970). Cleavage of structural proteins during the assembly of the head of bacteriophage T4. *Nature*, 227(5259), 680-685.
- Lauzon, A. M., Bates, J. H., Donovan, G., Tawhai, M., Sneyd, J., & Sanderson, M. J. (2012). A multi-scale approach to airway hyperresponsiveness: from molecule to organ. *Front*

Physiol, 3, 191. doi:10.3389/fphys.2012.00191

- Lauzon, A. M., Trybus, K. M., & Warshaw, D. M. (1998). Molecular mechanics of two smooth muscle heavy meromyosin constructs that differ by an insert in the motor domain. *Acta Physiol Scand.*, 164(4), 357-361.
- Lauzon, A. M., Tyska, M. J., Rovner, A. S., Freyzone, Y., Warshaw, D. M., & Trybus, K. M. (1998). A 7-amino-acid insert in the heavy chain nucleotide binding loop alters the kinetics of smooth muscle myosin in the laser trap. *J.Muscle Res.Cell Motil.*, 19(8), 825-837.
- Leguillette, R., Gil, F. R., Zitouni, N., Lajoie-Kadoch, S., Sobieszek, A., & Lauzon, A. M. (2005). (+)Insert smooth muscle myosin heavy chain (SM-B) isoform expression in human tissues. *Am.J.Physiol Cell Physiol*, 289(5), C1277-C1285.
- Lehman, W., Craig, R., & Vibert, P. (1994). Ca(2+)-induced tropomyosin movement in Limulus thin filaments revealed by three-dimensional reconstruction. *Nature*, 368(6466), 65-67.
- Levi-Valensin, G., Petit-Perrin, M., Amouroux, J., Caroit, M., Hubault, A., Denis, A., . . . Ryckewaert, A. (1979). [Synovial sarcoma]. *Ann Radiol (Paris)*, 22(1), 45-52.
- Linari, M., Caremani, M., Piperio, C., Brandt, P., & Lombardi, V. (2007). Stiffness and fraction of Myosin motors responsible for active force in permeabilized muscle fibers from rabbit psoas. *Biophys.J.*, 92(7), 2476-2490.
- Liu, X., & Pollack, G. H. (2002). Mechanics of F-actin characterized with microfabricated cantilevers. *Biophys.J.*, 83(5), 2705-2715.
- Liu, X., & Pollack, G. H. (2004). Stepwise sliding of single actin and Myosin filaments. *Biophys.J.*, 86(1 Pt 1), 353-358.
- Lohmann, K. (1934). Über die enzymatische ausspaltung der kreatinephosphorsaure; zugleich ein beitrage zum chemismus der muskelkontraktion. *Biochem. Z*, 271, 264-277.
- Low, R., Leguillette, R., & Lauzon, A. M. (2006). (+)Insert smooth muscle myosin heavy chain (SM-B): from single molecule to human. *Int.J.Biochem.Cell Biol.*, 38(11), 1862-1874.
- Lowey, S., Bretton, V., Joel, P. B., Trybus, K. M., Gulick, J., Robbins, J., . . . Rassier, D. E. (2018). Hypertrophic cardiomyopathy R403Q mutation in rabbit beta-myosin reduces contractile function at the molecular and myofibrillar levels. *Proc Natl Acad Sci U S A*, 115(44), 11238-11243. doi:10.1073/pnas.1802967115
- Lowey, S., Lesko, L. M., Rovner, A. S., Hodges, A. R., White, S. L., Low, R. B., . . . Robbins, J. (2008). Functional effects of the hypertrophic cardiomyopathy R403Q mutation are

- different in an alpha- or beta-myosin heavy chain backbone. *J.Biol.Chem.*, 283(29), 20579-20589.
- Luther, P. K. (2009). The vertebrate muscle Z-disc: sarcomere anchor for structure and signalling. *J Muscle Res Cell Motil*, 30(5-6), 171-185. doi:10.1007/s10974-009-9189-6
- Lymn, R. W., & Taylor, E. W. (1971). Mechanism of adenosine triphosphate hydrolysis by actomyosin. *Biochemistry*, 10(25), 4617-4624.
- Mansson, A., Rassier, D., & Tsiavaliaris, G. (2015). Poorly understood aspects of striated muscle contraction. *Biomed Res Int*, 2015, 245154. doi:10.1155/2015/245154
- Marieb, E. N., & Hoehn, K. (2008). *Human Anatomy & Physiology* (3 ed.): Pearson/Benjamin Cummings.
- Maruyama, K., Kimura, S., Yoshidomi, H., Sawada, H., & Kikuchi, M. (1984). Molecular size and shape of beta-connectin, an elastic protein of striated muscle. *J Biochem*, 95(5), 1423-1433.
- Matusovsky, O. S., Dobrzhanskaya, A. V., Pankova, V. V., Kiselev, K. V., Girich, U. V., & Shelud'ko, N. S. (2017). Crenomytilus grayanus 40kDa calponin-like protein: cDNA cloning, sequence analysis, tissue expression, and post-translational modifications. *Comp Biochem Physiol Part D Genomics Proteomics*, 22, 98-108. doi:10.1016/j.cbd.2017.02.006
- Mentes, A., Huehn, A., Liu, X., Zwolak, A., Dominguez, R., Shuman, H., . . . Sindelar, C. V. (2018). High-resolution cryo-EM structures of actin-bound myosin states reveal the mechanism of myosin force sensing. *Proc Natl Acad Sci U S A*, 115(6), 1292-1297. doi:10.1073/pnas.1718316115
- Mermall, V., Post, P. L., & Mooseker, M. S. (1998). Unconventional myosins in cell movement, membrane traffic, and signal transduction. *Science*, 279(5350), 527-533.
- Miller, C. J., Cheung, P., White, P., & Reisler, E. (1995). Actin's view of actomyosin interface. *Biophys J*, 68(4 Suppl), 50S-54S.
- Minozzo, F., & Rassier, D. E. (2013). Myosin Family Classification. *Encyclopedia of Biophysics*. doi:10.1007/978-3-642-16712-6
- Minozzo, F. C., Altman, D., & Rassier, D. E. (2015). MgADP activation contributes to force enhancement during fast stretch of isolated skeletal myofibrils. *Biochem Biophys Res Commun*, 463(4), 1129-1134. doi:10.1016/j.bbrc.2015.06.070
- Minozzo, F. C., & Rassier, D. E. (2013). The effects of Ca²⁺ and MgADP on force development

- during and after muscle length changes. *PLoS One*, 8(7), e68866. doi:10.1371/journal.pone.0068866
- Molloy, J. E., Burns, J. E., Kendrick-Jones, J., Tregear, R. T., & White, D. C. (1995). Movement and force produced by a single myosin head. *Nature*, 378(6553), 209-212.
- Mornet, D., Bertrand, R., Pantel, P., Audemard, E., & Kassab, R. (1981). Structure of the actin-myosin interface. *Nature*, 292(5821), 301-306.
- Mornet, D., Pantel, P., Audemard, E., & Kassab, R. (1979). The limited tryptic cleavage of chymotryptic S-1: an approach to the characterization of the actin site in myosin heads. *Biochem Biophys Res Commun*, 89(3), 925-932.
- Murphy, C. T., & Spudich, J. A. (1998). Dictyostelium myosin 25-50K loop substitutions specifically affect ADP release rates. *Biochemistry*, 37(19), 6738-6744.
- Murphy, C. T., & Spudich, J. A. (1999). The sequence of the myosin 50-20K loop affects Myosin's affinity for actin throughout the actin-myosin ATPase cycle and its maximum ATPase activity. *Biochemistry*, 38(12), 3785-3792.
- Murphy, C. T., & Spudich, J. A. (2000). Variable surface loops and myosin activity: accessories to a motor. *J.Muscle Res.Cell Motil.*, 21(2), 139-151.
- Needham, D. M., & Williams, J. M. (1963). Proteins of the Uterine Contractile Mechanism. *Biochem J*, 89, 552-561.
- Neumann, T., Fauver, M., & Pollack, G. H. (1998). Elastic properties of isolated thick filaments measured by nanofabricated cantilevers. *Biophys.J.*, 75(2), 938-947.
- Nikolaeva, O. P., Orlov, V. N., Bobkov, A. A., & Levitsky, D. I. (2002). Differential scanning calorimetric study of myosin subfragment 1 with tryptic cleavage at the N-terminal region of the heavy chain. *Eur J Biochem*, 269(22), 5678-5688.
- Odrionitz, F., & Kollmar, M. (2007). Drawing the tree of eukaryotic life based on the analysis of 2,269 manually annotated myosins from 328 species. *Genome Biol*, 8(9), R196. doi:10.1186/gb-2007-8-9-r196
- Ohtsuki, I. (1979). Molecular arrangement of troponin-T in the thin filament. *J Biochem*, 86(2), 491-497.
- Pearson, T., McArdle, A., & Jackson, M. J. (2015). Nitric oxide availability is increased in contracting skeletal muscle from aged mice, but does not differentially decrease muscle superoxide. *Free Radic Biol Med*, 78, 82-88. doi:10.1016/j.freeradbiomed.2014.10.505
- Perreault-Micale, C. L., Kalabokis, V. N., Nyitray, L., & Szent-Gyorgyi, A. G. (1996). Sequence

- variations in the surface loop near the nucleotide binding site modulate the ATP turnover rates of molluscan myosins. *J Muscle Res Cell Motil*, 17(5), 543-553.
- Pertici, I., Bongini, L., Melli, L., Bianchi, G., Salvi, L., Falorsi, G., . . . Bianco, P. (2018). A myosin II nanomachine mimicking the striated muscle. *Nat Commun*, 9(1), 3532. doi:10.1038/s41467-018-06073-9
- Piazzesi, G., Lucii, L., & Lombardi, V. (2002). The size and the speed of the working stroke of muscle myosin and its dependence on the force. *J.Physiol*, 545(Pt 1), 145-151.
- Pierobon-Bormioli, S., Sartore, S., Libera, L. D., Vitadello, M., & Schiaffino, S. (1981). "Fast" isomyosins and fiber types in mammalian skeletal muscle. *J Histochem Cytochem*, 29(10), 1179-1188. doi:10.1177/29.10.7028858
- Polis, B. D., & Meyerhof, O. (1947). Studies on adenosinetriphosphatase in muscle; concentration of the enzyme on myosin. *J Biol Chem*, 169(2), 389-401.
- Rayment, I. (1996). The Structural Basis of the Myosin ATPase Activity. *Journal of Biological Chemistry*, 271(27), 15850-15853. doi:10.1074/jbc.271.27.15850
- Rayment, I., Holden, H. M., Sellers, J. R., Fananapazir, L., & Epstein, N. D. (1995). Structural interpretation of the mutations in the beta-cardiac myosin that have been implicated in familial hypertrophic cardiomyopathy. *Proc Natl Acad Sci U S A*, 92(9), 3864-3868.
- Rayment, I., Holden, H. M., Whittaker, M., Yohn, C. B., Lorenz, M., Holmes, K. C., & Milligan, R. A. (1993). Structure of the actin-myosin complex and its implications for muscle contraction. *Science*, 261(5117), 58-65.
- Rayment, I., Rypniewski, W. R., Schmidt-Base, K., Smith, R., Tomchick, D. R., Benning, M. M., . . . Holden, H. M. (1993). Three-dimensional structure of myosin subfragment-1: a molecular motor. *Science*, 261(5117), 50-58.
- Reconditi, M., Linari, M., Lucii, L., Stewart, A., Sun, Y. B., Boesecke, P., . . . Lombardi, V. (2004). The myosin motor in muscle generates a smaller and slower working stroke at higher load. *Nature*, 428(6982), 578-581.
- Rief, M., Rock, R. S., Mehta, A. D., Mooseker, M. S., Cheney, R. E., & Spudich, J. A. (2000). Myosin-V stepping kinetics: a molecular model for processivity. *Proc.Natl.Acad.Sci.U.S.A*, 97(17), 9482-9486.
- Rovner, A. S., Freyzon, Y., & Trybus, K. M. (1997). An insert in the motor domain determines the functional properties of expressed smooth muscle myosin isoforms. *J.Muscle Res.Cell Motil.*, 18(1), 103-110.

- Ruff, C., Furch, M., Brenner, B., Manstein, D. J., & Meyhofer, E. (2001). Single-molecule tracking of myosins with genetically engineered amplifier domains. *Nat.Struct.Biol.*, 8(3), 226-229.
- Ruppel, K. M., & Spudich, J. A. (1996). Structure-function studies of the myosin motor domain: importance of the 50-kDa cleft. *Mol.Biol.Cell*, 7(7), 1123-1136.
- Sasaki, N., Shimada, T., & Sutoh, K. (1998). Mutational analysis of the switch II loop of Dictyostelium myosin II. *J Biol Chem*, 273(32), 20334-20340.
- Schroder, R. R., Manstein, D. J., Jahn, W., Holden, H., Rayment, I., Holmes, K. C., & Spudich, J. A. (1993). Three-dimensional atomic model of F-actin decorated with Dictyostelium myosin S1. *Nature*, 364(6433), 171-174.
- Scott, W., Stevens, J., & Binder-Macleod, S. A. (2001). Human skeletal muscle fiber type classifications. *Phys Ther*, 81(11), 1810-1816.
- Sellers, J. R., & Goodson, H. V. (1995). Motor proteins 2: myosin. *Protein Profile.*, 2(12), 1323-1423.
- Shevchenko, A., Tomas, H., Havlis, J., Olsen, J. V., & Mann, M. (2006). In-gel digestion for mass spectrometric characterization of proteins and proteomes. *Nat Protoc*, 1(6), 2856-2860. doi:10.1038/nprot.2006.468
- Shimada, T., Sasaki, N., Ohkura, R., & Sutoh, K. (1997). Alanine scanning mutagenesis of the switch I region in the ATPase site of Dictyostelium discoideum myosin II. *Biochemistry*, 36(46), 14037-14043. doi:10.1021/bi971837i
- Siemankowski, R. F., Wiseman, M. O., & White, H. D. (1985). ADP dissociation from actomyosin subfragment 1 is sufficiently slow to limit the unloaded shortening velocity in vertebrate muscle. *Proc Natl Acad Sci U S A*, 82(3), 658-662.
- Smith, C. A., & Rayment, I. (1996). X-ray structure of the magnesium(II).ADP.vanadate complex of the Dictyostelium discoideum myosin motor domain to 1.9 Å resolution. *Biochemistry*, 35(17), 5404-5417. doi:10.1021/bi952633+
- Smith, D., & Sleep, J. (2006a). Strain-dependent kinetics of the myosin working stroke, and how they could be probed with optical-trap experiments. *Biophys.J.*, 91(9), 3359-3369.
- Smith, D., & Sleep, J. (2006b). Strain-dependent kinetics of the myosin working stroke, and how they could be probed with optical-trap experiments. *Biophys J*, 91(9), 3359-3369. doi:10.1529/biophysj.106.082289
- Smith, D. A., & Geeves, M. A. (1995). Strain-dependent cross-bridge cycle for muscle.

- Biophys.J.*, 69(2), 524-537.
- Spudich, J. A. (1994). How molecular motors work. *Nature*, 372(6506), 515-518.
- Stein, L. A., Schwarz, R. P., Jr., Chock, P. B., & Eisenberg, E. (1979). Mechanism of actomyosin adenosine triphosphatase. Evidence that adenosine 5'-triphosphate hydrolysis can occur without dissociation of the actomyosin complex. *Biochemistry*, 18(18), 3895-3909.
- Straub, F. B. (1943). *Actin, II*. (Vol. III). Stud Inst Med Chem Univ Szeged.
- Sun, Y. B., & Irving, M. (2010). The molecular basis of the steep force-calcium relation in heart muscle. *J Mol Cell Cardiol*, 48(5), 859-865. doi:10.1016/j.yjmcc.2009.11.019
- Sutoh, K. (1983). Mapping of actin-binding sites on the heavy chain of myosin subfragment 1. *Biochemistry*, 22(7), 1579-1585.
- Sweeney, H. L., & Houdusse, A. (2010). Structural and functional insights into the Myosin motor mechanism. *Annu Rev Biophys*, 39, 539-557. doi:10.1146/annurev.biophys.050708.133751
- Szent-Gyorgyi, A. G. (2004). The early history of the biochemistry of muscle contraction. *J Gen Physiol*, 123(6), 631-641. doi:10.1085/jgp.200409091
- Takagi, Y., Homsher, E. E., Goldman, Y. E., & Shuman, H. (2006). Force generation in single conventional actomyosin complexes under high dynamic load. *Biophys.J.*, 90(4), 1295-1307.
- Tanaka, H., Ishijima, A., Honda, M., Saito, K., & Yanagida, T. (1998). Orientation dependence of displacements by a single one-headed myosin relative to the actin filament. *Biophys.J.*, 75(4), 1886-1894.
- Thompson, L. V., Lowe, D. A., Ferrington, D. A., & Thomas, D. D. (2001). Electron paramagnetic resonance: a high-resolution tool for muscle physiology. *Exerc Sport Sci Rev*, 29(1), 3-6.
- Tsiavaliaris, G., Fujita-Becker, S., Batra, R., Levitsky, D. I., Kull, F. J., Geeves, M. A., & Manstein, D. J. (2002). Mutations in the relay loop region result in dominant-negative inhibition of myosin II function in Dictyostelium. *EMBO Rep*, 3(11), 1099-1105. doi:10.1093/embo-reports/kvf214
- Tuck, S. A., Maghni, K., Poirier, A., Babu, G. J., Periasamy, M., Bates, J. H., . . . Lauzon, A. M. (2004). Time course of airway mechanics of the (+)insert myosin isoform knockout mouse. *Am.J.Respir.Cell Mol.Biol.*, 30(3), 326-332.
- Tyska, M. J., Dupuis, D. E., Guilford, W. H., Patlak, J. B., Waller, G. S., Trybus, K. M., . . .

- Lowey, S. (1999a). Two heads of myosin are better than one for generating force and motion. *Proc.Natl.Acad.Sci.U.S.A*, 96(8), 4402-4407.
- Tyska, M. J., Dupuis, D. E., Guilford, W. H., Patlak, J. B., Waller, G. S., Trybus, K. M., . . . Lowey, S. (1999b). Two heads of myosin are better than one for generating force and motion. *Proc Natl Acad Sci U S A*, 96(8), 4402-4407.
- Umemoto, S., & Sellers, J. R. (1990). Characterization of in vitro motility assays using smooth muscle and cytoplasmic myosins. *J.Biol.Chem.*, 265(25), 14864-14869.
- Uyeda, T. Q., Patterson, B., Mendoza, L., & Hiratsuka, Y. (2002). Amino acids 519-524 of Dictyostelium myosin II form a surface loop that aids actin binding by facilitating a conformational change. *J.Muscle Res.Cell Motil.*, 23(7-8), 685-695.
- Uyeda, T. Q., Ruppel, K. M., & Spudich, J. A. (1994). Enzymatic activities correlate with chimaeric substitutions at the actin-binding face of myosin. *Nature*, 368(6471), 567-569.
- Veigel, C., Coluccio, L. M., Jontes, J. D., Sparrow, J. C., Milligan, R. A., & Molloy, J. E. (1999). The motor protein myosin-I produces its working stroke in two steps. *Nature*, 398(6727), 530-533.
- Veigel, C., Molloy, J. E., Schmitz, S., & Kendrick-Jones, J. (2003). Load-dependent kinetics of force production by smooth muscle myosin measured with optical tweezers. *Nat.Cell Biol.*, 5(11), 980-986.
- Veigel, C., Schmitz, S., Wang, F., & Sellers, J. R. (2005). Load-dependent kinetics of myosin-V can explain its high processivity. *Nat.Cell Biol.*, 7(9), 861-869.
- Veigel, C., Wang, F., Bartoo, M. L., Sellers, J. R., & Molloy, J. E. (2002). The gated gait of the processive molecular motor, myosin V. *Nat.Cell Biol.*, 4(1), 59-65.
- Visscher, K., Schnitzer, M. J., & Block, S. M. (1999). Single kinesin molecules studied with a molecular force clamp. *Nature*, 400(6740), 184-189.
- Volkman, N., Hanein, D., Ouyang, G., Trybus, K. M., DeRosier, D. J., & Lowey, S. (2000). Evidence for cleft closure in actomyosin upon ADP release. *Nat Struct Biol*, 7(12), 1147-1155. doi:10.1038/82008
- von der Ecken, J., Heissler, S. M., Pathan-Chhatbar, S., Manstein, D. J., & Raunser, S. (2016). Cryo-EM structure of a human cytoplasmic actomyosin complex at near-atomic resolution. *Nature*, 534(7609), 724-728. doi:10.1038/nature18295
- von der Ecken, J., Muller, M., Lehman, W., Manstein, D. J., Penczek, P. A., & Raunser, S. (2015). Structure of the F-actin-tropomyosin complex. *Nature*, 519(7541), 114-117.

doi:10.1038/nature14033

- Warshaw, D. M., Desrosiers, J. M., Work, S. S., & Trybus, K. M. (1990). Smooth muscle myosin cross-bridge interactions modulate actin filament sliding velocity in vitro. *J Cell Biol*, *111*(2), 453-463.
- Weber, H. H. (1935). Der Feinbau und die mechanischen Eigenschaften des Myosinfadens. *Springer-Verlag*, *235*(1), 205-233. doi:<https://doi.org/10.1007/BF01764179>
- Wegner, A., & Isenberg, G. (1983). 12-fold difference between the critical monomer concentrations of the two ends of actin filaments in physiological salt conditions. *Proc Natl Acad Sci U S A*, *80*(16), 4922-4925.
- Weiss, S., Rossi, R., Pellegrino, M. A., Bottinelli, R., & Geeves, M. A. (2001). Differing ADP release rates from myosin heavy chain isoforms define the shortening velocity of skeletal muscle fibers. *J.Biol.Chem.*, *276*(49), 45902-45908.
- White, S. L., Zhou, M. Y., Low, R. B., & Periasamy, M. (1998). Myosin heavy chain isoform expression in rat smooth muscle development. *Am J Physiol*, *275*(2 Pt 1), C581-589.
- Wieczorek, D. F., Periasamy, M., Butler-Browne, G. S., Whalen, R. G., & Nadal-Ginard, B. (1985). Co-expression of multiple myosin heavy chain genes, in addition to a tissue-specific one, in extraocular musculature. *J Cell Biol*, *101*(2), 618-629.
- Witt, C. C., Burkart, C., Labeit, D., McNabb, M., Wu, Y., Granzier, H., & Labeit, S. (2006). Nebulin regulates thin filament length, contractility, and Z-disk structure in vivo. *EMBO J*, *25*(16), 3843-3855.
- Yamada, A., Ishii, N., Shimmen, T., & Takahashi, K. (1989). Mg-ATPase activity and motility of native thick filaments isolated from the anterior byssus retractor muscle of *Mytilus edulis*. *J Muscle Res Cell Motil*, *10*(2), 124-134.
- Yamada, T., Mishima, T., Sakamoto, M., Sugiyama, M., Matsunaga, S., & Wada, M. (2006). Oxidation of myosin heavy chain and reduction in force production in hyperthyroid rat soleus. *J.Appl.Physiol*, *100*(5), 1520-1526.
- Yang, Y., Gourinath, S., Kovacs, M., Nyitray, L., Reutzler, R., Himmel, D. M., . . . Cohen, C. (2007). Rigor-like structures from muscle myosins reveal key mechanical elements in the transduction pathways of this allosteric motor. *Structure*, *15*(5), 553-564. doi:10.1016/j.str.2007.03.010
- Young, D. M., Himmelfarb, S., & Harrington, W. F. (1964). The Relationship of the Meromyosins to the Molecular Structure of Myosin. *J Biol Chem*, *239*, 2822-2829.

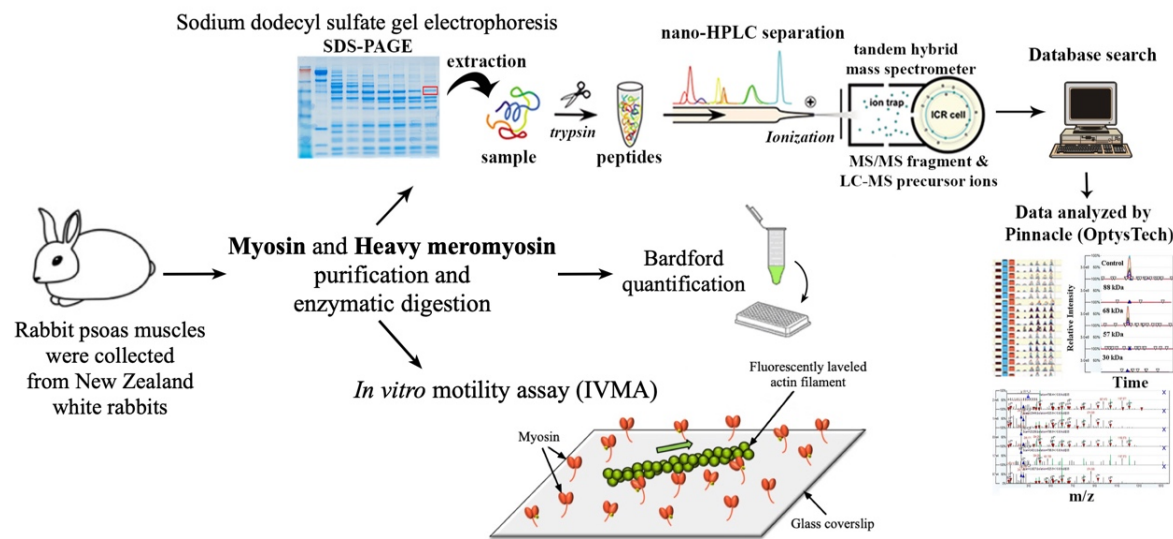
CHAPTER 5 –APPENDICES AND SUPPLEMENTAL INFORMATION

12. Supplemental Information

12.1. Detailed protocols and methods for the experimental study 2

12.1.1 Rationale

Muscle contraction is the result of cyclic interactions of protein filaments driven by energy released from adenosine triphosphate (ATP) hydrolysis for biological motility. Thin (actin-formed) filaments and the thick (myosin-formed) filaments that both are well organized into a crystalline hexagonal arrangement. These organized arrangement of the proteins plays an important role in active and passive force generation for muscle movement; there are many regions and loops accompany myosin interacts with actin. Loop 1 and loop 2, mainly, regulating the specific kinetic characteristics. The aims of this study were to investigate the effects of cleavage of loops 1 and 2 on the amino-acid structure of the myosin and to correlate these changes with myosin function by several methods and protocols. Our methods and protocols report myosin and heavy meromyosin (HMM) isolation from skeletal muscle, Bradford test, sodium dodecyl sulfate polyacrylamide gel electrophoresis (SDS-PAGE), in-vitro motility assay (IVMA) and mass spectrometry (MS). These methods were used to validate the loop 1 and loop 2 digestion from the myosin molecule.



Supplementary Figure 1. A flowchart of experimental study 2

12.1.2 Method details

Myosin preparation

Materials

- Rabbit psoas muscle, collected from New Zealand White rabbits. The study was approved by the animal ethic committee of McGill University
- Hasselbalch-Schneider buffer was prepared from 0.1 M $\text{KH}_2\text{PO}_4/\text{K}_2\text{HPO}_4$ at pH 6.4; 0.6 M KCl, 10 mM $\text{Na}_4\text{P}_2\text{O}_7 \cdot 10\text{H}_2\text{O}$, 1 mM MgCl_2 , and 20 mM ethylene glycol tetra-acetic acid.
- Omni mixer homogenizer (Omni International, Inc., Georgia, USA).
- 55mm hardened circle filter paper (No. 54, GE healthcare companies, UK).
- Buffer B was prepared from 20mM K_2HPO_4 at pH 7.2; 0.12M KCl; 1mM EDTA and 1mM DL-Dithiothreitol (DTT).
- buffer C was prepared from 50mM Sodium pyrophosphate and 1mM DTT at pH 7.8.

Procedure

1. 5 grams of psoas muscle tissue were homogenized with 15mL of Hasselbalch-Schneider buffer using an Omni mixer homogenizer.
2. The solution was stirred continuously for 15 min at 4°C, and the myosin extraction was stopped by the addition of 20 mL of distilled water at 4°C.
3. The mixture was centrifuged at 3,000×g for 10 min, while the supernatant (myosin solution) was filtrated through a 55mm hardened circle filter paper.
4. The filtrate was next diluted two-fold by distilled water at 4°C and centrifuged at 10,000×g for 15 min.
5. The resulting pellet was washed with buffer B, then re-suspended in 5 mL of buffer C, and centrifuged at 10,000×g for an additional 10 min.
6. The supernatant was filtered by hardened circle filter paper, and the myosin solution was kept on ice and stored at 4°C until the time of the experiment.

Myosin purification protocol has been previously described with minor modifications (Kalganov et al., 2013a).

Heavy meromyosin (HMM) preparation

Materials

- Solution 1: 0.1 mM NaHCO₃, 0.1 mM EGTA, and 1 mM DTT.
- Solution 2: 20 mM imidazole-HCl, 1 M KCl, 4 mM MgCl₂, and 10 mM DTT, pH 7.4.
- α-chymotrypsin (C-3142; Sigma-Aldrich, Canada).

- Water bath (2239-Isotemp®, Fisher Science, USA)

Procedure

1. Myosin stock was diluted in nine volumes of solution 1, left in ice for 15 min, and centrifuged at 25,000×g for 10 min.
2. The pellet was dissolved in an equal volume of solution 2. After a 10 minutes period of incubation at 25°C in a water bath, α -chymotrypsin was added to the solution to reach a final concentration of 12.5 μ g/ml. Molar ratio of enzyme to myosin equal to 1:50.
3. After 10 min of incubation, the solution was diluted in nine volumes of solution 1, mixed with 3 mM MgCl₂ and 0.1 mM PMSF, and kept in ice for 1 hour.
4. The suspension was centrifuged at 25,000×g for 90 min.
5. The supernatant containing HMM was collected and stored in ice for no more than 3 days before being used for experiments.

HMM preparation was adapted from a previous study (Kron, Uyeda, et al., 1991) and used to study loop 1 and loop 2 peptides content during proteolysis.

Quantification of proteins by Bradford method

Materials

- Quick Start™ Bradford 1x Dye Reagent (#5000205, BIO-RAD, Canada)
- Microplate reader (iMark Microplate Absorbance Reader, Bio Rad, USA).
- 96-Well Flat-Bottom EIA Plate (#2240096, Costar, BIO-RAD, Canada)

- Quick Start™ Bovine Serum Albumin (BSA) Standard (#5000206, BIO-RAD, Canada)

Procedure

Bradford method is used to quantify the amount of total protein (Myosin and HMM) in the solution (Bradford, 1976).

1. Prepare eight dilution of BSA standard solution buffer (1mL each) with a range, from 0, 0.03125, 0.0625, 0.125, 0.25, 0.5, 1 and 2 mg/mL.
2. Pipet 20uL of each standard and sample solution (unknown concentration of protein) into a dry 96-Well Flat-Bottom EIA Plate. Protein solutions are assayed in duplicate.
3. Add 200µl of Quick Start™ Bradford 1x Dye Reagent to each well and vortex for 5 second.
4. Measure absorbance of protein solution at 595nm by a microplate reader and calculate the protein concentration from BSA calibration curve.

Examination of protein purity by sodium dodecyl sulfate polyacrylamide gel electrophoresis (SDS-PAGE)

SDS-PAGE is commonly used for the separation of proteins based on the molecular weight (Laemmli, 1970).

Materials

- TEMED (Electrophoresis Grade, BioShop Canada)

- Acrylamide/Bis-acrylamide, 30% solution (BioReagent, suitable for electrophoresis, 29:1, A-3574; Sigma-Aldrich, Canada)
- Sodium Dodecyl Sulfate, (Powder, #1610302, BIO-RAD, Canada)
- Gel slab (Mini Protein® electrophoresis-BioRad, USA).
- SimpltBlue™ Safe Stain (Invitrogen, Carlsbad, CA).
- Molecular weight standards (SeeBlue™ Plus2 Pre-stained Protein Standard, LC5925, Thermo Fisher Scientific, Canada).
- 10% acrylamide resolving gel (H₂O 5235μL, Acrylamide/Bis-acrylamide mix 30% solution, 6665μl, 1.5M Tris at pH 8.8, 7500μL, 10% SDS 400μl, 100μL ammonium persulfate (APS) and 100μL TEMED)
- 4% acrylamide loading gel (H₂O 4400μL, Acrylamide/Bis-acrylamide mix 30% solution, 1360μl, 1.5M Tris at pH 6.8, 2000μL, 10% SDS 160μl, Ammonium persulfate (APS) 40μL and TEMED 40μL)

Procedure

SDS-PAGE was performed to determine the purity of myosin and HMM and as the initial step for mass-spectrometry analysis.

The gel was prepared using 0.75mm thick slab. 10% acrylamide resolving gel and a 4% bis/acrylamide loading gel were used for the stacking gels that were stained with SimpltBlue™ Safe Stain. The molecular mass of the protein fragments was determined by comparing their electrophoretic motilities to molecular weight standards.

In-vitro motility assay (IVMA)

Procedure

In-vitro motility assays were performed as previously described with minor modifications (Kalganov et al., 2013a). A flow-through chamber was constructed from a microscope glass coverslip (22x50-1.5, Fisherbrand®, USA) coated with 1.0% nitrocellulose (LADD Inc. VT, U.S.A).

1. The experiments were performed in a homemade chamber with a water thermal exchange column (SC-20, Harvard apparatus, Canada) that fixed the temperature at 30°C.
2. 100uL of 100µg/ml non-cleaved or cleaved HMM were passed through the chamber to allow it to randomly attach to coverslip coated with nitrocellulose.
3. 250 uL of assay buffer (0.1% fluorescence-labeled actin filament and 25 mM Imidazol, 25 mM KCl, 4 mM MgCl₂, 14 mM Glucose, 0.5 mM BSA, 0.018 mg/ml catalase, 0.1 mg/ml glucose oxidase, 17.8 mM dithiothreitol-containing 1mM ATP and an oxygen-scavenging system) was perfused into the chamber.
4. The velocity of actin propelled by non-cleaved and cleaved HMM was measured in different digestion times.
5. The actin filaments were imaged using fluorescence with a filter set using Exciter HQ480/40X, Dichroic Q505LP, Emitter HQ535/50m, Chroma, USA (dye: Alexa-488). The fluorescent light signals emitted by the actin were collected with a 100X oil-immersion objective (Nikon, Plan Fluor, NA: 0.5–1.3).

6. A video was recorded by a high-speed digital EMCCD Camera (Qimage, ROL-MGi-PLUS-F-M-14-C, 512 x 512 pixels BC, Canada).
7. The velocity of actin sliding was analyzed by a customized software (Matlab 8.3.0, MathWorks® Massachusetts, U.S.A.). All actin filaments were tracked during the experiments, but the results of filaments with velocities lower than 0.05 $\mu\text{m}/\text{sec}$ were discarded from analysis.

Mass spectrometry (MS) quantification of proteolytic fragments of HMM by Pinnacle software.

Procedure

1. The samples of rabbit skeletal HMM at different time points (from 0 to 60 min) of the alpha-chymotrypsin proteolysis (enzyme : protein molar ratio = 1:50) were run on the SDS-PAGE, and the gel bands were cut and extracted using standard methods described in detail here (Shevchenko et al., 2006).
2. The SDS-PAGE bands extracted from the gels used to study the content (expression) of myosin's loops 1 and 2, ATP-loop (P-loop) and actin binding domain by label-free quantitative liquid chromatography-tandem mass spectrometry (LC-MS/MS) with Ultimate 3000 nanoLC coupled to an Orbitrap Fusion Tribrid mass spectrometer (Thermo Fisher Scientific).
3. The resulting peptides were loaded onto a Thermo Acclaim Pepmap precolumn (Thermo, 75 μM ID X 2 cm C18 3 μM beads) and then onto an Acclaim Pepmap Easyspray analytical

column separation (Thermo, 75uM X 15cm with 2uM C18 beads) using a Dionex Ultimate 3000 uHPLC at 220 nl/min with a gradient of 2-35% organic solution (0.1% formic acid in acetonitrile) over 1 hour.

4. Peptides were analyzed using a Thermo Orbitrap Fusion Tribrid mass spectrometer with sequencing all peptides with a charge of 2+ or greater.
5. The obtained raw data were converted into *.mgf files (Mascot generic format) for search using the Mascot 2.3 search engine (Matrix Science) against a rabbit database (Uniprot, accession number Q28641) with 0.05 threshold, cysteine carbamidomethylation specified as a fixed modification and methionine oxidation as a variable modification. The control-enzyme was specified as trypsin and two miss cleavages were allowed. The *.mgf files then converted to Mascot *.dat files.
6. The database search results were loaded onto Scaffold Q+ Scaffold 4.4.8 (Proteome Software, USA) for statistical analysis and data visualization.
7. Scaffold (version 4.6.1, Proteome Software Inc., Portland, OR) was used to validate MS/MS based peptide and protein identifications. Peptide identifications were accepted if they could be established at >95.0% probability by the Peptide Prophet algorithm with Scaffold delta-mass correction.
8. The peptide sequences of rabbit skeletal myosin loops 1 and 2, ATP-loop (P-loop) and actin-binding domain were obtained from mass fingerprint search in Uniprot database (accession number Q28641). We were able to identify peptides in rabbit skeletal myosin sequence that cover the whole sequences of loop 1 (VIQYFATIAITGDKK and KEEATSGK:

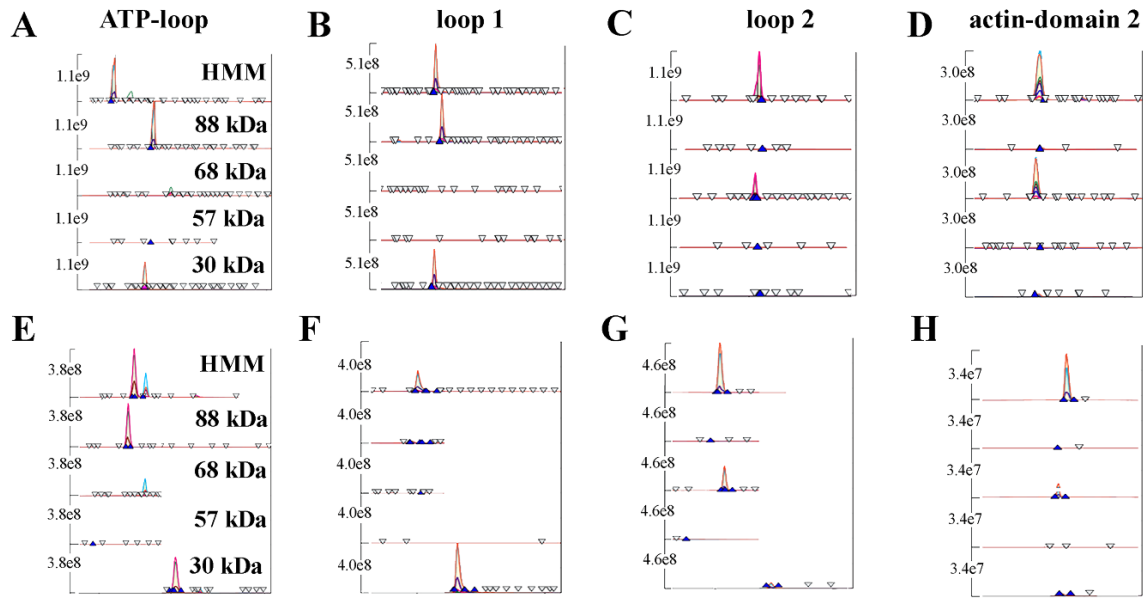
residues 192-207 and 208-214, respectively), the sequence of loop 2 (GSSFQTVSALFR: residues 644-655), the ATP-loop (ENQSILITGESGAGK: residues 171-185), and the actin-binding domain 2 (AGLLGLLEEMR: residues 770-780). The ATP-loop and actin-binding domain 2 were studied based on their close location to loop 1 and loop 2, respectively.

9. Ion currents (XIC's) for each peptide were analyzed and quantified by combining the *.raw files from the Thermo Orbitrap Fusion and the *.dat files from the output of Mascot 2.3 into Pinnacle software (v1.0.52.0, OptysTech, Thermo Scientific, USA, <http://optystech.com/>) using the Targeted Quantitation; label free DDA or pSMART workflow. This comprehensive software can be used for many applications in “*omics*” studies.
10. To analyze the peptide content / expression in Pinnacle software we create groups according to our sample dataset. For example, for the three different datasets the name of groups should be: 1, 2, 3, 4, 5, 1a, 2a, 3a, 4a, 5a, 1b, 2b, 3b, 4b, 5b etc. The numbers represent each band cut off from the SDS-PAGE, extracted and trypsinolized to study peptides content.
11. In Pinnacle software interface, mark the “reference” band for analysis. In our case it is the 1st band of control HMM before proteolysis for all analyzed datasets.
12. To each band in the group add the corresponding *.dat Mascot file and corresponding raw *.mgf file, then press start analysis.
13. For a quantitative data analysis of the myosin’s functional loops or any other protein domains, extracted ion chromatograms for the ¹²C, ¹³C and double ¹³C isotopes were used to calculate 50% peak area of eluted peptides in the Pinnacle software. 50% peak areas of specific

peptides corresponding to the loop 1, loop 2, ATP-loop and actin-binding domains (or any other interested domains) obtained during limited proteolysis of HMM were normalized to 50% peak area of non-trypsinized HMM peptides.

12.2. Supplemental material of Mass spectrometry for the experimental study 2

Figure S2 shows extracted ion chromatograms (MS1, 120K resolution, top 50% peak area) for the ^{12}C , ^{13}C and double ^{13}C isotopes of ENQSILITGESGAGK peptide (ATP loop); VIQYFATIAITGDKK peptide (loop 1); GSSFQTVSALFR peptide (actin binding domain 1 - loop 2) and AGLLGLLEEMRDDK peptide (actin binding domain 2) in the absence (A-D) and presence (E-H) of actin.



Supplementary Figure 2. Extracted ion chromatograms used to count peptide content in the loops and domains investigated in this study. Panels A-D: Representative peak area of selected peptides in different proteolytic fragments of HMM cleaved in both loops 1 and 2; Panels E-H: Representative peak area of selected peptides in different proteolytic fragments of HMM cleaved in loops 1 and 2 when loop 2 was partially protected with 2-fold excess of F-actin.

Supplementary Table 1: Protein-Peptide Database of rabbit skeletal HMM (Uniprot database: accession number Q28641, highlighted by blue color) and its tryptic fragments with corresponding peptide counted areas obtained without protection of loop 2. The highlighted peak area of peptides covering ATP-loop, loop 1, actin binding domain 1-loop 2 and actin-binding domain 2 are shown. Reproducibility of obtained data was tested in two independent experiments with at least three runs for quantification of peak area of selected peptides.



Protein-Peptide View

Name	HMM, 0 min File Area(s)	88 kDa, 1 min File Area(s)	68 kDa, 60 min File Area(s)	57 kDa, 60 min File Area(s)	30 kDa, 60 min File Area(s)
Protein G1SDF4=57014.31,Uncharacterized protein OS=Oryctolagus cuniculus GN=KRT	8.979E+06	2.218E+07	3.261E+07	1.209E+06	2.530E+07
Protein G1T2Y5=267359.82,Uncharacterized protein OS=Oryctolagus cuniculus GN=TPF	1.667E+09	4.301E+06	0.000E+00	1.208E+06	1.329E+06
Protein Q572T2=28921.06,Small inducible cytokine subfamily E, member 1 (Fragment)	2.429E+07	1.465E+07	5.499E+05	9.614E+05	8.736E+05
Protein G1SMU8=15434.61,Prefoldin subunit 4 OS=Oryctolagus cuniculus GN=PFND4 P	1.393E+07	2.659E+07	2.273E+05	5.462E+05	7.398E+05
Protein P02608=19130.39,Myosin regulatory light chain 2, skeletal muscle isoform type	0.000E+00	0.000E+00	0.000E+00	0.000E+00	0.000E+00
Protein U3KMU3=84748.15,Alpha-1,4 glucan phosphorylase OS=Oryctolagus cuniculus	0.000E+00	0.000E+00	0.000E+00	0.000E+00	0.000E+00
Protein G1SVG3=187858.64,Uncharacterized protein OS=Oryctolagus cuniculus GN=MY	1.369E+07	0.000E+00	0.000E+00	0.000E+00	0.000E+00
Protein P02602=20993.62,Myosin light chain 1/3, skeletal muscle isoform OS=Oryctolag	0.000E+00	0.000E+00	0.000E+00	0.000E+00	0.000E+00
Protein G1TN89=479309.59,Uncharacterized protein OS=Oryctolagus cuniculus GN=HS	2.860E+07	6.346E+06	3.877E+06	1.251E+07	3.105E+06
Protein G1TTW8=47126.84,Uncharacterized protein OS=Oryctolagus cuniculus GN=RNH	9.643E+06	0.000E+00	0.000E+00	9.307E+06	8.934E+06
Protein G1SWS9=53680.03,Uncharacterized protein OS=Oryctolagus cuniculus GN=VIM	1.450E+06	3.243E+05	3.655E+05	3.496E+05	4.050E+05
Protein G1TP66=55477.51,Uncharacterized protein OS=Oryctolagus cuniculus GN=LOC	0.000E+00	0.000E+00	0.000E+00	0.000E+00	0.000E+00
Protein G1SYF0=38940.29,Uncharacterized protein OS=Oryctolagus cuniculus GN=TNIH	1.567E+07	1.443E+05	6.135E+06	1.249E+05	2.428E+05
Protein G1T1I5=81548.32,Uncharacterized protein OS=Oryctolagus cuniculus PE=4 SV=	3.881E+07	2.206E+07	2.288E+07	1.827E+07	1.227E+07
Protein G1TS42=177328.11,Glycogen debranching enzyme (Fragment) OS=Oryctolagus	1.274E+07	1.172E+06	3.961E+05	0.000E+00	1.186E+04
Protein G1U9I8=64426.37,Uncharacterized protein OS=Oryctolagus cuniculus GN=KRT:	7.430E+08	3.146E+08	3.178E+08	4.790E+07	1.117E+08
Protein G1SHZ4=40888.73,Uncharacterized protein OS=Oryctolagus cuniculus GN=KRT	9.652E+07	4.479E+07	6.897E+07	7.772E+06	1.397E+07
Protein G1SKE3=53778.45,Uncharacterized protein OS=Oryctolagus cuniculus GN=LOC	8.973E+06	1.749E+05	0.000E+00	1.196E+06	0.000E+00
Protein G1SUH8=63653.30,Uncharacterized protein OS=Oryctolagus cuniculus GN=KRT	5.733E+07	3.244E+07	2.861E+07	4.321E+06	2.184E+07
Protein Q29426=64533.74,Keratin, type II cytoskeletal 3 OS=Oryctolagus cuniculus GN:	0.000E+00	0.000E+00	0.000E+00	0.000E+00	0.000E+00
Protein G1T0Q4=95502.43,Phospholipase A2 OS=Oryctolagus cuniculus GN=PLA2G4F F	5.755E+06	5.262E+05	6.865E+05	0.000E+00	0.000E+00
Protein G1T1Y7=48667.66,Uncharacterized protein OS=Oryctolagus cuniculus GN=KRT	4.796E+07	7.938E+06	1.485E+07	1.583E+06	3.998E+06
Protein G1T4S1=48714.92,Uncharacterized protein OS=Oryctolagus cuniculus GN=KRT:	3.525E+07	0.000E+00	1.232E+07	1.950E+06	4.361E+06
Protein G1T1V0=58263.42,Uncharacterized protein OS=Oryctolagus cuniculus GN=KRT	9.457E+07	4.043E+07	3.097E+07	6.872E+06	2.401E+07
Protein G1SPL2=135148.26,Uncharacterized protein OS=Oryctolagus cuniculus GN=NLF	5.043E+07	2.942E+07	2.851E+05	3.234E+04	1.208E+07
Protein G1TDN6=62416.94,Uncharacterized protein OS=Oryctolagus cuniculus GN=KRT	6.992E+07	1.431E+07	2.563E+07	3.949E+06	5.464E+06
Protein G1U9R3=224351.21,Uncharacterized protein OS=Oryctolagus cuniculus GN=MY	0.000E+00	0.000E+00	0.000E+00	0.000E+00	0.000E+00
Protein G1SYW9=223302.74,Uncharacterized protein OS=Oryctolagus cuniculus GN=M'	1.143E+10	2.115E+08	6.074E+09	1.045E+08	3.832E+08
Protein G1TW48=223676.68,Myosin-7 OS=Oryctolagus cuniculus GN=MYH7 PE=4 SV=	7.429E+08	5.442E+08	4.082E+07	3.862E+07	6.004E+07
Protein Q9GJP9=224536.89,Skeletal muscle myosin heavy chain MyHC-EO/IIL OS=Oryc	0.000E+00	0.000E+00	0.000E+00	0.000E+00	0.000E+00
Protein 0;"G1TY25":0:28:34:1	3.968E+07	2.137E+05	1.463E+07	9.289E+03	1.704E+04
Protein G1T4T6=166093.43,Uncharacterized protein OS=Oryctolagus cuniculus GN=MY	6.175E+08	4.501E+06	4.774E+05	1.105E+06	6.329E+06
Protein G1SJM7=224004.32, Uncharacterized protein OS=Oryctolagus cuniculus GN=LO	1.903E+09	1.463E+09	3.504E+06	1.053E+09	2.953E+08
Protein 0;"G1SX09":0:18:24:1	4.491E+06	2.694E+06	0.000E+00	0.000E+00	0.000E+00
Protein G1TKS9=224389.70,Uncharacterized protein OS=Oryctolagus cuniculus GN=MY	2.674E+08	5.151E+07	1.041E+05	1.124E+05	2.559E+06
Protein G1SJK4=224330.06,Uncharacterized protein OS=Oryctolagus cuniculus GN=MY	1.920E+10	1.817E+09	9.774E+09	1.531E+09	5.720E+08

Protein-Peptide View

Name	HMM, 0 min File Area(s)	88 kDa, 1 min File Area(s)	68 kDa, 60 min File Area(s)	57 kDa, 60 min File Area(s)	30 kDa, 60 min File Area(s)	
Protein	Q28641=223856.34,Myosin-4 OS=Oryctolagus cuniculus GN=MYH4 PE=1 SV=1	1.890E+09	7.836E+08	4.543E+08	5.575E+08	1.566E+08
Peptide	N[Deamid]TQGILK	9.571E+06	0.000E+00	4.829E+05	5.701E+05	3.342E+05
Peptide	KLEGLDK	2.627E+08	1.214E+08	1.280E+08	3.651E+07	9.222E+06
Peptide	LQDLVDK	3.729E+07	2.821E+08	3.367E+06	0.000E+00	5.883E+05
Peptide	IKEVTER	4.214E+08	3.742E+06	3.403E+08	2.336E+05	8.170E+04
Peptide	REAEFQK	4.755E+07	1.467E+07	2.024E+04	6.826E+05	6.388E+05
Peptide	TEEELEAK	4.269E+08	2.116E+08	1.964E+07	5.560E+06	1.928E+07
Peptide	MVALMQEK	7.381E+08	1.031E+06	9.492E+08	1.512E+07	7.786E+04
Peptide	RKLEGLDK	1.345E+07	6.341E+05	1.547E+07	1.959E+04	3.605E+04
Peptide	M[Oxid]VALMQEK	7.228E+08	9.354E+07	1.084E+08	2.702E+06	1.117E+05
Peptide	MVALM[Oxid]QEK	7.228E+08	5.821E+08	2.734E+08	3.356E+05	3.493E+05
Peptide	EQLAMVER	4.918E+07	2.056E+07	3.284E+06	2.649E+06	1.216E+05
Peptide	M[Oxid]VALM[Oxid]QEK	1.129E+09	3.114E+07	5.840E+08	9.949E+06	9.733E+05
Peptide	DEEIDQLK	1.849E+07	1.710E+07	0.000E+00	3.555E+07	4.034E+04
Peptide	EQLAM[Oxid]VER	6.664E+07	4.098E+07	3.192E+06	3.249E+06	3.766E+06
Peptide	TKEEHQK	9.998E+06	0.000E+00	1.458E+04	0.000E+00	0.000E+00
Peptide	ADIAESQVNK	5.381E+07	7.412E+05	2.408E+06	8.498E+05	4.161E+06
Peptide	TEEELEAKK	2.505E+07	0.000E+00	1.661E+06	6.029E+06	1.146E+06
Peptide	IQLELNQVK	7.080E+08	4.606E+08	3.424E+07	3.660E+07	0.000E+00
Peptide	IQLELN[Deamid]QVK	3.339E+07	1.379E+07	8.983E+05	6.499E+05	2.207E+03
Peptide	DEEIDQLKR	2.843E+07	1.380E+07	1.299E+06	1.196E+06	5.358E+04
Peptide	EQDTSAHLER	4.082E+08	2.133E+08	2.807E+07	2.120E+07	1.353E+07
Peptide	AGLLGLEEMR	1.378E+09	5.453E+06	5.274E+08	2.165E+06	3.110E+06
Peptide	AGLLGLEEM[Oxid]R	3.108E+09	5.681E+07	1.372E+09	1.860E+07	1.400E+08
Peptide	DIDDLELTLAK	4.286E+08	1.990E+08	4.393E+09	9.446E+07	9.563E+05
Peptide	EQYEEQEAKE	2.356E+09	3.187E+08	9.316E+06	5.390E+06	1.813E+07
Peptide	ELTYQTEEDR	7.490E+07	3.377E+07	0.000E+00	0.000E+00	0.000E+00
Peptide	KEQDTSAHLER	5.033E+06	1.507E+06	2.861E+04	2.902E+03	0.000E+00
Peptide	KDIDDLELTLAK	3.406E+08	8.059E+06	1.598E+08	2.714E+06	5.194E+05
Peptide	LQHELEEAEEER	2.487E+07	0.000E+00	0.000E+00	3.324E+06	6.109E+05
Peptide	SAETEKEM[Oxid]ANMK	2.047E+07	2.144E+05	2.710E+07	5.463E+05	0.000E+00
Peptide	EMANMKKEFEK	1.422E+08	1.765E+07	3.859E+08	6.543E+06	2.232E+06
Peptide	EMANM[Oxid]KEFEK	4.486E+07	1.903E+06	1.092E+08	1.029E+06	8.939E+05
Peptide	ELTYQTEEDRK	5.526E+08	3.397E+08	4.321E+06	1.657E+06	5.071E+05
Peptide	EM[Oxid]ANM[Oxid]KEFEK	1.570E+09	2.647E+07	4.886E+08	6.832E+06	1.731E+07
Peptide	EM[Oxid]AN[Deamid]M[Oxid]KEFEK	1.044E+08	2.808E+05	1.280E+07	3.517E+06	1.574E+06
Peptide	IAEKDEEIDQLK	3.212E+08	1.166E+08	1.220E+07	9.310E+06	3.736E+05
Peptide	IEEEEEIEAER	1.571E+10	4.624E+08	9.012E+09	6.499E+07	2.884E+07

Protein-Peptide View

Name	HMM, 0 min File Area(s)	88 kDa, 1 min File Area(s)	68 kDa, 60 min File Area(s)	57 kDa, 60 min File Area(s)	30 kDa, 60 min File Area(s)	
Peptide	N[Deamid]DLQLQVQAEADSLADAEER	6.911E+08	6.294E+07	1.122E+08	2.038E+07	0.000E+00
Peptide	NDLQLQVQ[Deamid]AEADSLADAEER	6.911E+08	1.535E+07	0.000E+00	5.334E+06	5.232E+06
Peptide	NDLQLQ[Deamid]VQAEADSLADAEER	2.777E+08	5.926E+06	1.909E+08	2.157E+06	0.000E+00
Peptide	TKLEQQVDDLEGSLEQEKK	7.066E+09	2.328E+08	3.329E+09	6.134E+07	9.044E+06
Peptide	LETDISIQGEMEDIVQEAR	4.354E+07	1.496E+04	2.156E+05	5.146E+03	8.710E+04
Peptide	KALQEAHQQTLLDDLQAEEDK	6.446E+07	1.291E+05	3.734E+07	6.720E+05	3.662E+04
Peptide	LETDISIQGEM[Oxid]EDIVQEAR	2.983E+07	1.888E+07	2.131E+06	4.457E+05	9.975E+05
Peptide	KLETDISIQGEMEDIVQEAR	1.047E+08	6.505E+06	1.415E+05	2.670E+04	3.795E+04
Peptide	KLETDISIQGEM[Oxid]EDIVQEAR	8.303E+07	6.457E+07	3.535E+06	1.950E+06	4.594E+06
Peptide	ALQEAHQQTLLDDLQAEEDKVNLT	1.388E+10	4.995E+08	8.201E+09	1.057E+08	2.434E+07
Peptide	ALQEAHQQTLLDDLQAEEDKVN[Deamid]TLTK	7.560E+08	3.267E+08	3.291E+08	3.217E+06	7.131E+05
Peptide	ALQEAHQQTLLDDLQ[Deamid]AEEDKVNLT	3.934E+09	7.937E+07	7.969E+07	0.000E+00	7.064E+04
Peptide	KALQEAHQQTLLDDLQAEEDKVNLT	7.259E+08	4.364E+07	7.271E+08	4.483E+06	8.682E+05
Peptide	MAAEALR	2.846E+07	1.474E+06	4.284E+06	2.928E+06	4.899E+05
Peptide	KEEATSGK: part of loop 1 [residues: 208-214]	2.732E+06	2.498E+04	0.000E+00	1.159E+06	0.000E+00
Peptide	IHFGTTGK	2.737E+09	2.174E+09	4.206E+06	2.917E+09	1.070E+06
Peptide	ILYADF	1.033E+10	2.218E+08	5.450E+09	9.771E+07	4.380E+08
Peptide	QLEEEIK	2.041E+09	2.483E+08	0.000E+00	1.077E+07	1.029E+07
Peptide	VGNEYVTK	7.337E+09	7.265E+09	2.102E+07	9.464E+09	1.817E+07
Peptide	VGN[Deamid]EYVTK	5.084E+08	1.642E+08	1.924E+05	5.071E+08	2.418E+05
Peptide	ATLEQTER	5.491E+08	2.753E+08	2.537E+07	2.643E+07	1.631E+07
Peptide	SSVFVADPK	5.271E+09	6.240E+09	1.537E+08	5.463E+06	4.583E+09
Peptide	INQQLDTK	8.939E+09	8.557E+09	2.651E+07	1.004E+10	2.470E+07
Peptide	INQ[Deamid]LDTK	1.262E+09	2.434E+08	7.771E+06	6.636E+06	6.887E+05
Peptide	IN[Deamid]QQQLDTK	3.345E+08	2.434E+08	1.543E+06	2.736E+08	6.887E+05
Peptide	TEAGATVTVK	5.902E+09	5.868E+09	4.061E+06	4.950E+06	4.147E+09
Peptide	LYEQHLGK	2.359E+09	1.852E+09	6.219E+06	2.575E+09	6.544E+06
Peptide	DSLVSQLSR	4.327E+09	2.259E+08	0.000E+00	1.837E+06	0.000E+00
Peptide	LINDLSAQR	1.115E+10	3.204E+08	2.748E+07	1.839E+06	2.965E+06
Peptide	LINDLSAQ[Deamid]R	8.967E+06	4.203E+06	2.740E+05	1.869E+05	0.000E+00
Peptide	LIN[Deamid]DLSAQR	1.599E+09	3.327E+07	0.000E+00	0.000E+00	0.000E+00
Peptide	ANSEVAQWR	5.002E+08	2.936E+08	1.136E+07	6.351E+06	2.112E+07
Peptide	AN[Deamid]SEVAQWR	5.574E+06	1.021E+07	5.071E+04	3.637E+05	2.332E+05
Peptide	M[Oxid]FLWMVTR	1.574E+08	7.481E+07	9.230E+05	2.989E+08	0.000E+00
Peptide	MFLWM[Oxid]VTR	5.329E+08	1.774E+08	1.946E+06	2.989E+08	1.979E+06
Peptide	M[Oxid]FLWM[Oxid]VTR	3.067E+09	2.015E+09	5.789E+06	1.458E+07	6.982E+06
Peptide	SALAHALQSAR	9.684E+08	9.735E+07	2.890E+06	1.392E+06	4.505E+06
Peptide	LQTESGEFSR	5.972E+09	2.902E+08	1.351E+06	1.660E+06	1.109E+06

Protein-Peptide View

Name	HMM, 0 min File Area(s)	88 kDa, 1 min File Area(s)	68 kDa, 60 min File Area(s)	57 kDa, 60 min File Area(s)	30 kDa, 60 min File Area(s)	
Peptide	ILYADFKQR	1.297E+07	0.000E+00	2.312E+06	0.000E+00	9.326E+04
Peptide	TLEDQVSELK	1.118E+10	3.364E+08	4.122E+07	0.000E+00	3.522E+06
Peptide	DDKLAQLITR	3.332E+07	1.621E+06	1.177E+08	0.000E+00	8.718E+05
Peptide	EFEMSNLQSK	1.979E+09	3.717E+06	1.835E+09	1.492E+07	0.000E+00
Peptide	TKYETDAIQR	5.567E+08	3.429E+08	2.506E+07	8.175E+06	2.154E+07
Peptide	EFEM[Oxid]SNLQSK	1.566E+09	5.668E+07	5.880E+08	7.635E+06	9.285E+03
Peptide	EFEM[Oxid]SN[Deamid]LQSK	2.846E+07	1.614E+04	9.065E+06	3.828E+05	3.565E+05
Peptide	SNNFQKPKPAK	1.186E+08	7.341E+06	0.000E+00	1.498E+08	1.563E+03
Peptide	SNN[Deamid]FQKPKPAK	5.818E+06	1.306E+07	0.000E+00	1.556E+07	0.000E+00
Peptide	IEAQNKPFDAK	2.965E+09	3.020E+09	1.604E+06	5.655E+07	1.901E+09
Peptide	IEAQN[Deamid]KPFDAK	1.118E+07	0.000E+00	1.451E+04	2.671E+05	4.516E+08
Peptide	ELEAEVESEQK	2.203E+08	9.215E+07	6.624E+05	1.577E+06	4.580E+05
Peptide	DTQLHLDDALR	5.393E+08	3.655E+08	3.347E+07	4.180E+07	1.669E+07
Peptide	GSSFQTVSALFR: actin binding domain 1 / part of loop2 [residues:644-655]	8.174E+09	1.865E+08	4.266E+09	4.782E+07	3.265E+08
Peptide	GSSFQ[Deamid]TVSALFR	8.392E+05	9.356E+06	3.000E+06	2.707E+06	4.396E+07
Peptide	EDQVFPMPNPPK	7.692E+08	7.483E+07	4.117E+05	7.073E+05	6.963E+08
Peptide	EDQVFPM[Oxid]NPPK	5.637E+09	3.612E+09	7.313E+05	5.724E+05	2.911E+09
Peptide	LTGAVMHYGNMK	4.063E+07	2.293E+06	8.230E+04	1.685E+08	0.000E+00
Peptide	QAFTQQIEELK	6.091E+08	3.637E+07	6.966E+03	1.606E+05	1.717E+06
Peptide	LTGAVMHYGNM[Oxid]K	4.617E+08	5.900E+07	1.100E+05	7.209E+08	2.411E+05
Peptide	LTGAVM[Oxid]HYGNMK	1.836E+08	5.900E+07	1.880E+06	5.044E+08	0.000E+00
Peptide	LTGAVMHYGN[Deamid]M[Oxid]K	1.278E+07	8.783E+05	2.143E+04	1.672E+07	0.000E+00
Peptide	KEFEMSNLQSK	2.676E+07	7.512E+04	3.135E+07	2.474E+05	4.434E+05
Peptide	INQLDITKQPR	3.000E+07	2.135E+07	9.452E+04	2.036E+07	1.288E+05
Peptide	LTGAVM[Oxid]HYGNM[Oxid]K	1.963E+09	1.843E+09	5.257E+06	2.022E+09	3.302E+05
Peptide	LTGAVM[Oxid]HYGN[Deamid]M[Oxid]K	4.616E+07	1.119E+07	4.877E+04	2.378E+07	0.000E+00
Peptide	KEFEM[Oxid]SNLQSK	1.273E+08	8.054E+06	4.981E+07	9.290E+06	5.260E+05
Peptide	VAEQELLDASER	6.333E+08	3.361E+08	2.555E+07	2.126E+07	1.635E+07
Peptide	ANLLQAEIEELR	6.992E+08	4.066E+08	2.853E+07	2.372E+07	1.618E+07
Peptide	KGSSFQTVSALFR	3.228E+09	5.967E+07	1.528E+09	1.352E+07	1.095E+08
Peptide	ELEAEVESEQKR	3.262E+08	2.736E+08	2.695E+06	4.960E+06	0.000E+00
Peptide	LASADIETYLLEK	1.590E+10	1.479E+10	3.982E+07	1.518E+10	3.892E+05
Peptide	DPLNETVWGLYQK	2.279E+09	2.027E+09	5.711E+06	2.709E+09	1.383E+06
Peptide	DPLN[Deamid]ETVWGLYQK	2.893E+08	1.546E+07	6.148E+07	4.009E+08	2.601E+07
Peptide	KVAEQELLDASER	5.171E+08	3.161E+08	2.926E+07	2.089E+07	3.381E+05
Peptide	QAFTQQIEELKR	4.915E+09	5.652E+08	4.542E+05	7.582E+06	2.081E+07
Peptide	LAQESTMDIENDK	1.027E+08	5.684E+05	1.614E+08	0.000E+00	6.375E+04
Peptide	LAQESTMDIEN[Deamid]DK	7.679E+06	2.375E+05	4.199E+06	4.095E+04	0.000E+00

Protein-Peptide View

Name	HMM, 0 min File Area(s)	88 kDa, 1 min File Area(s)	68 kDa, 60 min File Area(s)	57 kDa, 60 min File Area(s)	30 kDa, 60 min File Area(s)	
Peptide	ENQSILITGESGAGK: ATP-loop (P-loop) [residues: 171-185]	1.385E+10	1.194E+10	1.990E+06	1.176E+07	7.558E+09
Peptide	ENQ[Deamid]SILITGESGAGK	5.233E+09	3.200E+08	0.000E+00	0.000E+00	3.059E+09
Peptide	LAQESTM[Oxid]DIENDK	8.112E+08	1.208E+07	1.739E+08	1.700E+06	1.414E+06
Peptide	IEDEQALAMQLQK	1.162E+09	2.553E+06	1.726E+09	8.706E+06	1.015E+06
Peptide	EEQAEPDGTVEADK	3.310E+09	3.028E+09	0.000E+00	4.003E+09	0.000E+00
Peptide	VIQYFATIAVTGDK: part of loop 1 [residues:192-207]	5.883E+09	5.803E+09	5.459E+05	2.631E+06	4.822E+09
Peptide	SYHIFYQIMSNK	7.700E+08	2.295E+08	4.054E+06	1.281E+09	3.551E+06
Peptide	IEDEQALAM[Oxid]QLQK	4.011E+09	1.209E+08	1.336E+09	4.953E+07	1.250E+07
Peptide	YEETHAELEASQK	9.019E+07	4.305E+07	5.570E+06	5.177E+06	4.470E+06
Peptide	ERIEAQNKPFDAK	8.844E+07	1.385E+08	1.232E+05	1.104E+05	9.827E+07
Peptide	SYHIFYQIM[Oxid]SNK	3.258E+09	3.077E+09	8.734E+07	3.137E+09	2.572E+06
Peptide	LQDAEEHVEAVNAK	5.196E+08	3.710E+08	2.894E+07	1.152E+07	3.416E+07
Peptide	LQDAEEHVEAVN[Deamid]AK	3.034E+07	2.619E+07	7.820E+06	1.220E+06	6.101E+06
Peptide	RANLLQAEIEELR	1.081E+08	1.050E+08	6.468E+06	8.271E+04	3.073E+06
Peptide	AGLLGLEEMRDDK: actin binding domain 2 [residues: 770-780]	2.744E+08	1.533E+06	1.648E+08	5.148E+05	6.025E+05
Peptide	AGLLGLEEM[Oxid]RDDK	6.676E+09	1.312E+08	4.017E+09	4.407E+07	2.926E+08
Peptide	QLDEKDSLVSQLSR	3.437E+07	3.138E+07	6.059E+06	6.628E+05	0.000E+00
Peptide	GQEDLKEQLAMVER	2.387E+07	1.993E+06	2.903E+06	2.691E+06	8.616E+04
Peptide	GQTVQQVYNAV GALAK	1.517E+10	1.692E+10	3.173E+07	1.609E+10	3.003E+07
Peptide	GQTVQQVYN[Deamid]AVGALAK	7.457E+08	1.613E+09	7.736E+06	1.815E+09	2.409E+06
Peptide	GQTVQ[Deamid]QVYNAV GALAK	1.892E+07	7.383E+09	0.000E+00	5.595E+09	6.978E+06
Peptide	GQTVQQ[Deamid]VYNAV GALAK	6.489E+09	7.383E+09	0.000E+00	5.595E+09	0.000E+00
Peptide	NAYEESLDQLETLK	5.666E+08	2.531E+08	2.259E+07	1.741E+07	2.013E+07
Peptide	N[Deamid]AYEESLDQLETLK	3.728E+07	1.491E+07	0.000E+00	1.812E+06	9.067E+05
Peptide	VIQYFATIAVTGDKK	5.671E+08	8.857E+08	2.458E+04	1.783E+06	7.833E+08
Peptide	GQEDLKEQLAM[Oxid]VER	3.078E+07	3.473E+07	0.000E+00	2.415E+06	2.475E+06
Peptide	RVIQYFATIAVTGDK	2.875E+08	5.047E+08	4.966E+05	4.999E+04	3.354E+08
Peptide	MEIDDLASNMETVSK	3.007E+08	5.743E+05	2.016E+06	1.301E+05	5.409E+05
Peptide	VLNASAIPEGQFIDSK	2.579E+10	4.282E+08	1.376E+10	1.612E+08	8.985E+08
Peptide	VLN[Deamid]ASAIPEGQFIDSK	9.045E+08	1.041E+08	5.687E+09	4.343E+07	3.197E+08
Peptide	MEIDDLASNM[Oxid]ETVSK	4.659E+08	1.692E+06	0.000E+00	1.568E+05	2.775E+05
Peptide	M[Oxid]EIDDLASNMETVSK	3.741E+08	2.094E+05	2.756E+06	4.077E+04	2.651E+05
Peptide	LQNEVEDLMIDVER	8.374E+07	1.093E+07	8.142E+06	1.498E+06	1.536E+05
Peptide	LASADIETYLLEKSR	5.483E+07	5.129E+07	1.585E+04	1.377E+07	3.381E+06
Peptide	M[Oxid]EIDDLASNM[Oxid]ETVSK	9.113E+08	4.336E+07	4.133E+06	2.079E+05	0.000E+00
Peptide	M[Oxid]EIDDLASN[Deamid]M[Oxid]ETVSK	3.387E+07	1.164E+07	1.572E+06	0.000E+00	3.212E+03
Peptide	NKDP LN ET VVGLYQK	1.710E+10	1.529E+10	3.940E+07	2.322E+10	1.679E+07
Peptide	LQNEVEDLM[Oxid]IDVER	1.136E+08	9.757E+07	7.357E+06	1.116E+06	1.277E+07

Supplementary Table 2: Protein-Peptide Database of rabbit skeletal HMM (Uniprot database: accession number Q28641) and its tryptic fragments with corresponding peptide counted areas obtained with protection of loop 2. The highlighted peak area of peptides covering ATP-loop, loop 1, actin binding domain 1-loop 2 (part of loop 2) and actin-binding domain 2 are shown. Reproducibility of obtained data were tested in two independent experiments with at least three runs for quantification of peak area of selected peptides.



Our Passion Translating into Your Success

Protein-Peptide View

Name	HMM, 0 min File Area(s)	88 kDa, 1 min File Area(s)	68 kDa, 60 min File Area(s)	57 kDa, 60 min File Area(s)	30 kDa, 60 min File Area(s)
Protein HNRH2_BOVIN=49523.27,Heterogeneous nuclear ribonucleoprotein H2 OS=Bos taurus GN=HNRH2 PE=1 SV=1	0.000E+00	0.000E+00	1.076E+05	3.732E+04	2.180E+06
Protein OSBP1_RABIT=90292.57,Oxysterol-binding protein 1 OS=Oryctolagus cuniculus GN=OSBP1 PE=1 SV=1	1.502E+06	0.000E+00	0.000E+00	1.210E+05	6.226E+06
Protein GLYR1_BOVIN=61098.08,Putative oxidoreductase GLYR1 OS=Bos taurus GN=GLYR1 PE=1 SV=1	3.190E+06	7.869E+03	3.484E+06	0.000E+00	3.412E+06
Protein TM38A_RABIT=33265.13,Trimeric intracellular cation channel type A OS=Oryctolagus cuniculus GN=TM38A PE=1 SV=1	9.500E+03	6.911E+02	3.463E+03	1.788E+02	2.298E+06
Protein HBA_TALEU=15294.80,Hemoglobin subunit alpha OS=Talpa europaea GN=HBA1 PE=1 SV=1	2.659E+05	7.901E+04	2.406E+05	8.655E+04	2.061E+07
Protein KAC4_RABIT=11268.31,Ig kappa-b4 chain C region OS=Oryctolagus cuniculus PE=1 SV=1	2.475E+06	1.223E+04	9.462E+05	2.789E+05	4.183E+06
Protein KCRS_BOVIN=47723.28,Creatine kinase S-type, mitochondrial OS=Bos taurus GN=KCRS PE=1 SV=1	0.000E+00	0.000E+00	0.000E+00	0.000E+00	0.000E+00
Protein HCD2_BOVIN=27297.30,3-hydroxyacyl-CoA dehydrogenase type-2 OS=Bos taurus GN=HCD2 PE=1 SV=1	0.000E+00	0.000E+00	0.000E+00	0.000E+00	4.364E+06
Protein MYOM1_BOVIN=37281.13,Myomesin-1 (Fragments) OS=Bos taurus GN=MYOM1 PE=1 SV=1	3.071E+07	0.000E+00	1.236E+07	1.854E+05	1.222E+08
Protein KAD1_BOVIN=21766.32,Adenylate kinase isoenzyme 1 OS=Bos taurus GN=AK1 PE=1 SV=1	4.670E+05	2.011E+06	1.548E+05	0.000E+00	1.609E+06
Protein HS90B_HORSE=83533.12,Heat shock protein HSP 90-beta OS=Equus caballus GN=HS90B PE=1 SV=1	0.000E+00	0.000E+00	0.000E+00	0.000E+00	0.000E+00
Protein MYL6_BOVIN=17093.15,Myosin light polypeptide 6 OS=Bos taurus GN=MYL6 PE=1 SV=1	0.000E+00	0.000E+00	0.000E+00	0.000E+00	0.000E+00
Protein ANXA2_SHEEP=38877.79,Annexin A2 OS=Ovis aries GN=ANXA2 PE=1 SV=1	0.000E+00	0.000E+00	0.000E+00	0.000E+00	0.000E+00
Protein TPM1_RABIT=32718.68,Tropomyosin alpha-1 chain OS=Oryctolagus cuniculus GN=TPM1 PE=1 SV=1	0.000E+00	0.000E+00	0.000E+00	0.000E+00	0.000E+00
Protein ACTN3_BOVIN=103724.06,Alpha-actinin-3 OS=Bos taurus GN=ACTN3 PE=2 SV=1	0.000E+00	0.000E+00	0.000E+00	0.000E+00	2.782E+06
Protein QOR_BOVIN=35534.64,Zeta-crystallin OS=Bos taurus GN=CRYZ PE=2 SV=2	1.004E+08	4.089E+06	1.108E+07	9.130E+06	2.029E+06
Protein 1433E_SHEEP=29329.43,14-3-3 protein epsilon OS=Ovis aries GN=YWHAE PE=1 SV=1	0.000E+00	0.000E+00	0.000E+00	0.000E+00	0.000E+00
Protein GGCT_BOVIN=21337.44,Gamma-glutamylcyclotransferase OS=Bos taurus GN=GGCT PE=1 SV=1	0.000E+00	2.731E+05	1.552E+05	0.000E+00	2.570E+06
Protein CAPZB_BOVIN=34183.96,F-actin-capping protein subunit beta OS=Bos taurus GN=CAPZB PE=1 SV=1	0.000E+00	0.000E+00	0.000E+00	0.000E+00	0.000E+00
Protein K1C14_BOVIN=10773.43,Keratin, type I cytoskeletal 14 (Fragment) OS=Bos taurus GN=K1C14 PE=1 SV=1	1.043E+08	2.784E+06	0.000E+00	1.344E+05	4.069E+07
Protein KCC2D_PIG=56991.60,Calcium/calmodulin-dependent protein kinase type II subunit gamma OS=Sus scrofa GN=KCC2D PE=1 SV=1	0.000E+00	0.000E+00	0.000E+00	0.000E+00	0.000E+00
Protein ARG1_RABIT=34601.05,Arginase-1 OS=Oryctolagus cuniculus GN=ARG1 PE=2 SV=1	0.000E+00	0.000E+00	0.000E+00	0.000E+00	0.000E+00
Protein DSG1_CANLF=114887.68,Desmoglein-1 OS=Canis lupus familiaris GN=DSG1 PE=1 SV=1	0.000E+00	0.000E+00	0.000E+00	0.000E+00	0.000E+00
Protein DDX4_PIG=79514.71,Probable ATP-dependent RNA helicase DDX4 OS=Sus scrofa GN=DDX4 PE=1 SV=1	0.000E+00	0.000E+00	0.000E+00	0.000E+00	0.000E+00
Protein CO1A1_MACSX=85044.97,Collagen alpha-1(I) chain (Fragments) OS=Macrauchenia patachonica GN=CO1A1 PE=1 SV=1	0.000E+00	0.000E+00	0.000E+00	0.000E+00	0.000E+00
Protein 1433G_BOVIN=28408.95,14-3-3 protein gamma OS=Bos taurus GN=YWHAG PE=1 SV=1	0.000E+00	0.000E+00	0.000E+00	0.000E+00	0.000E+00
Protein TRY1_BOVIN=26464.67,Cationic trypsin OS=Bos taurus PE=1 SV=3	4.632E+07	2.215E+07	1.596E+07	3.334E+07	1.320E+10
Protein OLA1_BOVIN=44947.30,Obg-like ATPase 1 OS=Bos taurus GN=OLA1 PE=2 SV=1	1.062E+06	0.000E+00	3.237E+05	2.671E+06	5.030E+06
Protein MDHM_BOVIN=36109.81,Malate dehydrogenase, mitochondrial OS=Bos taurus GN=MDHM PE=1 SV=1	0.000E+00	0.000E+00	0.000E+00	0.000E+00	0.000E+00
Protein PSA2_BOVIN=25998.28,Proteasome subunit alpha type-2 OS=Bos taurus GN=PSA2 PE=1 SV=1	0.000E+00	3.137E+05	0.000E+00	3.937E+05	1.423E+06
Protein HBA_PIPAB=15561.92,Hemoglobin subunit alpha OS=Pipistrellus abramus GN=HBA PE=1 SV=1	0.000E+00	0.000E+00	0.000E+00	0.000E+00	0.000E+00
Protein K1C9_CANLF=77004.17,Keratin, type I cytoskeletal 9 OS=Canis lupus familiaris GN=K1C9 PE=1 SV=1	2.521E+07	3.213E+06	1.386E+07	4.404E+07	4.758E+08
Protein PGAM2_BOVIN=28840.80,Phosphoglycerate mutase 2 OS=Bos taurus GN=PGAM2 PE=1 SV=1	4.259E+05	1.594E+06	3.453E+05	2.009E+06	8.159E+07
Protein ABCF1_PIG=92044.29,ATP-binding cassette sub-family F member 1 OS=Sus scrofa GN=ABCF1 PE=1 SV=1	0.000E+00	0.000E+00	0.000E+00	0.000E+00	2.401E+06
Protein CTRA_BOVIN=26229.82,Chymotrypsinogen A OS=Bos taurus PE=1 SV=1	1.798E+05	4.902E+04	1.219E+05	3.806E+05	9.582E+07
Protein SYPL2_RABIT=29699.39,Synaptophysin-like protein 2 OS=Oryctolagus cuniculus GN=SYPL2 PE=1 SV=1	1.463E+05	1.397E+05	1.090E+06	2.118E+05	5.324E+07

Protein-Peptide View

Name	HMM, 0 min File Area(s)	88 kDa, 1 min File Area(s)	68 kDa, 60 min File Area(s)	57 kDa, 60 min File Area(s)	30 kDa, 60 min File Area(s)
Protein PFKAM_CANLF=86376.69,ATP-dependent 6-phosphofructokinase, muscle type O	0.000E+00	0.000E+00	0.000E+00	0.000E+00	0.000E+00
Protein PRDX1_MYOLU=22342.32,Peroxioredoxin-1 OS=Myotis lucifugus GN=PRDX1 PE=1	0.000E+00	0.000E+00	0.000E+00	0.000E+00	0.000E+00
Protein PRDX1_BOVIN=22427.42,Peroxioredoxin-1 OS=Bos taurus GN=PRDX1 PE=2 SV=	4.221E+04	1.822E+04	0.000E+00	2.881E+04	6.617E+06
Protein KAP2_BOVIN=45413.61,cAMP-dependent protein kinase type II-alpha regulatory	1.673E+05	1.177E+05	7.656E+04	4.314E+04	8.039E+06
Protein PLAK_BOVIN=82522.85,Junction plakoglobin OS=Bos taurus GN=JUP PE=2 SV=	0.000E+00	0.000E+00	0.000E+00	0.000E+00	0.000E+00
Protein K1C19_BOVIN=43858.06,Keratin, type I cytoskeletal 19 OS=Bos taurus GN=KRT	0.000E+00	1.225E+06	1.332E+05	0.000E+00	7.824E+06
Protein K1C17_BOVIN=48972.30,Keratin, type I cytoskeletal 17 OS=Bos taurus GN=KRT	4.501E+06	1.083E+06	3.623E+06	2.767E+06	4.684E+07
Protein K1C15_SHEEP=48740.10,Keratin, type I cytoskeletal 15 OS=Ovis aries GN=KRT1	0.000E+00	0.000E+00	0.000E+00	0.000E+00	0.000E+00
Protein K1C10_CANLF=57850.14,Keratin, type I cytoskeletal 10 OS=Canis lupus familiaris	8.636E+07	5.404E+06	4.361E+07	1.555E+07	7.336E+08
Protein G3P_FELCA=36022.24,Glyceraldehyde-3-phosphate dehydrogenase OS=Felis cati	0.000E+00	0.000E+00	0.000E+00	0.000E+00	0.000E+00
Protein TNNC2_RABIT=18142.34,Troponin C, skeletal muscle OS=Oryctolagus cuniculus	0.000E+00	0.000E+00	0.000E+00	0.000E+00	2.201E+07
Protein TNNC2_PIG=18071.31,Troponin C, skeletal muscle OS=Sus scrofa GN=TNNC2 P	1.030E+04	2.784E+04	6.707E+05	0.000E+00	7.031E+06
Protein K2C5_BOVIN=63072.35,Keratin, type II cytoskeletal 5 OS=Bos taurus GN=KRT5	3.230E+07	4.577E+06	1.879E+07	7.507E+06	1.466E+08
Protein MYSS_RABIT=125760.24,Myosin heavy chain, skeletal muscle (Fragments) OS=C	5.855E+06	1.958E+06	3.880E+05	1.033E+06	4.928E+07
Protein MYH8_CANLF=223657.48,Myosin-8 OS=Canis lupus familiaris GN=MYH8 PE=3 S	0.000E+00	0.000E+00	0.000E+00	0.000E+00	7.015E+06
Protein MYH7_CANLF=223649.70,Myosin-7 OS=Canis lupus familiaris GN=MYH7 PE=1 S	2.448E+05	9.901E+03	5.769E+04	0.000E+00	2.395E+07
Protein MYH4_PIG=224025.37,Myosin-4 OS=Sus scrofa GN=MYH4 PE=2 SV=1	2.646E+04	0.000E+00	6.733E+03	9.224E+05	5.008E+06
Protein MYH1_BOVIN=223779.57,Myosin-1 OS=Bos taurus GN=MYH1 PE=2 SV=2	1.964E+09	5.587E+08	1.573E+06	0.000E+00	1.360E+10
Protein MYH13_CANLF=224304.36,Myosin-13 OS=Canis lupus familiaris GN=MYH13 PE=	1.928E+07	3.924E+07	9.819E+06	6.496E+06	2.404E+08
Protein PGM1_RABIT=61809.67,Phosphoglucomutase-1 OS=Oryctolagus cuniculus GN=P	1.624E+07	0.000E+00	4.669E+06	1.293E+07	1.713E+06
Protein ACTS_BOVIN=42371.89,Actin, alpha skeletal muscle OS=Bos taurus GN=ACTA1	0.000E+00	0.000E+00	0.000E+00	0.000E+00	0.000E+00
Protein ACTB_CANLF=42057.76,Actin, cytoplasmic 1 OS=Canis lupus familiaris GN=ACTE	0.000E+00	0.000E+00	0.000E+00	0.000E+00	0.000E+00
Protein DDX1_BOVIN=83347.89,ATP-dependent RNA helicase DDX1 OS=Bos taurus GN=	9.056E+04	2.861E+06	1.282E+05	1.336E+05	7.171E+07
Protein ABEC2_BOVIN=26177.91,Probable C->U-editing enzyme APOBEC-2 OS=Bos taur	0.000E+00	0.000E+00	0.000E+00	0.000E+00	7.191E+06
Protein ALBU_RABIT=70895.48,Serum albumin OS=Oryctolagus cuniculus GN=ALB PE=1	4.682E+06	1.104E+08	5.925E+05	1.122E+07	1.332E+08
Protein HSP7C_BOVIN=71428.38,Heat shock cognate 71 kDa protein OS=Bos taurus GN=	0.000E+00	0.000E+00	0.000E+00	0.000E+00	0.000E+00
Protein ALDOA_RABIT=39782.31,Fructose-bisphosphate aldolase A OS=Oryctolagus cuni	1.237E+08	1.861E+06	3.173E+06	2.750E+06	2.897E+08
Protein MYH4_RABIT=223856.34,Myosin-4 OS=Oryctolagus cuniculus GN=MYH4 PE=1 S	4.366E+06	9.598E+06	2.957E+06	6.506E+06	5.708E+09
Protein MYH2_CANLF=224000.00,Myosin-2 OS=Canis lupus familiaris GN=MYH2 PE=3 S	0.000E+00	0.000E+00	0.000E+00	0.000E+00	0.000E+00
Protein MYH1_PIG=223962.62,Myosin-1 OS=Sus scrofa GN=MYH1 PE=2 SV=1	0.000E+00	0.000E+00	0.000E+00	0.000E+00	0.000E+00
Protein MYH1_HORSE=223788.37,Myosin-1 OS=Equus caballus GN=MYH1 PE=2 SV=1	0.000E+00	0.000E+00	0.000E+00	0.000E+00	0.000E+00
Protein MYH1_CANLF=223937.64,Myosin-1 OS=Canis lupus familiaris GN=MYH1 PE=3 S	0.000E+00	0.000E+00	0.000E+00	0.000E+00	0.000E+00
Protein MYL1_RABIT=20993.62,Myosin light chain 1/3, skeletal muscle isoform OS=Oryc	1.503E+07	5.408E+07	3.896E+06	2.271E+07	1.457E+08
Protein U3KLU4=125468.04,Uncharacterized protein OS=Oryctolagus cuniculus GN=DMC	0.000E+00	0.000E+00	0.000E+00	0.000E+00	0.000E+00
Protein G1TKC1=120179.91,Uncharacterized protein OS=Oryctolagus cuniculus GN=MYB	7.879E+08	0.000E+00	2.097E+06	0.000E+00	2.263E+07
Protein G1T658=162762.82,Uncharacterized protein OS=Oryctolagus cuniculus GN=UAC	1.557E+07	1.645E+05	1.999E+07	2.946E+05	4.944E+05
Protein G1T933=194577.41,Uncharacterized protein OS=Oryctolagus cuniculus GN=COL	3.398E+06	1.558E+06	1.380E+05	2.300E+06	0.000E+00
Protein G1SZ44=10921.89,Uncharacterized protein OS=Oryctolagus cuniculus GN=LOC1	1.075E+07	3.357E+05	7.426E+04	3.116E+05	0.000E+00

Protein-Peptide View

Name	HMM, 0 min File Area(s)	88 kDa, 1 min File Area(s)	68 kDa, 60 min File Area(s)	57 kDa, 60 min File Area(s)	30 kDa, 60 min File Area(s)
Protein G1TDN6=62416.94,Uncharacterized protein OS=Oryctolagus cuniculus GN=KRT5	4.167E+05	0.000E+00	1.428E+06	2.508E+06	4.770E+07
Protein G1T9F3=98472.15,Uncharacterized protein OS=Oryctolagus cuniculus GN=KPNB:	0.000E+00	6.034E+04	1.023E+04	0.000E+00	0.000E+00
Protein G1SGV5=95464.53,Uncharacterized protein OS=Oryctolagus cuniculus GN=ABCF	4.130E+05	3.981E+05	0.000E+00	3.481E+06	3.920E+05
Protein G1U9I8=64426.37,Uncharacterized protein OS=Oryctolagus cuniculus GN=KRT1	8.499E+07	1.539E+07	1.819E+07	8.128E+07	7.803E+08
Protein Q28888=40218.86,Decorin OS=Oryctolagus cuniculus GN=DCN PE=2 SV=1	4.566E+05	3.518E+06	5.110E+03	0.000E+00	0.000E+00
Protein G1U383=155595.77,Uncharacterized protein OS=Oryctolagus cuniculus GN=DHX	5.479E+04	0.000E+00	2.835E+05	0.000E+00	0.000E+00
Protein G1U754=61551.81,Histidine-rich glycoprotein OS=Oryctolagus cuniculus GN=HR	0.000E+00	0.000E+00	0.000E+00	0.000E+00	0.000E+00
Protein G1TN89=479309.59,Uncharacterized protein OS=Oryctolagus cuniculus GN=HSP	1.036E+08	1.223E+07	5.402E+07	1.271E+07	2.413E+07
Protein G1SXA5=85410.02,Uncharacterized protein OS=Oryctolagus cuniculus GN=HNRN	9.719E+05	5.594E+05	4.696E+05	0.000E+00	8.336E+06
Protein P12798=126317.63,Phosphorylase b kinase regulatory subunit beta OS=Oryctola	0.000E+00	0.000E+00	0.000E+00	0.000E+00	0.000E+00
Protein G1TXS2=257451.03,Uncharacterized protein OS=Oryctolagus cuniculus GN=MYO	1.083E+07	1.478E+07	5.863E+04	7.032E+05	3.613E+04
Protein G1U6N8=227599.13,Uncharacterized protein OS=Oryctolagus cuniculus GN=NUM	1.540E+07	1.648E+07	7.430E+07	1.027E+06	1.702E+08
Protein G1T4T6=166093.43,Uncharacterized protein OS=Oryctolagus cuniculus GN=MYO	1.701E+10	1.042E+08	8.907E+07	4.544E+07	6.341E+08
Protein D7NHU9=34848.38,Adenosine monophosphate deaminase 1 (Fragment) OS=Ory	0.000E+00	0.000E+00	0.000E+00	0.000E+00	0.000E+00
Protein G1T9M9=71270.37,Uncharacterized protein (Fragment) OS=Oryctolagus cuniculu	4.271E+08	1.090E+08	3.430E+07	1.396E+07	3.607E+06
Protein G1U7L4=72506.57,Uncharacterized protein (Fragment) OS=Oryctolagus cuniculu	8.021E+05	1.052E+07	7.135E+06	2.389E+06	1.697E+04
Protein G1SR03=89961.78,Uncharacterized protein OS=Oryctolagus cuniculus GN=VCP P	2.638E+06	6.137E+06	1.042E+07	9.677E+06	9.992E+07
Protein P68135=42371.89,Actin, alpha skeletal muscle OS=Oryctolagus cuniculus GN=AC	0.000E+00	0.000E+00	0.000E+00	0.000E+00	0.000E+00
Protein G1T1I5=81548.32,Uncharacterized protein OS=Oryctolagus cuniculus PE=4 SV=:	4.176E+06	2.947E+06	1.004E+06	5.300E+06	8.299E+07
Protein G1U9S2=70950.56,Serum albumin OS=Oryctolagus cuniculus GN=ALB PE=1 SV=	8.327E+06	3.028E+07	1.336E+06	9.851E+05	5.398E+07
Protein P04191=111779.56,Sarcoplasmic/endoplasmic reticulum calcium ATPase 1 OS=O	0.000E+00	0.000E+00	0.000E+00	0.000E+00	0.000E+00
Protein G1T1H3=87242.88,Uncharacterized protein (Fragment) OS=Oryctolagus cuniculu	7.648E+08	5.336E+07	2.115E+07	7.138E+06	5.416E+07
Protein G1T8Q6=84991.86,Heat shock protein HSP 90-beta OS=Oryctolagus cuniculus GI	7.346E+06	3.153E+05	7.734E+04	2.872E+06	3.843E+06
Protein G1TDQ5=86021.43,ATP-dependent 6-phosphofructokinase OS=Oryctolagus cunic	0.000E+00	0.000E+00	0.000E+00	0.000E+00	0.000E+00
Protein P30946=80089.14,Heat shock protein HSP 90-alpha OS=Oryctolagus cuniculus G	0.000E+00	0.000E+00	0.000E+00	0.000E+00	0.000E+00
Protein G1SS73=83430.75,Uncharacterized protein OS=Oryctolagus cuniculus GN=DDX1	1.053E+09	9.217E+07	1.256E+07	1.168E+08	8.630E+07
Protein G1SGZ6=98991.53,Alpha-1,4 glucan phosphorylase (Fragment) OS=Oryctolagus	0.000E+00	0.000E+00	0.000E+00	0.000E+00	0.000E+00
Protein G1T4R6=49883.51,Uncharacterized protein OS=Oryctolagus cuniculus GN=KRT1	0.000E+00	0.000E+00	0.000E+00	0.000E+00	0.000E+00
Protein G1T1V0=58263.42,Uncharacterized protein OS=Oryctolagus cuniculus GN=KRT1	0.000E+00	0.000E+00	0.000E+00	0.000E+00	0.000E+00
Protein G1SJN7=224004.32,Uncharacterized protein OS=Oryctolagus cuniculus GN=LOC:	9.430E+08	2.404E+08	6.431E+07	6.266E+08	5.439E+08
Protein G1TKS9=224389.70,Uncharacterized protein OS=Oryctolagus cuniculus GN=MYH	0.000E+00	0.000E+00	0.000E+00	0.000E+00	0.000E+00
Protein G1SJQ4=224330.06,Uncharacterized protein OS=Oryctolagus cuniculus GN=MYH	5.443E+08	6.669E+07	1.998E+08	8.691E+07	1.022E+08
Protein G1U9R3=224351.21,Uncharacterized protein OS=Oryctolagus cuniculus GN=MYH	0.000E+00	0.000E+00	0.000E+00	0.000E+00	0.000E+00
Protein G1TW48=223676.68,Myosin-7 OS=Oryctolagus cuniculus GN=MYH7 PE=4 SV=1	4.954E+05	8.644E+06	2.023E+05	2.740E+07	3.881E+06
Protein Q9GJP9=224536.89,Skeletal muscle myosin heavy chain MyHC-EO/IIL OS=Oryct	0.000E+00	0.000E+00	0.000E+00	0.000E+00	0.000E+00
Protein Q28641=223856.34,Myosin-4 OS=Oryctolagus cuniculus GN=MYH4 PE=1 SV=1	2.558E+06	4.477E+04	8.969E+05	2.833E+05	3.206E+07
Peptide KLEGDLK	1.428E+09	3.032E+07	1.124E+09	3.930E+05	7.954E+06
Peptide LQDLVDK	6.557E+06	1.942E+07	9.940E+05	6.727E+05	2.279E+07

Protein-Peptide View

Name	HMM, 0 min File Area(s)	88 kDa, 1 min File Area(s)	68 kDa, 60 min File Area(s)	57 kDa, 60 min File Area(s)	30 kDa, 60 min File Area(s)	
Peptide	KKEEATSGK: part of loop 1 [residues: 208-214]	0.000E+00	0.000E+00	0.000E+00	1.630E+06	0.000E+00
Peptide	LINDLSAQR	3.251E+09	6.298E+07	1.772E+07	4.678E+05	4.268E+08
Peptide	LIN[Deamid]DLSAQR	4.829E+08	4.987E+06	1.662E+06	4.003E+05	2.770E+07
Peptide	ANSEVAQWR	1.188E+07	2.769E+07	7.640E+06	2.739E+06	4.176E+07
Peptide	MFLWMVTR	1.208E+09	4.208E+08	2.606E+06	9.877E+08	1.449E+07
Peptide	MFLWM[Oxid]VTR	1.554E+08	8.994E+07	6.273E+04	3.219E+08	8.572E+06
Peptide	M[Oxid]FLWMVTR	1.278E+08	6.337E+07	9.651E+05	2.715E+08	2.769E+06
Peptide	SALAHALQSAR	3.572E+08	1.287E+07	1.787E+06	5.994E+05	0.000E+00
Peptide	LQTESGFSR	2.213E+09	4.602E+07	2.186E+06	1.187E+09	4.478E+08
Peptide	TLEDQVSELK	5.252E+09	7.853E+07	2.015E+07	1.628E+06	2.550E+08
Peptide	TNAACAALDKK	1.984E+08	0.000E+00	1.201E+06	8.368E+05	3.662E+05
Peptide	DDKLAQLITR	3.060E+08	3.964E+06	2.096E+08	7.039E+06	1.025E+08
Peptide	TKYETDAIQR	1.662E+07	3.444E+07	1.184E+07	2.142E+05	1.838E+08
Peptide	VKVGNEYVTK	1.298E+07	2.459E+07	0.000E+00	1.538E+08	6.040E+06
Peptide	VKVG[Deamid]EYVTK	3.398E+05	1.086E+06	2.703E+04	7.861E+06	0.000E+00
Peptide	ESFVKATVQSR	2.374E+06	1.313E+06	1.139E+04	1.065E+05	5.043E+07
Peptide	SNN[Deamid]FQKPKPAK	1.281E+08	1.288E+08	0.000E+00	3.828E+08	1.586E+07
Peptide	IEAQNKPFDAK	1.166E+09	9.144E+08	0.000E+00	1.044E+07	2.887E+09
Peptide	LQDLVDKLAQAK	4.050E+06	2.118E+07	7.750E+05	1.630E+05	2.139E+08
Peptide	DTQLHLDDALR	2.028E+07	4.325E+07	1.099E+07	7.168E+06	5.941E+07
Peptide	GSSFQTVSALFR: actin binding domain 1 / part of loop2 [residues:644-655]	5.423E+09	8.072E+07	2.269E+09	4.511E+07	7.321E+08
Peptide	EDQVFPMNPPK	2.923E+08	8.507E+07	0.000E+00	2.398E+06	2.089E+08
Peptide	EDQVFPM[Oxid]NPPK	1.028E+09	9.281E+08	2.067E+06	1.445E+06	2.541E+09
Peptide	LTGAVMHYGNMK	2.286E+07	4.858E+06	1.118E+05	2.269E+07	1.344E+06
Peptide	LTGAVMHYGNM[Oxid]K	9.424E+07	3.918E+07	0.000E+00	1.298E+08	1.746E+04
Peptide	SNNFQKPKPAK	1.927E+08	3.219E+08	1.256E+07	1.067E+09	2.382E+06
Peptide	LTGAVM[Oxid]HYGNM[Oxid]K	6.703E+07	6.493E+07	9.977E+04	1.685E+08	0.000E+00
Peptide	VAEQELLDASER	1.192E+07	2.463E+07	7.670E+06	4.195E+06	3.279E+08
Peptide	ANLLQAEIEELR	2.785E+07	3.682E+07	1.659E+07	9.452E+06	3.189E+08
Peptide	KGSSFQTVSALFR	1.938E+09	2.911E+07	9.444E+08	1.589E+07	2.973E+08
Peptide	GSSFQ[Deamid]TVSALFR	7.390E+06	6.371E+06	8.355E+08	2.947E+06	1.006E+08
Peptide	ELEAEVESEQKR	6.621E+06	1.890E+07	9.618E+03	9.870E+05	1.060E+08
Peptide	LASADIETYLLEK	8.605E+09	2.302E+09	1.000E+08	1.187E+10	4.327E+08
Peptide	DPLNETVVGlyQK	5.864E+08	4.456E+08	4.355E+06	6.725E+08	1.749E+07
Peptide	KVAEQELLDASER	1.495E+07	3.201E+07	1.238E+07	5.210E+06	2.777E+08
Peptide	INQQLDTKQPR	1.384E+07	7.225E+06	0.000E+00	1.273E+07	5.123E+07
Peptide	QAFTQIEELKR	2.795E+09	9.672E+07	4.590E+06	3.184E+06	2.125E+08
Peptide	ENQSILITGESGAGK: ATP-loop (P-loop) [residues: 171-185]	4.659E+09	3.537E+09	8.180E+06	4.835E+06	4.000E+09

Protein-Peptide View

Name	HMM, 0 min File Area(s)	88 kDa, 1 min File Area(s)	68 kDa, 60 min File Area(s)	57 kDa, 60 min File Area(s)	30 kDa, 60 min File Area(s)	
Peptide	ENQ[Deamid]SILITGESGAGK	1.866E+09	1.356E+09	1.244E+06	6.368E+05	1.387E+09
Peptide	EEQAEPDGTEVADK	9.407E+08	8.492E+08	1.590E+07	1.443E+09	1.801E+08
Peptide	VIQYFATIAVTGDK: part of loop 1 [residues:192-207]	3.141E+09	3.594E+08	2.359E+06	1.036E+06	8.116E+09
Peptide	SYHIFYQIMSNK	5.522E+08	2.044E+08	7.605E+06	6.972E+08	1.713E+07
Peptide	IEDEQALAM[Oxid]QLQK	1.538E+09	2.763E+07	1.255E+09	3.050E+06	1.072E+09
Peptide	ERIEAQNKPFDAK	2.948E+07	3.263E+07	1.365E+06	1.197E+06	4.511E+08
Peptide	SYHIFYQIM[Oxid]SNK	1.404E+09	9.625E+08	1.806E+07	2.401E+09	1.073E+08
Peptide	LQDAEEHVAVNAK	1.902E+07	2.951E+07	1.379E+07	3.219E+06	1.849E+08
Peptide	AAYLQSLNSXDLLK	2.396E+06	0.000E+00	7.661E+05	9.928E+04	2.730E+07
Peptide	LLGSIDVDHTQYK	1.663E+07	1.506E+06	6.818E+07	0.000E+00	0.000E+00
Peptide	QLDEKDSLVSQLSR	1.113E+09	2.084E+07	0.000E+00	2.114E+06	3.775E+08
Peptide	GQTVQQVYNAV GALAK	8.479E+09	7.116E+09	1.044E+08	1.330E+10	5.553E+08
Peptide	GQTVQQVYN[Deamid]AVGALAK	3.658E+09	5.822E+08	1.906E+07	1.122E+09	1.386E+08
Peptide	GQTVQQ[Deamid]VYNAV GALAK	3.443E+09	2.742E+09	1.834E+07	5.645E+09	1.342E+08
Peptide	NAYEESLDQLETLK	9.852E+06	1.444E+07	4.657E+06	2.657E+06	3.300E+07
Peptide	VIQYFATIAVTGDKK	5.200E+08	1.158E+08	0.000E+00	1.214E+04	2.356E+09
Peptide	RVIQYFATIAVTGDK	3.444E+08	3.669E+07	0.000E+00	0.000E+00	8.703E+08
Peptide	VLNASAIPEGQFIDSK	1.211E+10	1.914E+08	8.658E+09	1.208E+08	2.643E+09
Peptide	VRELEAEVESEQKR	1.431E+06	3.761E+06	5.206E+06	1.867E+04	1.153E+08
Peptide	NKDPLNETVWGLYQK	7.942E+09	6.322E+09	8.570E+07	1.211E+10	2.068E+08
Peptide	NKDPLN[Deamid]ETVWGLYQK	3.214E+09	2.918E+09	2.307E+07	5.696E+09	2.428E+06
Peptide	KKGSSFQTVSALFR	4.202E+07	6.431E+06	1.611E+08	0.000E+00	1.274E+08
Peptide	EDQVFPM[Oxid]NPPKYDK	1.561E+08	9.869E+07	1.870E+06	1.220E+05	3.175E+09
Peptide	TPGAM[Oxid]EHELVLHQLR	1.731E+09	2.762E+07	1.129E+09	2.093E+07	1.703E+09
Peptide	AGLLGLLEEM[Oxid]RDDK	2.641E+09	4.574E+04	2.175E+09	4.404E+07	9.288E+08
Peptide	QREEQAEPDGTEVADK	2.558E+09	1.656E+09	3.917E+07	3.515E+09	2.274E+08
Peptide	NAYEESLDQLETLKR	2.172E+07	4.151E+07	1.555E+07	1.047E+07	2.802E+08
Peptide	RVIQYFATIAVTGDKK	4.845E+07	1.202E+07	0.000E+00	0.000E+00	3.601E+08
Peptide	GQTVQQ[Deamid]QVYNAV GALAK	3.443E+09	2.742E+09	1.834E+07	5.645E+09	1.342E+08
Peptide	TLAFLFTGTA AAAEAGGGK	1.150E+09	3.401E+07	3.917E+06	6.210E+07	8.182E+07
Peptide	DLEEATLQHEATAATLR	9.279E+09	1.172E+08	2.467E+07	0.000E+00	3.709E+08
Peptide	TLAFLFTGTA AAAEAGGGKK	6.388E+08	1.926E+07	2.005E+06	1.156E+08	2.900E+07
Peptide	LQQFFNHMM[Oxid]FVLEQE EYK	1.247E+09	7.041E+08	1.466E+06	1.993E+09	1.245E+08
Peptide	VLN[Deamid]ASAIPEGQFIDSK	5.156E+09	1.057E+07	3.757E+09	3.536E+07	9.479E+08
Peptide	N[Deamid]KDPLNETVWGLYQK	3.214E+09	2.918E+09	2.307E+07	5.696E+09	4.244E+07
Peptide	INQ[Deamid]QLDTK	8.300E+07	5.802E+07	3.687E+05	6.852E+06	5.760E+06
Peptide	TPGAMEHELVLHQLR	4.009E+08	2.338E+06	6.707E+07	2.672E+06	2.203E+08
Peptide	LYEQHLGK	7.333E+08	6.940E+08	1.739E+07	1.369E+09	9.438E+07

Protein-Peptide View

Name	HMM, 0 min File Area(s)	88 kDa, 1 min File Area(s)	68 kDa, 60 min File Area(s)	57 kDa, 60 min File Area(s)	30 kDa, 60 min File Area(s)	
Peptide	YKVLNASAIPEGQFIDSK	3.213E+07	2.973E+05	3.503E+07	4.940E+04	1.092E+08
Peptide	VTFQLKAER	0.000E+00	2.043E+05	0.000E+00	1.124E+06	5.769E+05
Peptide	M[Oxid]FLWM[Oxid]VTR	8.068E+08	5.236E+08	1.105E+07	4.814E+06	1.104E+08
Peptide	EFEM[Oxid]SNLQSK	4.834E+08	1.234E+07	5.590E+08	3.366E+06	3.543E+08
Peptide	IKELQAR	9.065E+07	0.000E+00	2.009E+08	0.000E+00	3.449E+07
Peptide	LTGAVM[Oxid]HYGN[Deamid]M[Oxid]K	0.000E+00	6.400E+06	0.000E+00	2.817E+07	0.000E+00
Peptide	YETDAIQR	5.986E+05	2.900E+06	1.294E+06	6.145E+05	2.778E+07
Peptide	AAYLQSLN[Deamid]SXDLLK	1.619E+05	4.477E+04	1.308E+05	1.840E+05	4.762E+06
Peptide	LASADIETYLLEKSR	3.754E+07	4.418E+06	0.000E+00	1.489E+07	1.433E+06
Peptide	EFEMSNLQSK	4.578E+08	6.315E+04	1.790E+08	1.375E+06	2.118E+07
Peptide	KEFEMSNLQSK	5.119E+06	5.128E+04	2.704E+06	2.622E+05	0.000E+00
Peptide	KEFEM[Oxid]SNLQSK	4.246E+07	2.880E+04	6.214E+07	3.358E+05	4.786E+07
Peptide	ESIFCIQYNIR	2.791E+05	0.000E+00	1.314E+06	7.786E+05	3.558E+06
Peptide	KKEFEM[Oxid]SNLQSK	1.058E+08	2.843E+06	2.683E+08	1.069E+06	1.453E+08
Peptide	LAQESTM[Oxid]DIENDK	4.442E+07	7.517E+04	5.732E+07	1.097E+04	2.257E+07
Peptide	IEDEQALAMQLQK	4.144E+08	1.735E+06	1.042E+08	1.010E+07	1.372E+08
Peptide	VLNASAIPEGQFIDSKK	2.634E+08	0.000E+00	3.313E+08	1.464E+04	8.314E+08
Peptide	LAQESTM[Oxid]DIENDKQLDEK	1.301E+09	3.463E+07	1.642E+09	2.277E+04	4.898E+07
Peptide	LAQESTM[Oxid]DIEN[Deamid]DKQQLDEK	1.088E+08	8.132E+05	1.585E+08	6.320E+05	3.396E+08
Peptide	QLEEEIK	9.462E+08	2.864E+05	3.543E+06	7.421E+05	8.165E+07
Peptide	LINDLSAQ[Deamid]R	6.021E+06	0.000E+00	0.000E+00	1.998E+04	0.000E+00
Peptide	IEAQN[Deamid]KPFDAK	3.797E+06	1.847E+08	0.000E+00	2.903E+04	1.301E+09
Peptide	QAFTQIEELK	1.144E+08	0.000E+00	1.711E+04	5.914E+04	1.773E+06
Peptide	ESIFCIQYN[Deamid]IR	6.737E+05	1.659E+05	8.059E+05	4.536E+06	3.992E+04
Peptide	KKEFEMSNLQSK	4.021E+07	2.905E+05	4.681E+07	2.386E+05	6.479E+06
Peptide	LAQESTMDIENDK	7.816E+06	0.000E+00	1.569E+06	0.000E+00	6.130E+04
Peptide	AGLLGLEEMRDDK: actin binding domain 2 [residues: 770-780]	7.638E+07	5.507E+04	8.279E+06	2.227E+05	1.570E+06
Peptide	Q[Deamid]LDEKDSLVSQLSR	1.453E+08	4.988E+06	8.152E+05	0.000E+00	8.938E+07
Peptide	MEIDDLASNMETVSK	1.812E+08	1.149E+03	0.000E+00	6.907E+04	0.000E+00
Peptide	M[Oxid]EIDDLASNMETVSK	3.748E+07	1.515E+05	3.202E+04	0.000E+00	0.000E+00
Peptide	MEIDDLASNM[Oxid]ETVSK	1.091E+08	3.685E+05	0.000E+00	0.000E+00	0.000E+00
Peptide	M[Oxid]EIDDLASNM[Oxid]ETVSK	1.177E+08	3.252E+04	0.000E+00	3.623E+05	0.000E+00
Peptide	DLEEATLQ[Deamid]HEATAATLR	3.931E+09	3.983E+07	5.956E+06	1.333E+06	1.177E+08
Peptide	RDLEEATLQHEATAATLR	5.140E+08	8.731E+06	2.080E+06	1.516E+07	2.267E+07
Peptide	NLQQEISDLTEQIAEGGKR	8.032E+06	1.588E+06	6.398E+02	0.000E+00	1.434E+08
Peptide	SELKM[Oxid]EIDDLASNMETVSK	1.612E+07	3.036E+04	2.365E+05	2.402E+04	2.161E+05
Peptide	SELKM[Oxid]EIDDLASNM[Oxid]ETVSK	2.401E+08	1.695E+04	5.809E+04	0.000E+00	6.215E+07
Peptide	HDCDLLREQYEEEQEAK	4.559E+06	0.000E+00	5.460E+06	1.285E+05	0.000E+00

Supplementary Table 3: Mean velocities ($\mu\text{m}/\text{sec}$) of actin filaments in the in-vitro motility assay form enzymatic HMM.

Myosin digestion time(minutes)	Control group			Loop1 digestion group			Loop1&2 digestion group		
	Mean velocity ($\mu\text{m}/\text{sec}$)	SEM	Number of filaments	Mean velocity ($\mu\text{m}/\text{sec}$)	SEM	Number of filaments	Mean velocity ($\mu\text{m}/\text{sec}$)	SEM	Number of filaments
0	3.386	0.108	101	3.780	0.049	574	3.385	0.058	193
1	3.927	0.126	77	3.985	0.067	438	3.831	0.063	516
2	3.662	0.102	66	3.906	0.067	466	4.499	0.083	289
4	3.875	0.102	87	2.519	0.13	144	4.196	0.084	297
8	3.443	0.076	114	0	0	0	2.951	0.089	231
10	3.338	0.119	87	0	0	0	0	0	0
30	3.564	0.127	102	0	0	0	0	0	0

Supplementary Table 4: Mean of motile fraction (fraction of time that filaments are moving) of actin filaments in the in-vitro motility assay form enzymatic HMM.

Myosin digestion time(minutes)	Control group			Loop1 digestion group			Loop1&2 digestion group		
	Mean velocity ($\mu\text{m}/\text{sec}$)	SEM	Number of filaments	Mean velocity ($\mu\text{m}/\text{sec}$)	SEM	Number of filaments	Mean velocity ($\mu\text{m}/\text{sec}$)	SEM	Number of filaments
0	0.959	0.015	101	0.925	0.026	571	0.894	0.011	193
1	0.966	0.007	77	0.913	0.019	438	0.892	0.013	516
2	0.791	0.079	66	0.898	0.008	466	0.862	0.051	289
4	0.971	0.016	87	0.703	0.089	144	0.736	0.112	297
8	0.891	0.021	114	0	0	0	0.807	0.028	231
10	0.910	0.039	87	0	0	0	0	0	0
30	0.929	0.014	102	0	0	0	0	0	0

Supplementary Table 5: Mean velocities of actin filaments cooperated with α -actinin in the in-vitro motility assay form enzymatic HMM.

α-actinin concentration (μM)	Control group			Loop1 digestion group			Loop1&2 digestion group		
	Mean velocity (μ m/sec)	SEM	Number of filaments	Mean velocity (μ m/sec)	SEM	Number of filaments	Mean velocity (μ m/sec)	SEM	Number of filaments
0	3.292	0.1355	127	4.057	0.363	123	3.841	0.052	193
0.5	2.352	0.5231	88	2.623	1.392	182	2.300	1.345	154
0.75	1.856	0.7837	109	1.515	1.180	138	1.634	0.759	107
1	1.769	0.9673	57	0.921	0.572	87	1.074	0.593	130
1.25	1.367	0.7763	135	0.774	0.691	47	0.951	1.220	293
1.5	0.900	0.8454	271	0	0	0	0.776	0.607	39